CTD-75

Applied Science Associates, Inc.

OIL SPILL - FISHERY
IMPACT ASSESSMENT
ON
GEORGES BANK:
EFFECTS OF SPILL TIMING
AND SPILL SITE LOCATION

PREPARED FOR:

U.S. DEPARTMENT OF INTERIOR
NEW YORK
OUTER CONTINENTAL SHELF OFFICE
AND
U.S. DEPARTMENT OF STATE
WASHINGTON, D.C.

JUNE 10, 1982

P.O. Box 537, West Kingston, Rhode Island 02892
(401) 789-6224

OIL SPILL - FISHERY IMPACT ASSESSMENT ON GEORGES BANK: EFFECTS OF SPILL TIMING AND SPILL SITE LOCATION

DR. MARK REED
DR. MALCOLM L. SPAULDING
MR. ERIC L. ANDERSON
MR. ERNESTO LORDA

APPLIED SCIENCE ASSOCIATES, INC.
529 MAIN STREET
WAKEFIELD, RHODE ISLAND 02879

PREPARED FOR:

U.S. DEPARTMENT OF INTERIOR
NEW YORK
OUTER CONTINENTAL SHELF OFFICE
AND
U.S. DEPARTMENT OF STATE
WASHINGTON, D.C.

JUNE 10, 1982

TABLE OF CONTENTS

1. INTRODUCTION

2. METHODOLOGICAL BACKGROUND

3. OVERVIEW OF PREVIOUS SYSTEM SENSITIVITY ANALYSES

4. CASE DESCRIPTIONS

5. OIL SPILL SURFACE AND SUBSURFACE TRAJECTORY ANALYSES

6. ICHTHYOPLANKTON TRANSPORT AND FATES ANALYSIS

7. GEORGES BANK COD FISHERY IMPACTS

8. SUMMARY OF FINDINGS

9. FURTHER SUPPORTING STUDIES

REFERENCES

APPENDIX A. SUMMARY OF WIND STATISTICS

1. INTRODUCTION

In response to a request from the U.S. State Department through the U.S. Department of Interior, Bureau of Land Management (BLM), Applied Science Associates (ASA) personnel have executed 16 simulations (four spill locations (Fig. 1), four seasonal scenarios at each site) of the behavior and fate of oil spills on Georges Bank, and the estimated impact of these spills on the Georges Bank cod fishery. The modeling methodology follows that of Reed, Spaulding, and Cornillon (1979, 1980, 1981), as further refined under contract #AA851-CTO-75 to the BLM-New York Outer Continental Shelf Office (Anderson and Spaulding, 1981; Lorda et al. 1982; Spaulding and Reed, 1982; Spaulding and Saila et al. 1981, 1982a, 1982b, 1982c; Reed et al. 1982).

This report includes a brief description of the underlying methodology followed by an overview of the 16 simulations performed, case-by-case analyses of the surface and subsurface hydrocarbon trajectories, ichthyoplankton and fishery impact estimates, a summary of findings, and a set of recommendations for further supporting work.

2. METHODOLOGICAL BACKGROUND

The basis for the present work is an oil spill - fishery impact assessment computer model system composed of an oil spill fates model, a continental shelf hydrodynamics model, an ichthyoplankton transport and fates model, and a fish population

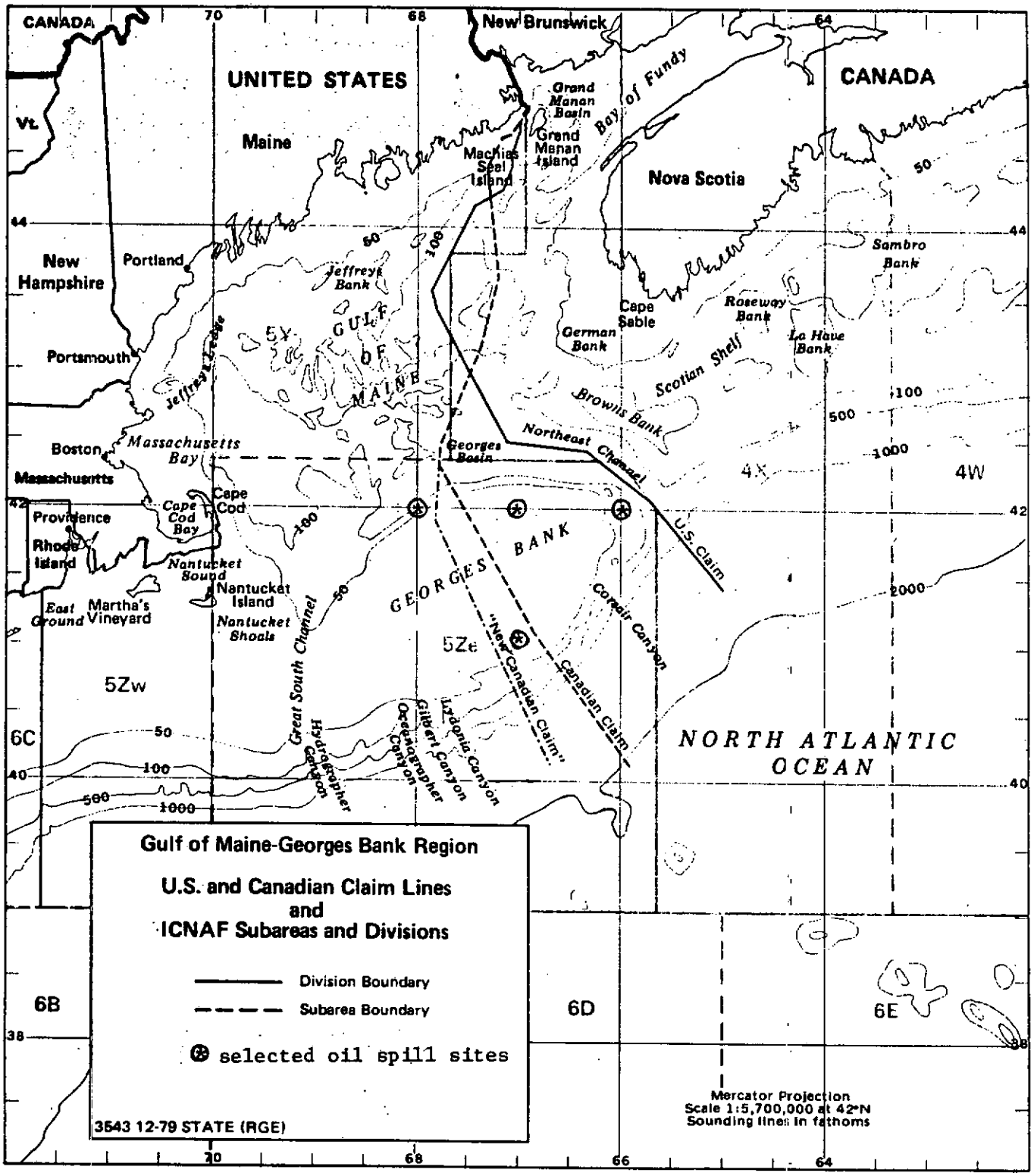

Figure 1. Study area map, showing the four selected spill sites and U.S. and Canadian boundary claim lines.

model. The model system addresses direct impacts of oil on a fishery through hydrocarbon-induced egg and larval mortality. This early life stage mortality is estimated by dynamically mapping the spatial intersection of the surface and subsurface oil distributions resulting from the spill with the distribution of developing eggs and larvae. Ichthyoplankton entering a volume of water with hydrocarbon concentrations in excess of a specified threshold (50 parts per billion) Reed (1980) or under a surface spillet are assumed lost. Model ouput is given in terms of differential catch at uniform effort, comparing the non-impacted and the hydrocarbon impacted fisheries, stochastically including the effects of environmental variability.

In the present study, the hydrodynamic field is composed of a long term net transport regime inferred from several decades of drifter observations (Bumpus and Day, 1957; Bumpus and Lauzier, 1965). One net transport field has been compiled for four seasons centered on January 1, April 1, July 1, and October 1. To obtain transport estimates at intermediate days, the currents are linearly interpolated in time at each node of the transport grid (Fig. 2). Thus an annually repetitive long term net transport field varying smoothly from day to day is provided.

Noting that this net transport field already contains the effect of the net wind forcing, seasonal means are removed from a wind record for the time period of interest. This de-meaned record is then used to drive a slab flow model of the upper 10 meters of the water column. This second transport field, incorporating transport phenomena with coherence scales ranging from approximately 1 to 10 days, is then juxtaposed with the

drifter inferred field described above. A random walk model simulates dispersive processes occurring on shorter time scales. For more information, the reader is referred to Reed et al. (1980). In addition to this flow regime, the surface spillets are also transported at 3.5% of the wind speed (full wind, not de-meaned) in the direction of the wind.

The wind record used here is taken from Nantucket Airport, and spans from September 1972 through August 1973. This record can be considered typical for the Georges Bank area, with the qualifications discussed in Appendix A. Comparison of the wind record from Nantucket Airport with that taken at the spill site during the Argo Merchant oil spill of 1976-77 suggests that the airport data underestimates peak wind magnitudes by as much as a factor of two (Grose and Mattson, 1977), although Godshall et al. (1980) suggest that an overall multiplication factor of 1.1 to 1.5 is representative. The latter reference also suggests spatially and seasonally variable adjustments to wind direction as reported at Nantucket, with values ranging from -20 to +30 degrees. To maintain consistency with earlier work (Spaulding et al. 1981, 1982a, 1982b) none of these corrections has been incorporated in the work reported here.

It should be noted that a sophisticated continental shelf numerical hydrodynamic model for the Georges Bank - Gulf of Maine region exists as a functioning part of the oil spill - fishery impact model system. The complexity of the topography of the Georges Bank region results in complex flow fields, especially in the area of the Northeast Channel. The authors strongly believe that scientifically sounder estimates of the surface and

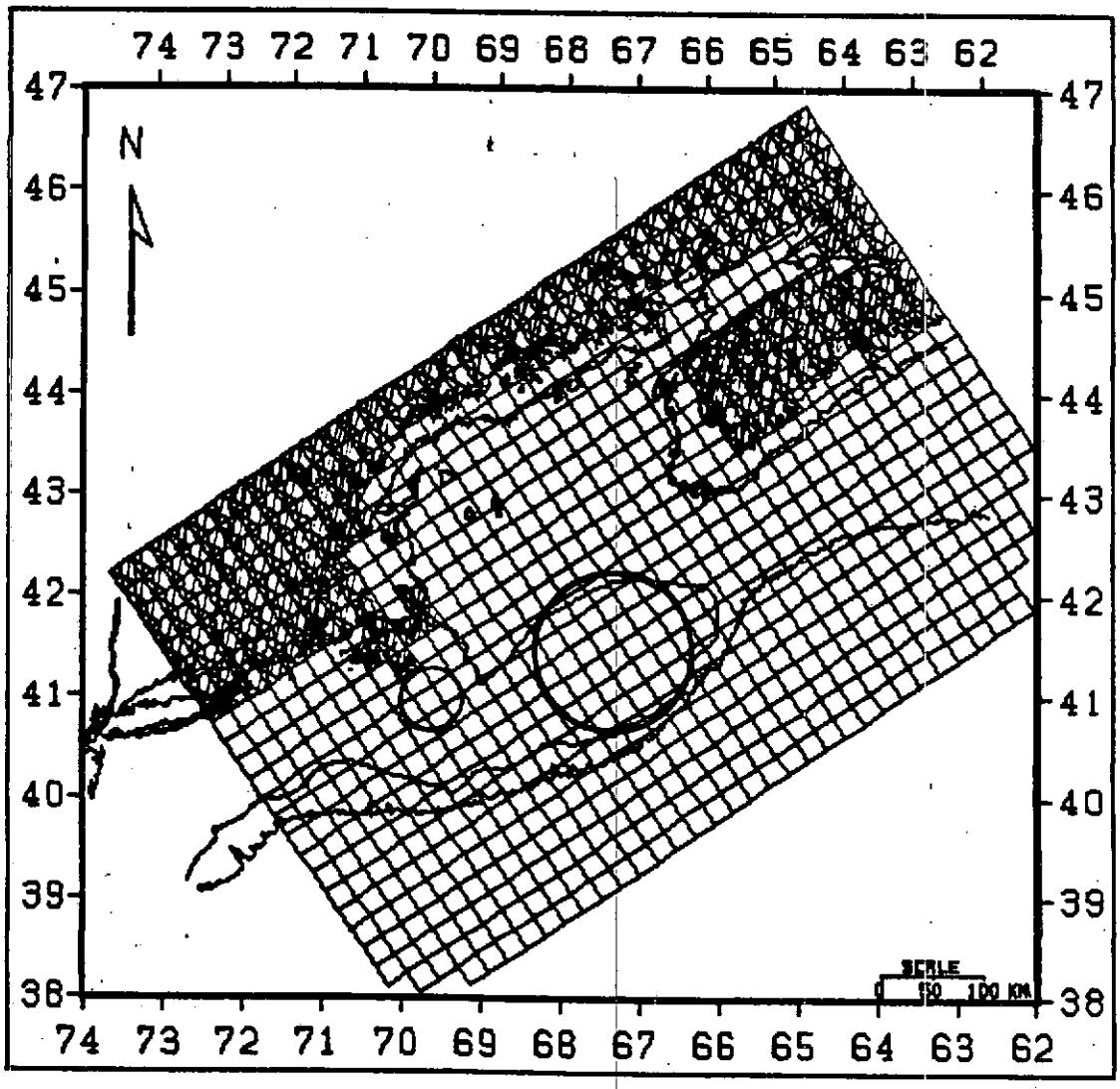

Figure 2. Rectangular transport grid used for the oil spill and ichthyoplankton transport and fates models. Land cells are shaded. The two circles designate the modeled cod spawning grounds.

subsurface fates of hydrocarbons and ichthyoplankton can be made with this numerical hydrodynamic model. This option was not employed for the work discussed here due to time constraints.

3. OVERVIEW OF PREVIOUS SYSTEM SENSITIVITY ANALYSES

Difficulties in establishing stock-recruit relationships, and the current inability to predict recruitment even one year ahead make the quantification of absolute catch losses impossible. Output of the model system discussed here is therefore limited to relative rather than absolute catch losses. The sensitivities of these impact estimates to pre-recruit (year 0) mortality formulations, hydrocarbon toxicity threshold, spill timing, stochastic environmental variability, and transport field have been evaluated (Reed, et al. 1982; Spaulding et al. 1982c).

For any given species, we can define an "impact window" with a temporal range from the beginning of the spawning season for that species to the last day of spawning plus the maximum number of days required for the larvae or post larvae to become demersal or pelagic and self-motile such that polluted areas can be avoided. This window dimension reflects the assumption that only the planktonic eggs, larvae, and post-larvae are susceptible to the toxic action of hydrocarbons. The impact window also has two horizontal spatial dimensions, defined by that area of the ocean occupied by the developing ichthyoplankton.

Clearly, the location of a spill, combined with wind and ocean current transport fields, can place the spill outside this

impact window, regardless of spill duration. For cod, the species considered here, the temporal dimension of the impact window begins with the initiation of spawning on December 1, and ends 120 days after cessation of spawning at the end of April. Thus the window is closed, regardless of spill location, for the month of September. For spills of release duration less than about 30 days, the transport regime during October and November is sufficient to remove all residual hydrocarbons from Georges Bank by the time cod spawning begins in early December.

Thus it can be said that the impact estimates are most sensitive to spill timing and location, in that these two factors, together with the transport mechanisms of wind and currents, determine whether or not any impact occurs at all. However, given a situation in which an impact is found to be probable, the magnitude of this impact is most dependent upon the characterization of the stock-recruit relationship (Reed, Spaulding, and Cornillon, 1980; Reed, Spaulding, and Lorda, 1982), and is much less sensitive to the toxicity threshold level or the hydrocarbon entrainment rate.

Impact variations associated with different spill sites around the perimeter of Georges Bank (Fig. 1) will also be sensitive to the hydrodynamic fields underlying the simulations, as discussed in the previous section and in Section 8.

4. CASE DESCRIPTIONS

For the present study, four spill sites have been selected by the U.S. State Department (Fig. 1), and an oil well blowout of 30 days' duration has been simulated at each site for each of

TABLE 1
OIL SPILL FATES MODEL INPUT DATA

SPILL LOCATIONS:	N LATITUDE	W LONGITUDE
	42	66
	42	67
	42	68
	41	67

MIXED LAYER DEPTH: 10 METERS

WIND: NANTUCKET WEATHER STATION 1972-73, 3 HOUR INTERVALS

CURRENTS: DERIVED FROM BUMPUS et al. (1965), SEASONAL DRIFTER DATA PLUS WIND-DRIVEN SLAB FLOW

SURFACE OIL DRIFT RATE: VECTORAL SUM OF CURRENTS PLUS 3.5% WIND SPEED DOWNWIND

OIL:

DENSITY	0.8338	GM/CM**3
INTERFACIAL TENSION	30.0	DYNES/CM**2
KINEMATIC VISCOSITY	7.95	CENTISTOKE

OIL FRACTION (STATFJORD NORWAY CRUDE) % BY WEIGHT

PARAFFIN C6 - C12	15.0
PARAFFIN C13 - C22	13.0
CYCLOPARAFFIN C6 - C12	14.0
CYCLOPARAFFIN C13 - C22	12.0
AROMATIC C6 - C11	7.0
AROMATIC C12 - C18	3.5
NAPTHENO-AROMATIC C9 - C25	3.5
RESIDUAL	32.0

SPILL SIZE AND RELEASE RATE: WELL BLOWOUT, 68,000,000 GALLON RELEASE OVER 30 DAYS (60 SPILLETS, 1 RELEASED EVERY 12 HOURS)

TOTAL SPILL SIMULATION TIME: 90 DAYS

TIME STEP (OIL SPILL MODEL): 3 HOURS

HORIZONTAL DISPERSION RATE: 10 M**2/SEC

four starting days: March 1, June 1, September 1, and December 1. Other details of the simulations are summarized in Table 1.

5. SURFACE AND SUBSURFACE HYDROCARBON TRAJECTORY ANALYSES

Figures 3 through 18 show the trajectories of the surface and subsurface hydrocarbon centers of mass for 90 days subsequent to the initiation of each spill. These figures represent summaries of the transport properties associated with each of the 16 cases simulated, as governed by the combined drifter-inferred (Figs. 19 through 22) and de-meaned-wind driven current fields and raw wind data as described above.

Certain seasonal patterns of ocean currents and winds have been historically typical of the Georges Bank - Nantucket Shoals - Gulf of Maine region. Because this area lies between the summer and winter normal positions of the North American polar front (see Appendix A), seasonal shifts in wind direction usually occur in April and September. Winter winds come typically from the northwest, summer winds from the southwest. Long term ocean transport velocities in this area are on the order of 5-10 cm/sec. Wind-induced drift magnitudes of surface hydrocarbons are estimated here at 3.5% of the wind speed, so that surface wind effects in excess of the background transports are not unusual. Figures 19 through 22 show seasonal long term transport fields. The reliability of these estimated fields depends on the number of returns from drifter releases. Thus the reliability is generally high on Georges Bank, except during the winter, and low on the Scotian Shelf. For detailed analyses, the reader is referred to Bumpus and Day (1957) and Bumpus and Lauzier (1965).

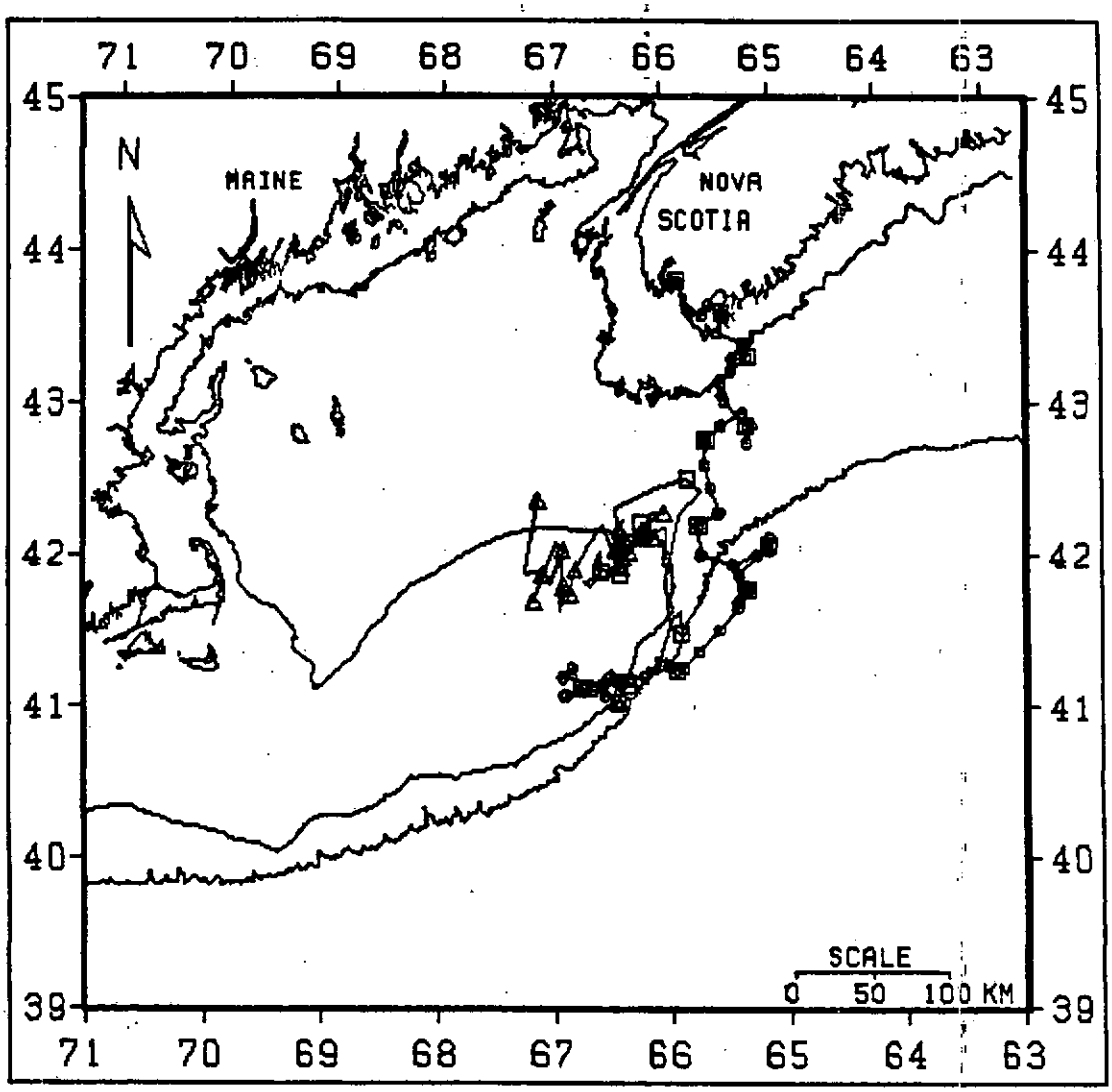

Surface (■) and Subsurface (▲) Center of Mass Trajectories

Spill Site: 42° N, 66° W Spill Start Day: March 1

Figure 3.

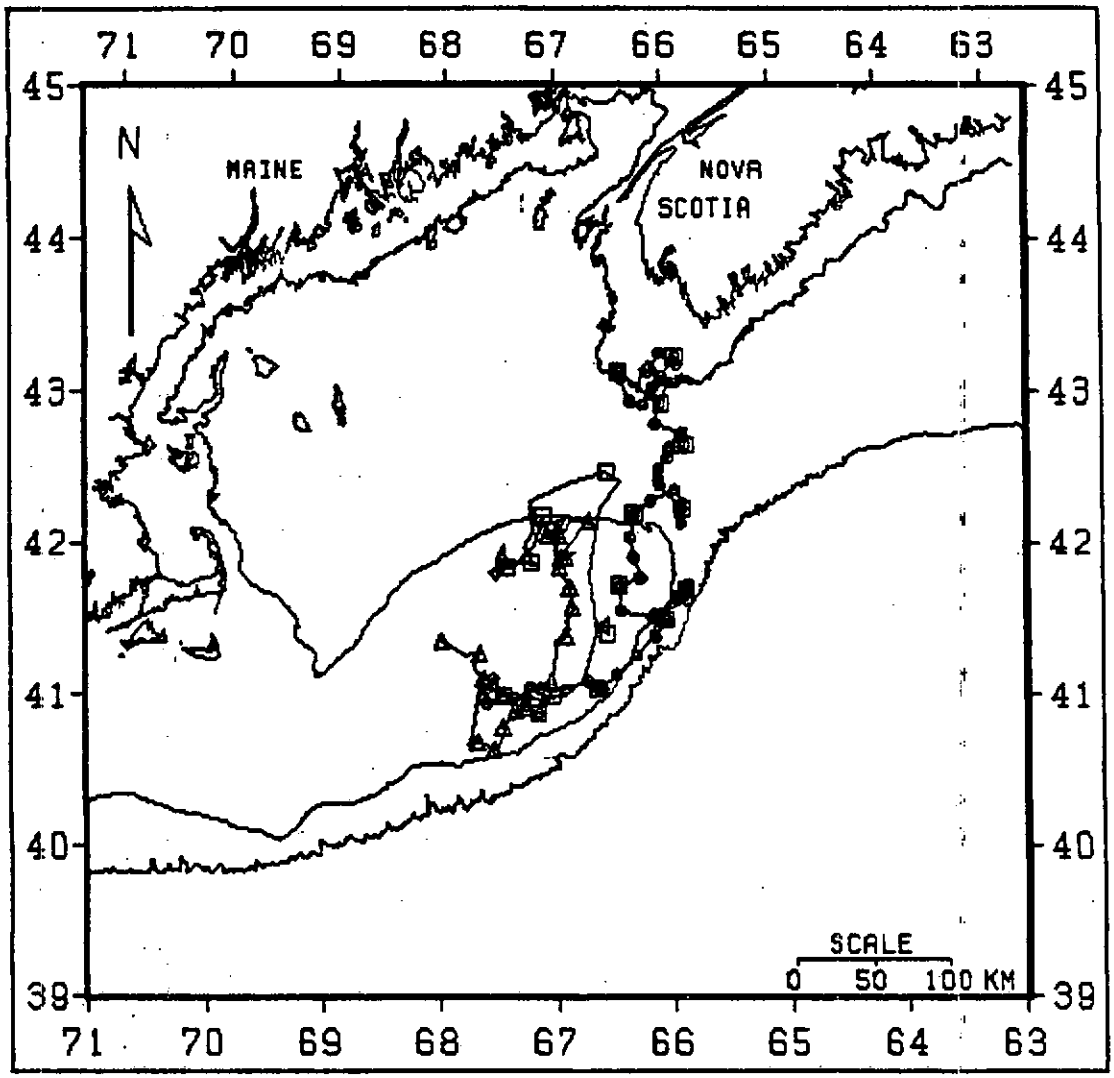

Surface (■) and Subsurface (▲) Center of Mass Trajectories

Spill Site: 42° N, 67° W Spill Start Day: March 1

Figure 4.

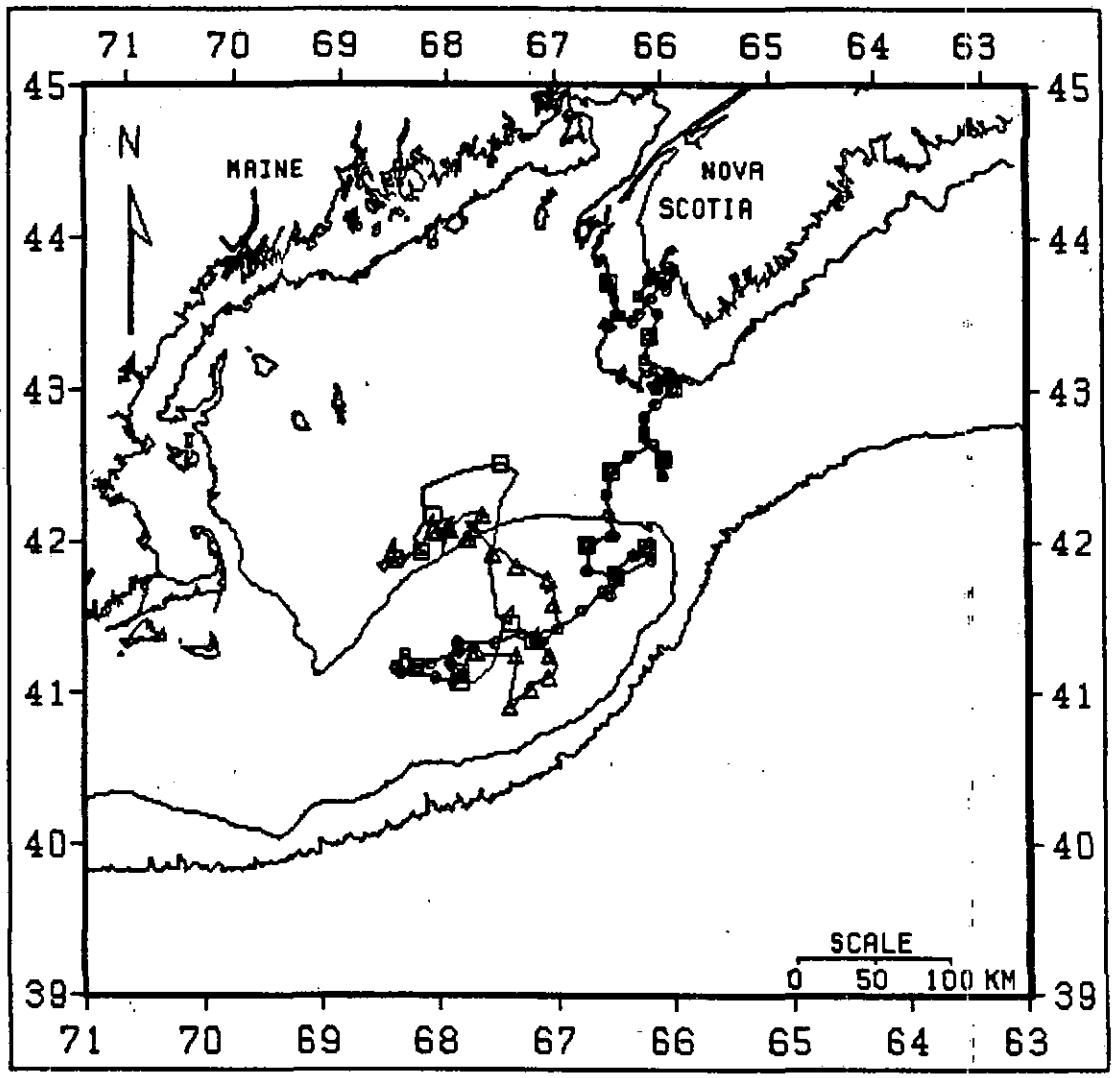

Surface (■) and Subsurface (▲) Center of Mass Trajectories

Spill Site: 42° N, 68° W Spill Start Day: March 1

Figure 5.

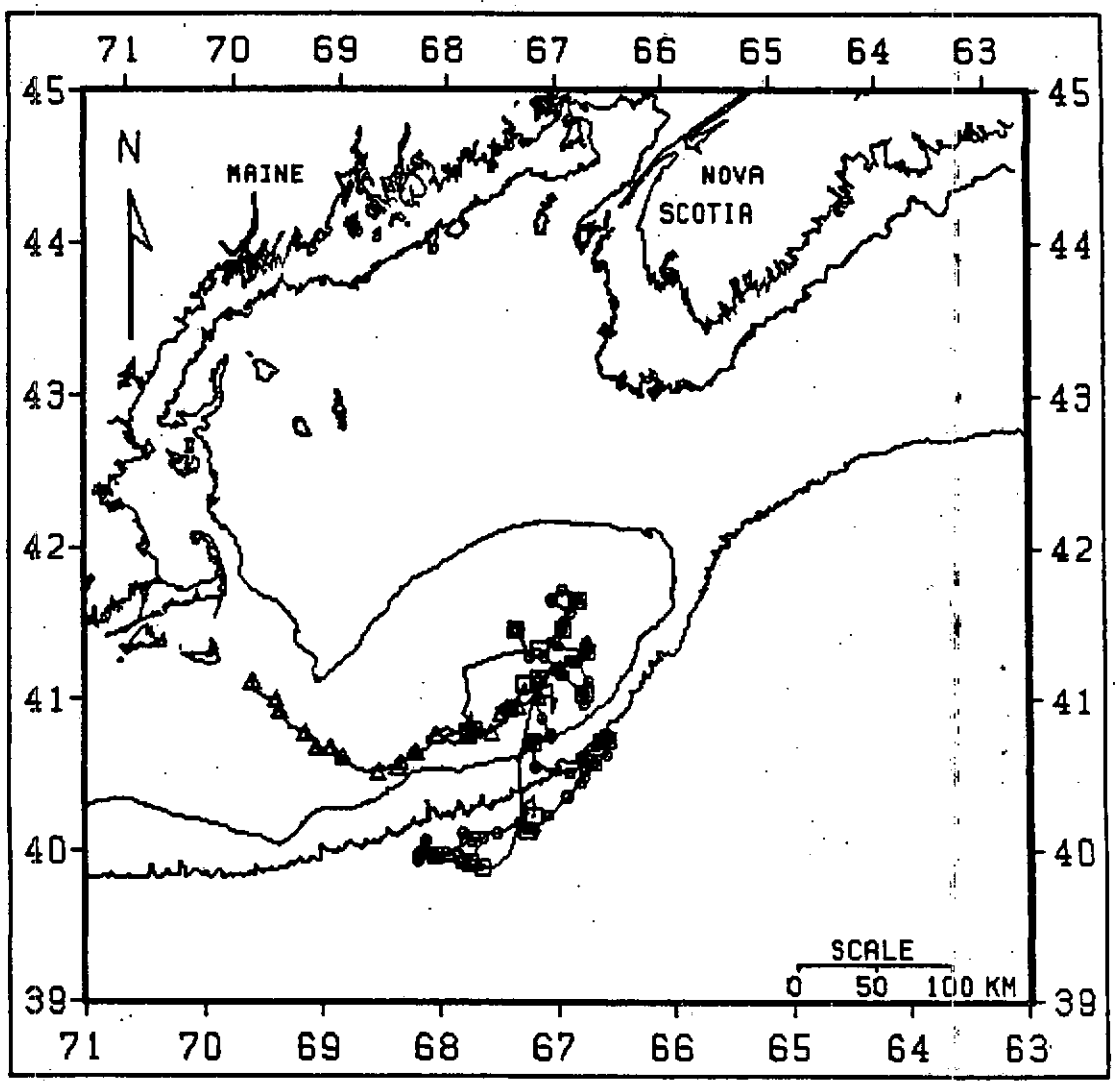

Surface (■) and Subsurface (▲) Center of Mass Trajectories

Spill Site: 41° N, 67° W Spill Start Day: March 1

Figure 6.

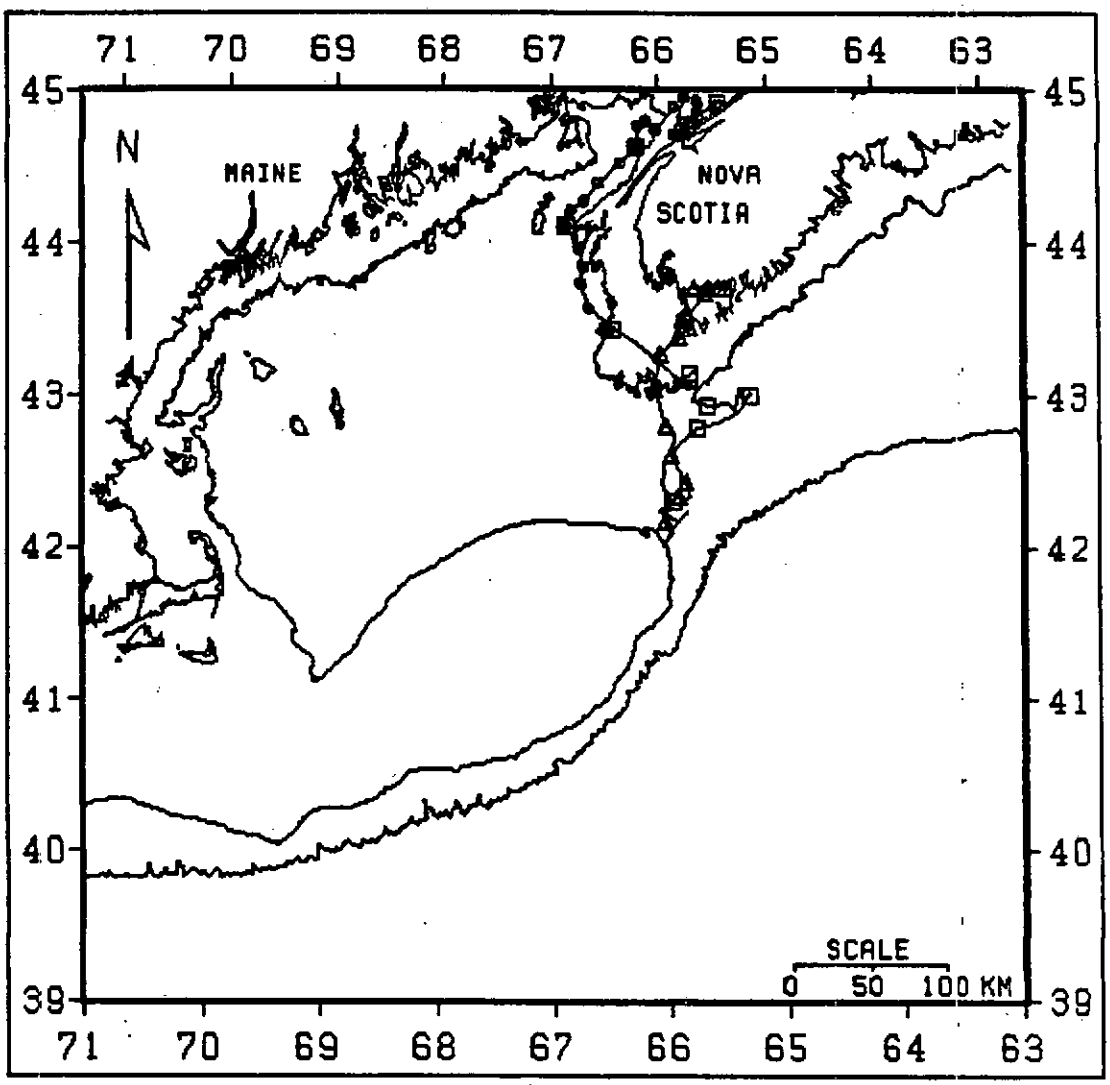

Surface (■) and Subsurface (▲) Center of Mass Trajectories

Spill Site: 42° N, 66° W Spill Start Day: June 1

Figure 7.

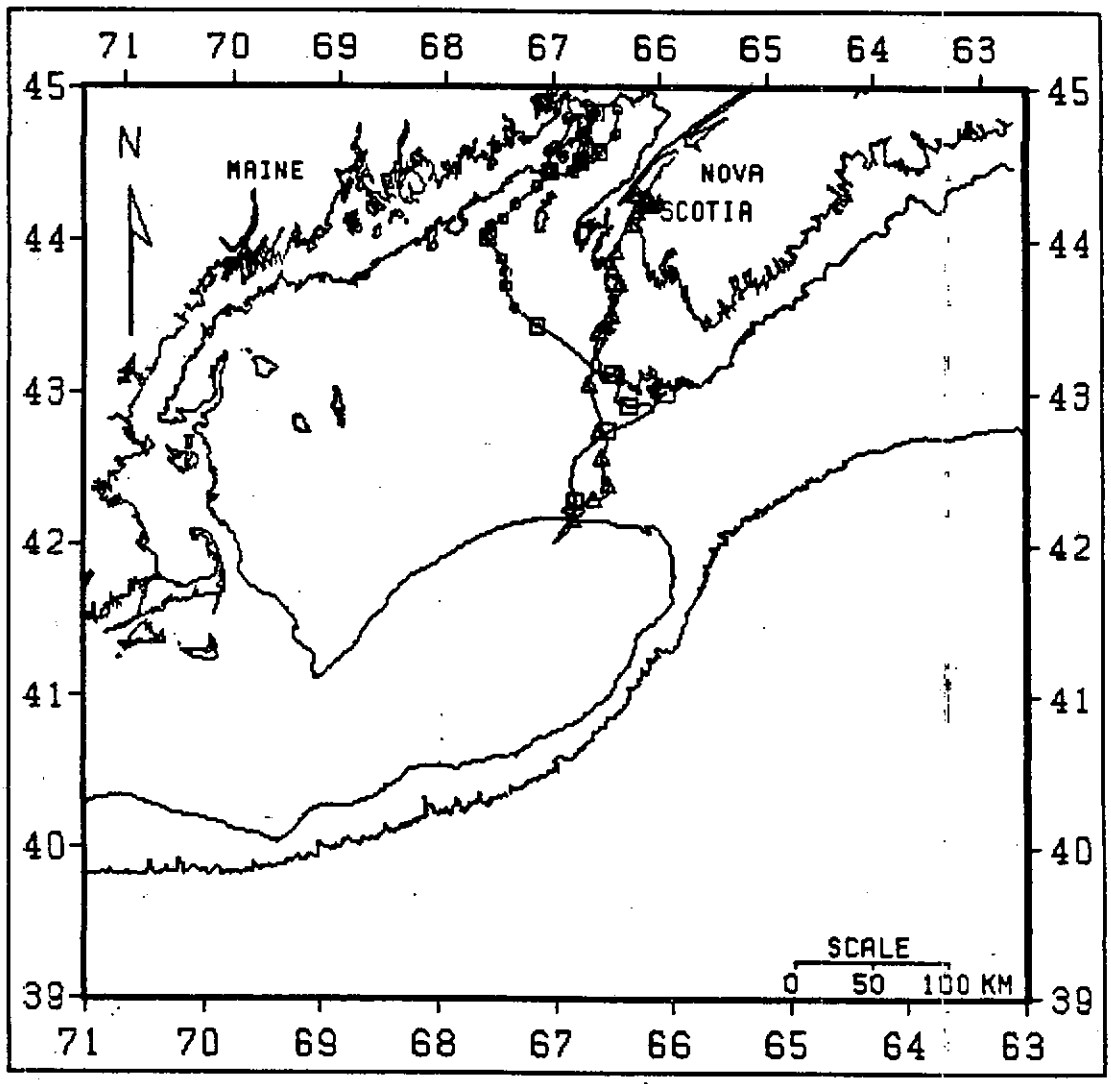

Surface (■) and Subsurface (▲) Center of Mass Trajectories

Spill Site: 42° N, 67° W Spill Start Day: June 1

Figure 8.

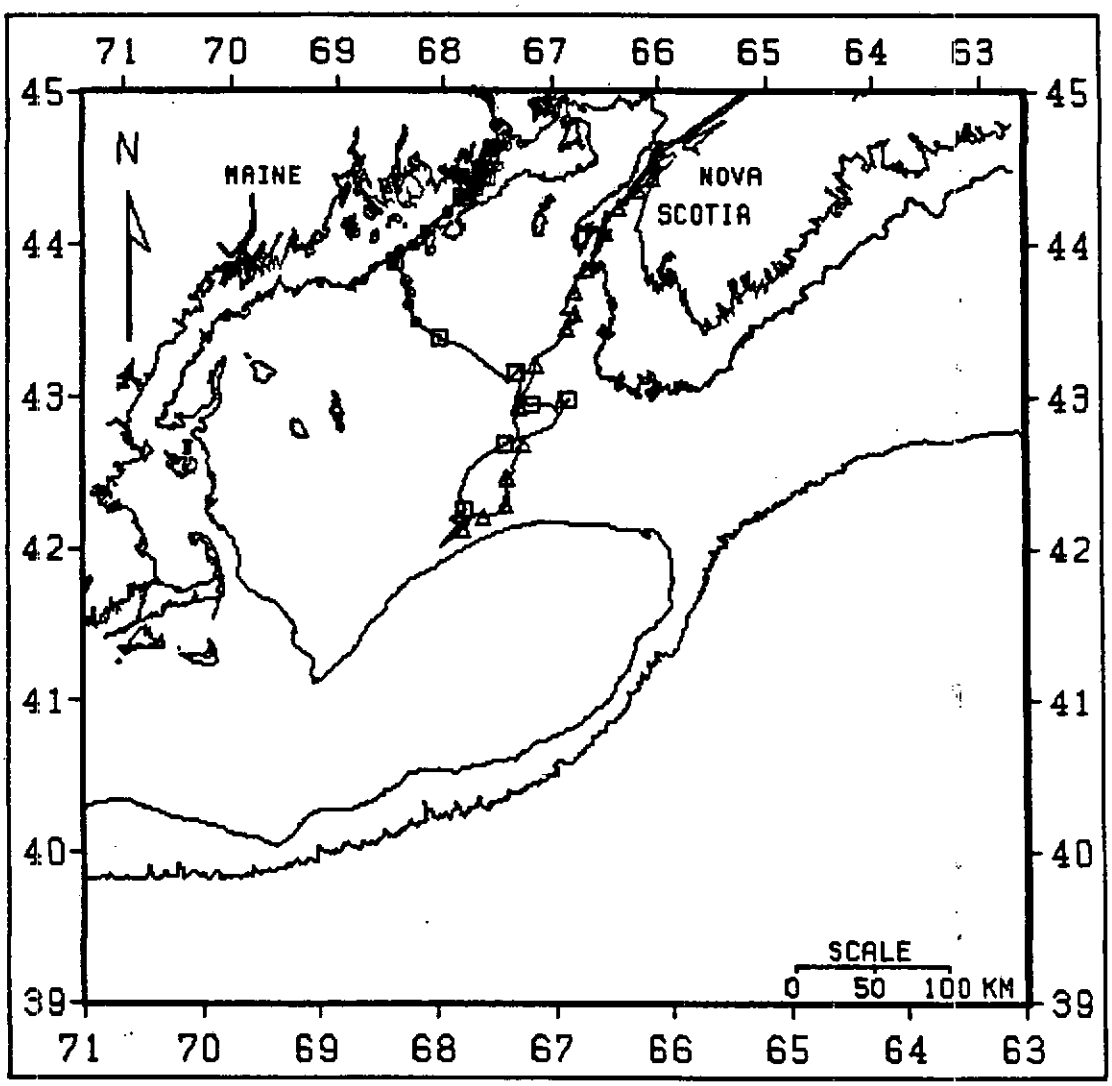

Surface (■) and Subsurface (▲) Center of Mass Trajectories

Spill Site: 42° N, 68° W Spill Start Day: June 1

Figure 9.

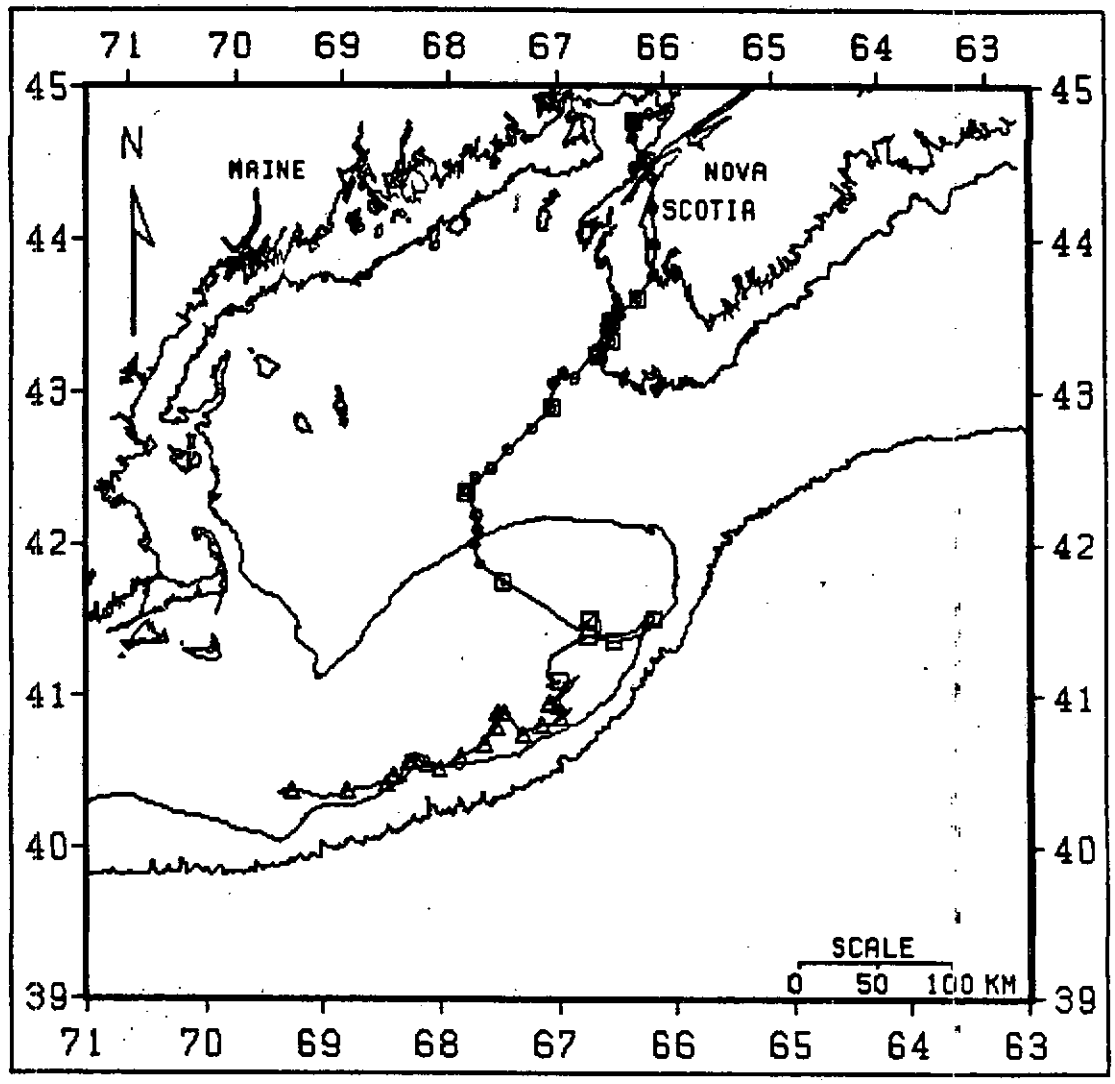

Surface (■) and Subsurface (▲) Center of Mass Trajectories

Spill Site: 41° N, 67° W Spill Start Day: June 1

Figure 10.

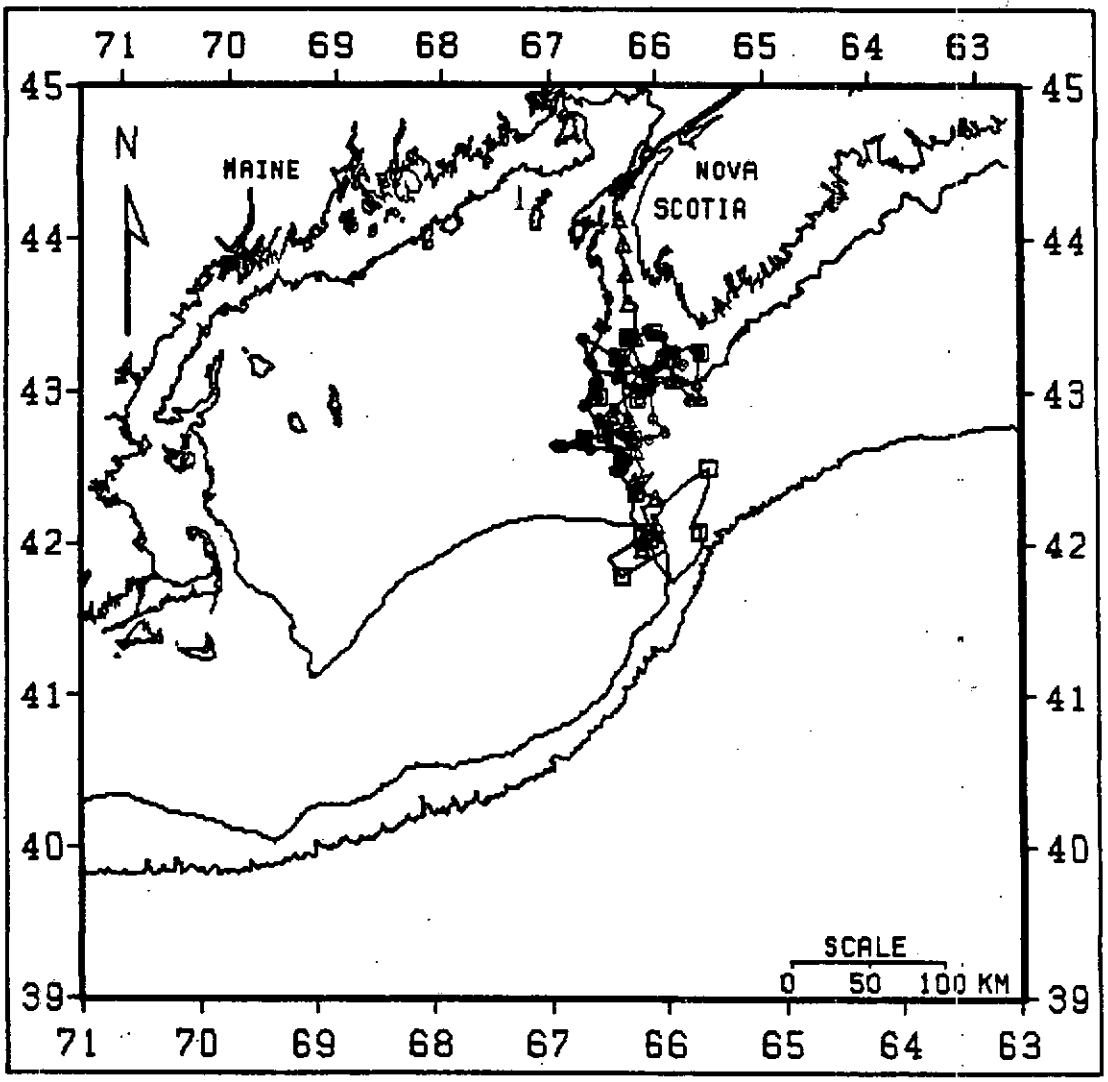

Surface (■) and Subsurface (▲) Center of Mass Trajectories

Spill site: 42° N, 66° W Spill Start Day: September 1

Figure 11.

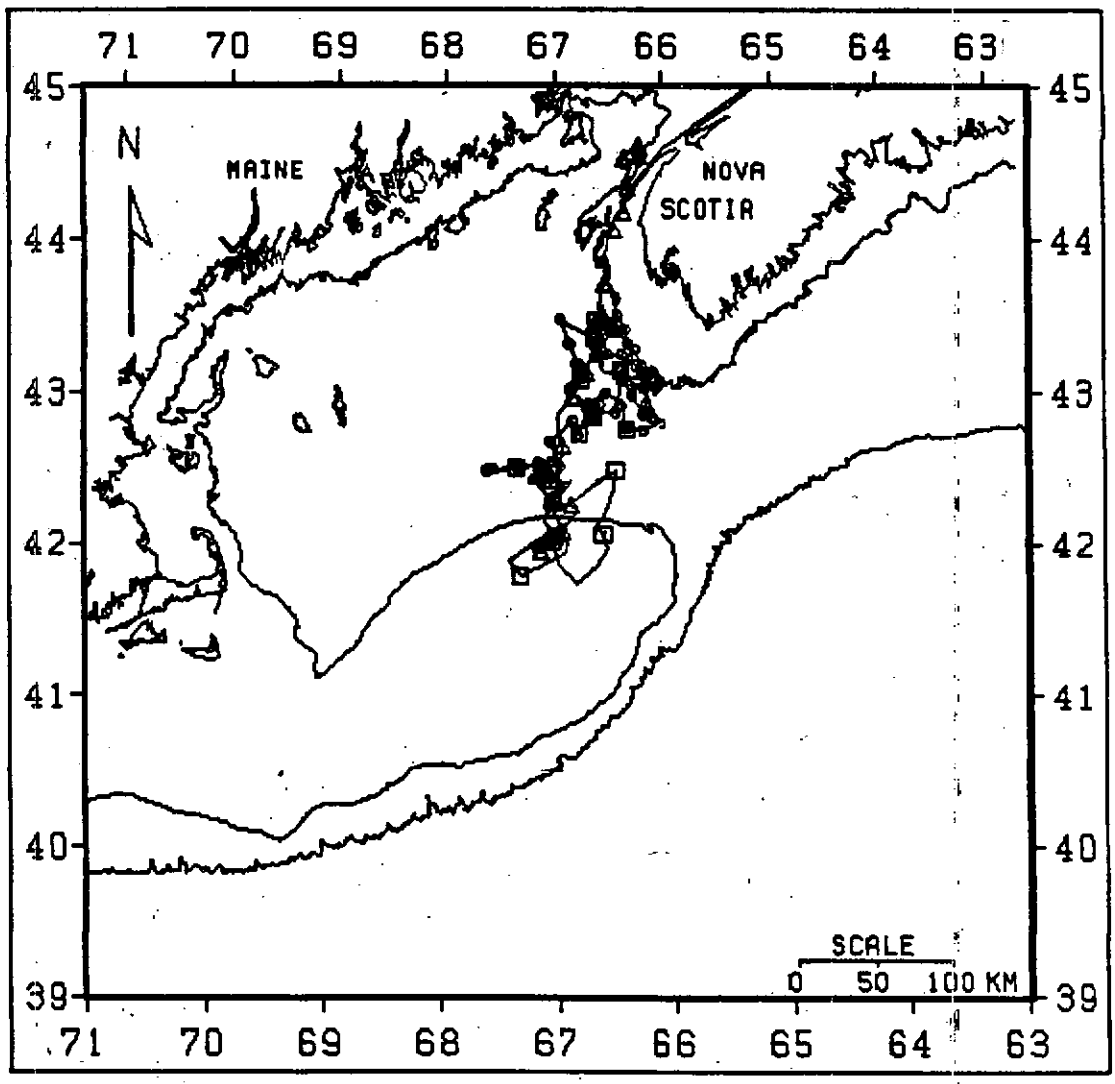

Surface (■) and Subsurface (▲) Center of Mass Trajectories

Spill Site: 42° N, 67° W Spill Start Day: September 1

Figure 12.

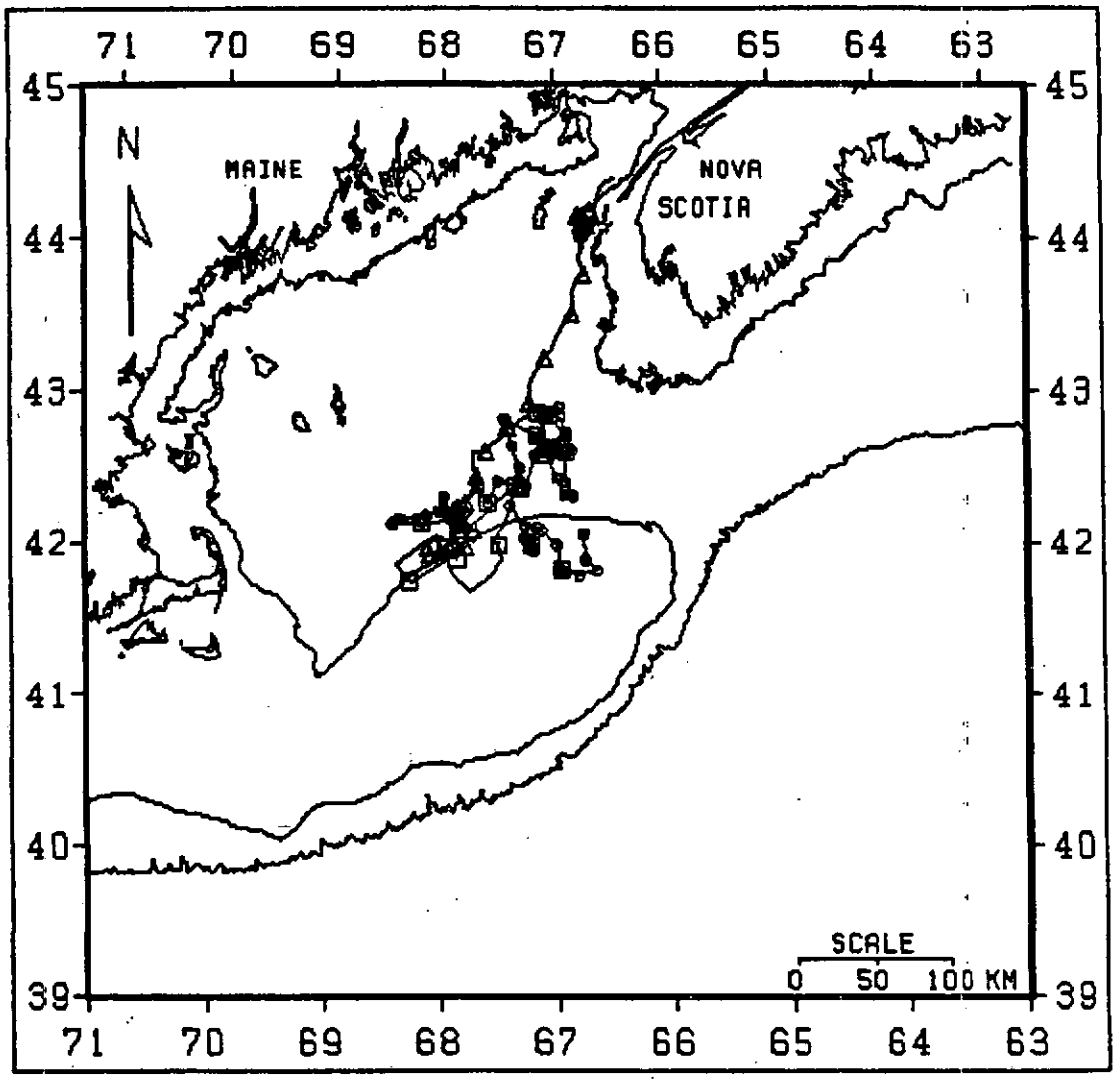

Surface (■) and Subsurface (▲) Center of Mass Trajectories

Spill Site: 42° N, 68° W Spill Start Day: September 1

Figure 13.

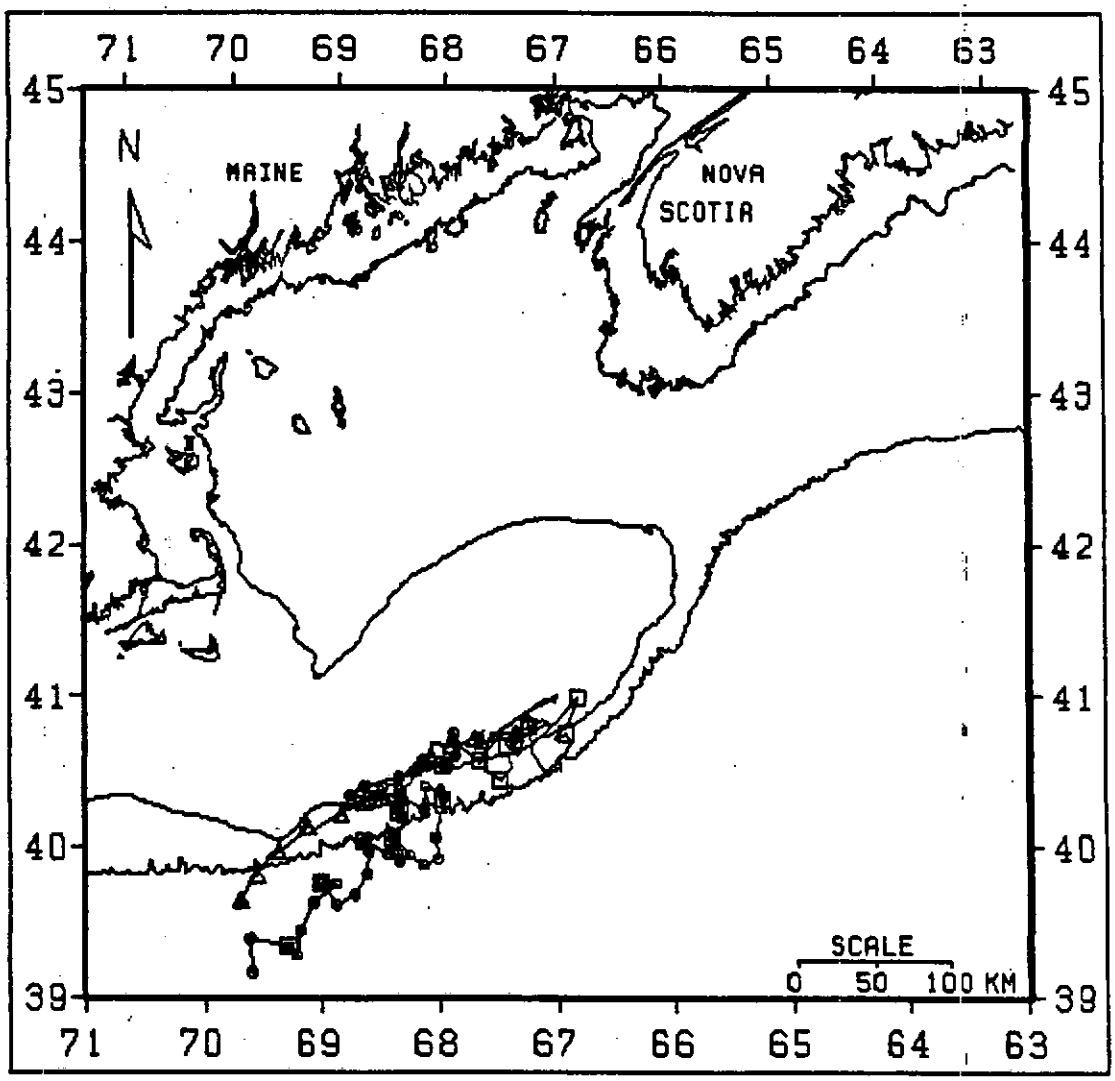

Surface (■) and Subsurface (▲) Center of Mass Trajectories

Spill Site: 41° N, 67° W Spill Start Day: September 1

Figure 14.

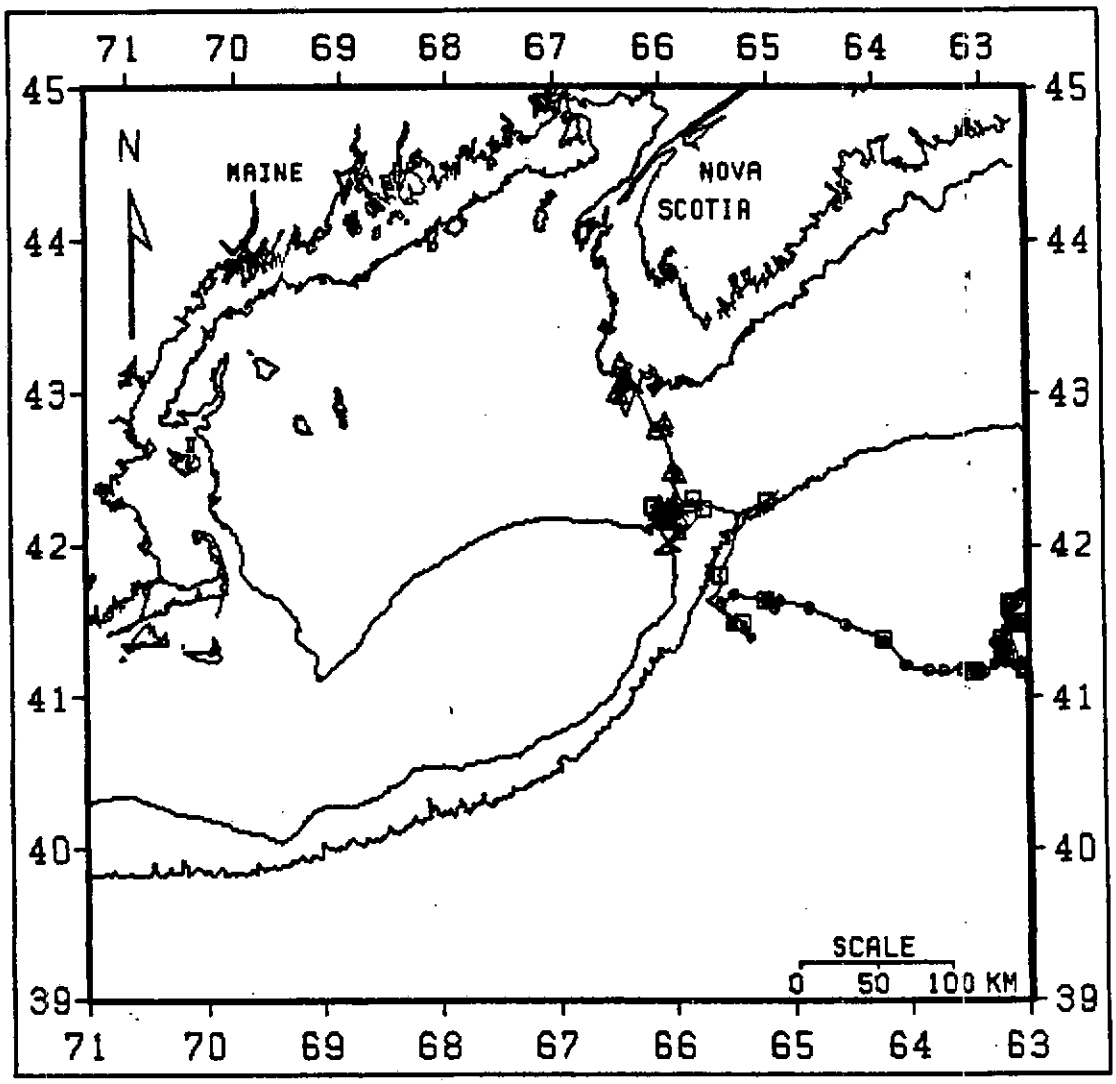

Surface (■) and Subsurface (▲) Center of Mass Trajectories

Spill Site: 42° N, 66° W Spill Start Day: December 1

Figure 15.

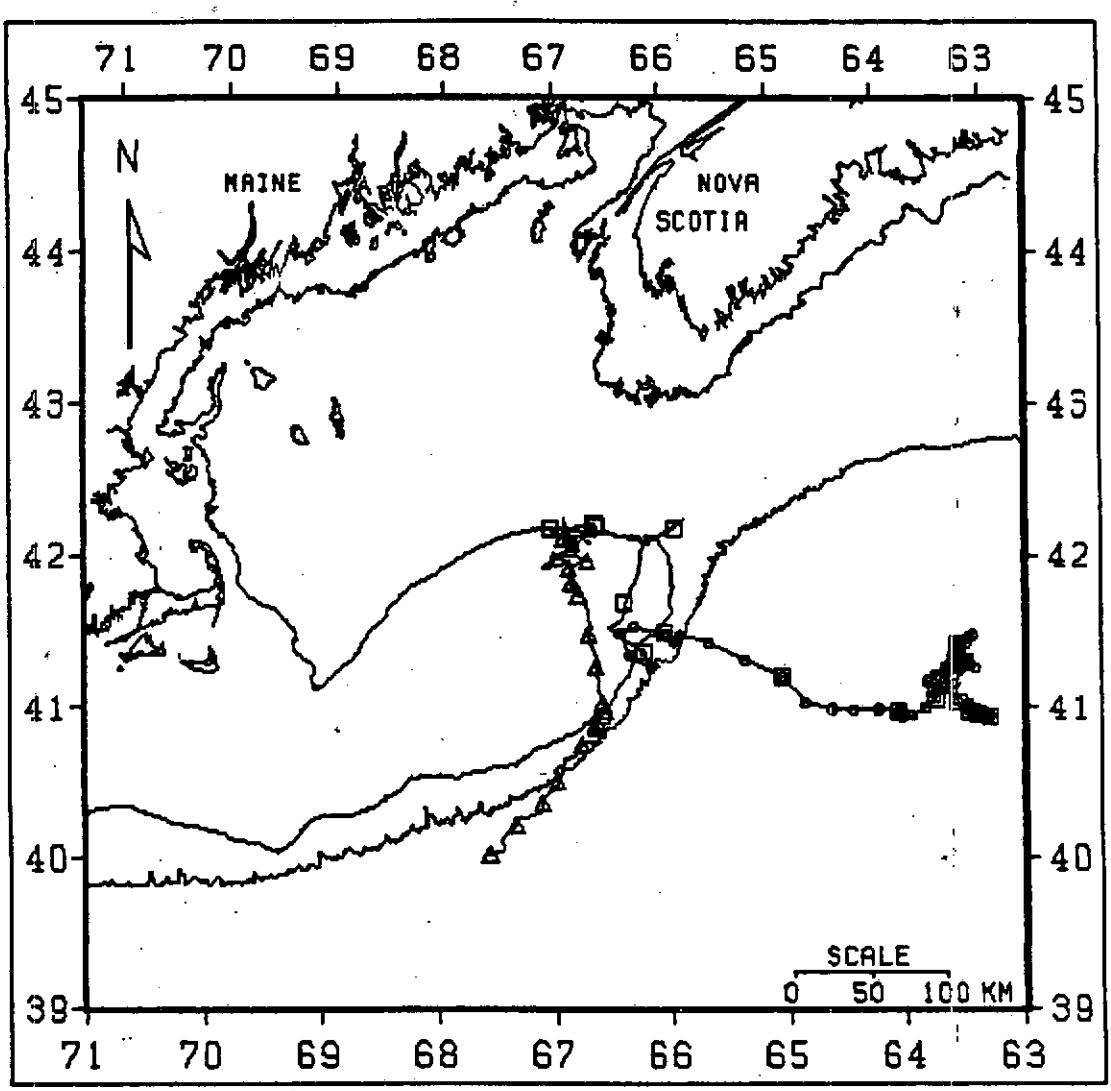

Surface (■) and Subsurface (▲) Center of Mass Trajectories

Spill Site: 42° N, 67° W Spill Start Day: December 1

Figure 16.

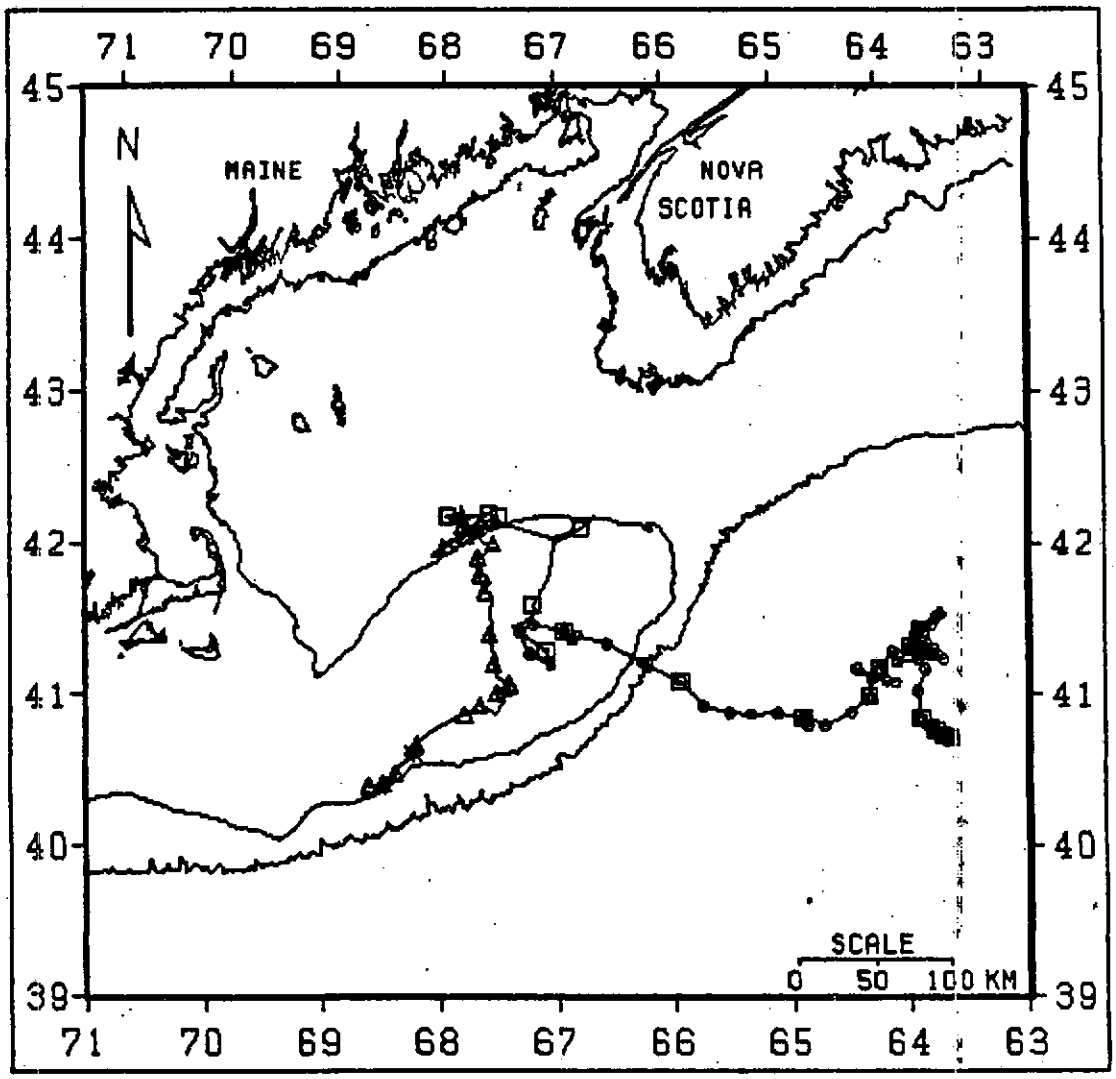

Surface (■) and Subsurface (▲) Center of Mass Trajectories

Spill Site: 42° N, 68° W Spill Start Day: December 1

Figure 17.

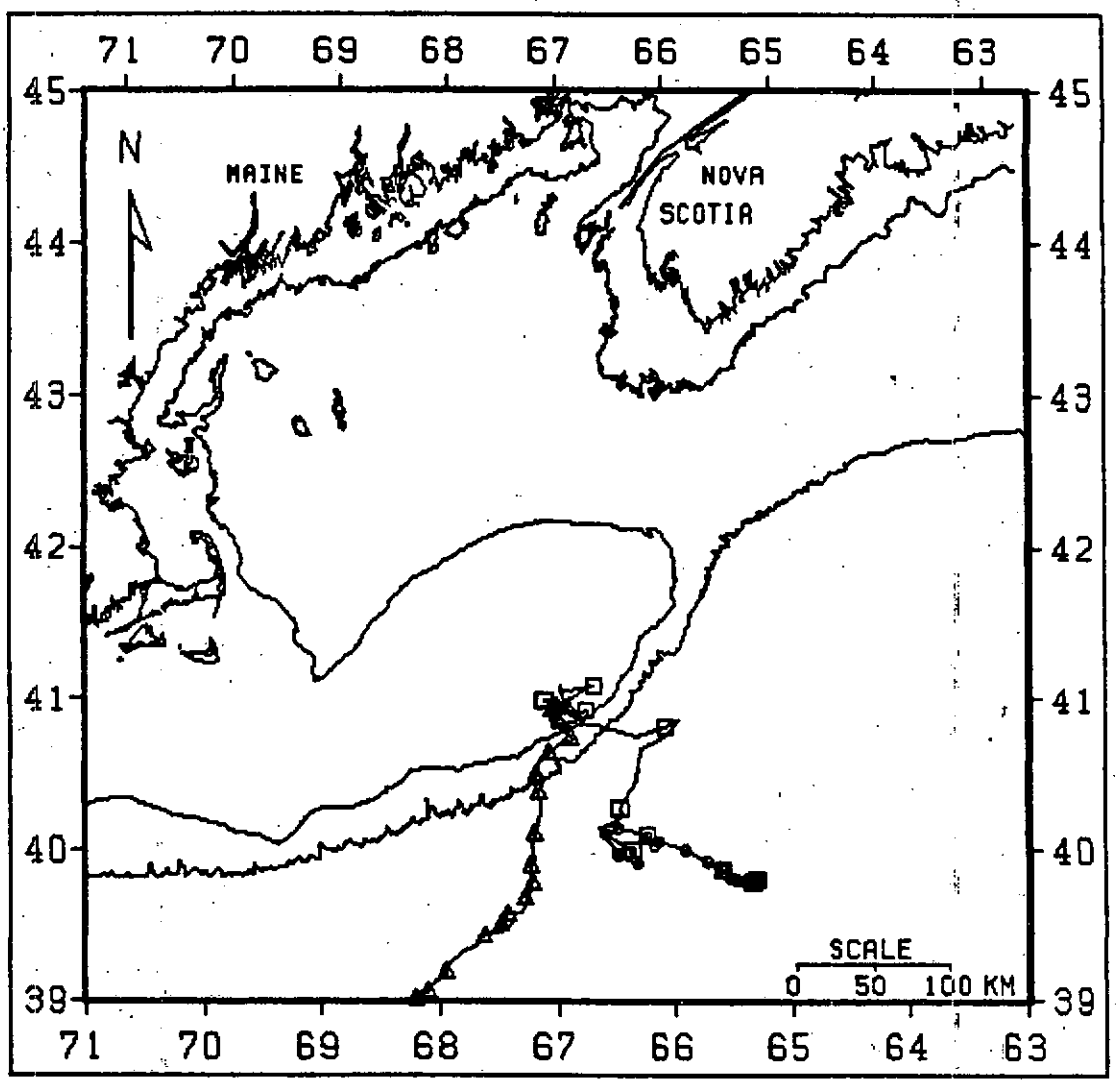

Surface (■) and Subsurface (▲) Center of Mass Trajectories

Spill Site: 41° N, 67° W Spill Start Day: December 1

Figure 18.

To summarize the information in this family of trajectory plots, it is useful to consider them first in seasonal groups:

(1) Four spill sites, spills beginning on March 1 (Julian Day 60)

As is true with all oil spills, details of the surface trajectories are dominated by wind events. This explains the characteristic signature evident in the surface track of Figs. 3, 4, and 5. The same signature exists in Fig. 6 (spill location 41 N, 67 W, Julian Day 060, hereafter 4167.060), but is obscured by the dense overlays of surface and subsurface tracks during the first 30 days of the spill. The difference in flow patterns north and south of Georges Bank during the spring is also evident from 4167.060, as compared to the other three sites on this day (4266.060, 4267.060, 4268.060). These patterns concur with those reported by EG&G (1978b) for moored current measurements.

(2) Spills beginning on June 1 (Julian Day 152)

Case 4167.152 (Fig. 10) reflects the southwesterly currents on the south side of Georges Bank, which oppose the typically southwesterly summer winds in the study area, explaining the striking divergence between the surface and subsurface hydrocarbon trajectories. Of particular interest is the prediction that summer pollutant releases between 66 W and 68 W on the northern edge of the bank will be transported north. Inspection of the governing net current fields (Figs. 20 and 21) clearly shows a transport divergence along parallel 42. This divergence is probably a reality (Bigelow, 1927; Godshall et al.

1980; Bumpus and Day, 1965; Spaulding et al. 1982c), but because it is probably induced by westerly flows entering the Gulf of Maine through the Northeast Channel, a flow to the north around the tip of Nova Scotia, and a counter clockwise circulation in the Gulf of Maine, one might expect the surface layer divergence to be more closely related to the steep bathymetric slope on the north flank of the bank, and therefore appear farther north (e.g. at 42.5 N). If this transport divergence occurs 50 km farther north, the trajectories from sites along parallel 42 will be south or east rather than north. This question can be adequately addressed only with a proper integration of the three dimensional numerical hydrodynamic model, as discussed earlier, and recently collected in situ current data (EG&G, 1981).

(3) Spills beginning September 1 (Julian Day 244)

Again, 4167.244 underscores the difference in transport patterns north and south of Georges Bank. Because autumn and winter winds come typically from the northwest, both surface and subsurface components of 4167.244 (Fig. 14) are approximately down wind and down current. In Figs. 11, 12, and 13, the wind and currents north of the bank oppose each other to some extent, producing highly convoluted surface trajectories.

(4) Spills beginning December 1 (Julian Day 335)

Here 4266.335 is the exception, although all four surface trajectories are similar due to the strength and coherence of the winter wind and net current field (Fig. 22).

If the 16 trajectory plots of Figs. 3-18 are arranged by site, other generalizations can be made:

(1) 42 N, 66 W

This is the site least likely to impact Georges Bank fisheries. Smallest cod fishery impacts are associated with this site for all seasons.

(2) 42 N, 67 W

At this site, the summer and fall seasons show surface and subsurface transports toward the north. Winter brings hydrocarbons south across the bank. (Because of the high sea state typically associated with this area during the winter, well blowouts and tanker accidents are most probable at this time of year (Devanney et al. 1974). Thus winter trajectories are perhaps more important to consider than summer trajectories). The spring case (Fig. 7) begins towards the south, with the surface track eventually veering north with the wind shift from the winter to the summer regime.

(3) 42 N, 68 W

Seasonal transport at this site is similar to that at 4267, although impacts on the cod fishery are slightly higher due to the location of the cod spawning area relative to the spill site.

(4) 41 N, 67 W

The impact associated with a March 1 spill at this site is

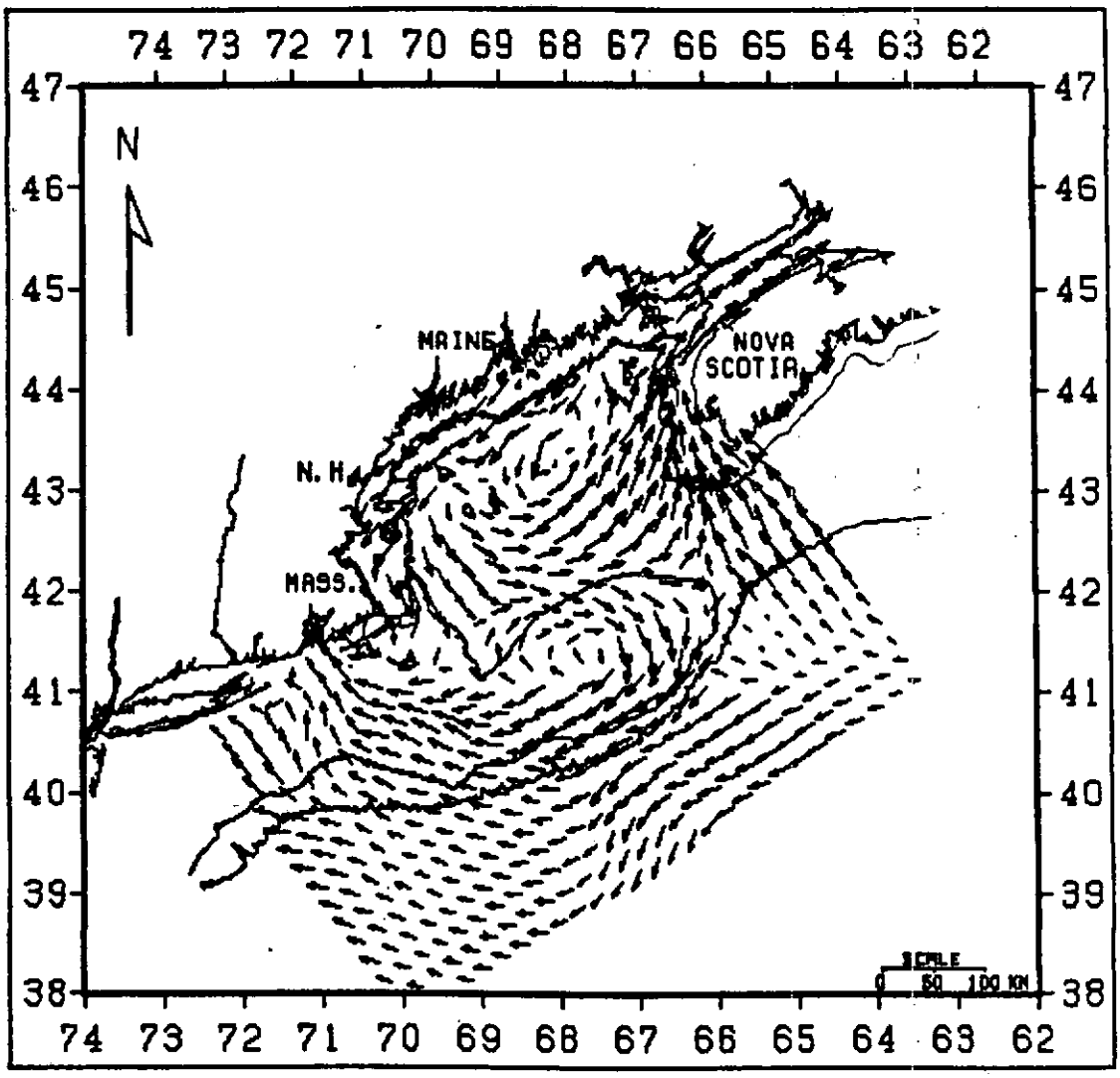

VMAX = 5.45 CM/SEC.

Figure 19. Julian day 60 drifter inferred advective surface currents.

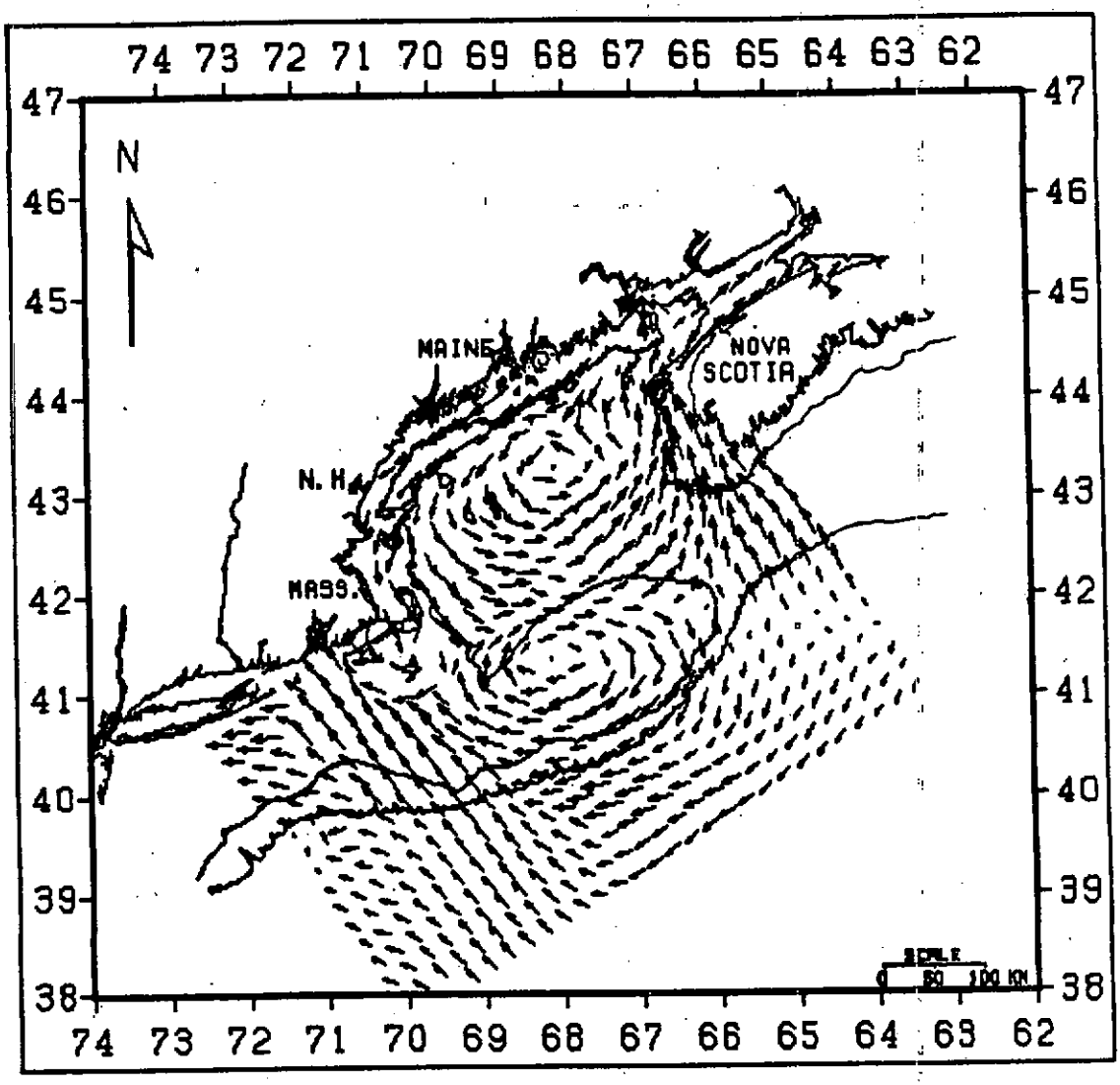

VMAX = 7.91 CM/SEC.

Figure 20. Julian day 152 drifter inferred advective surface currents.

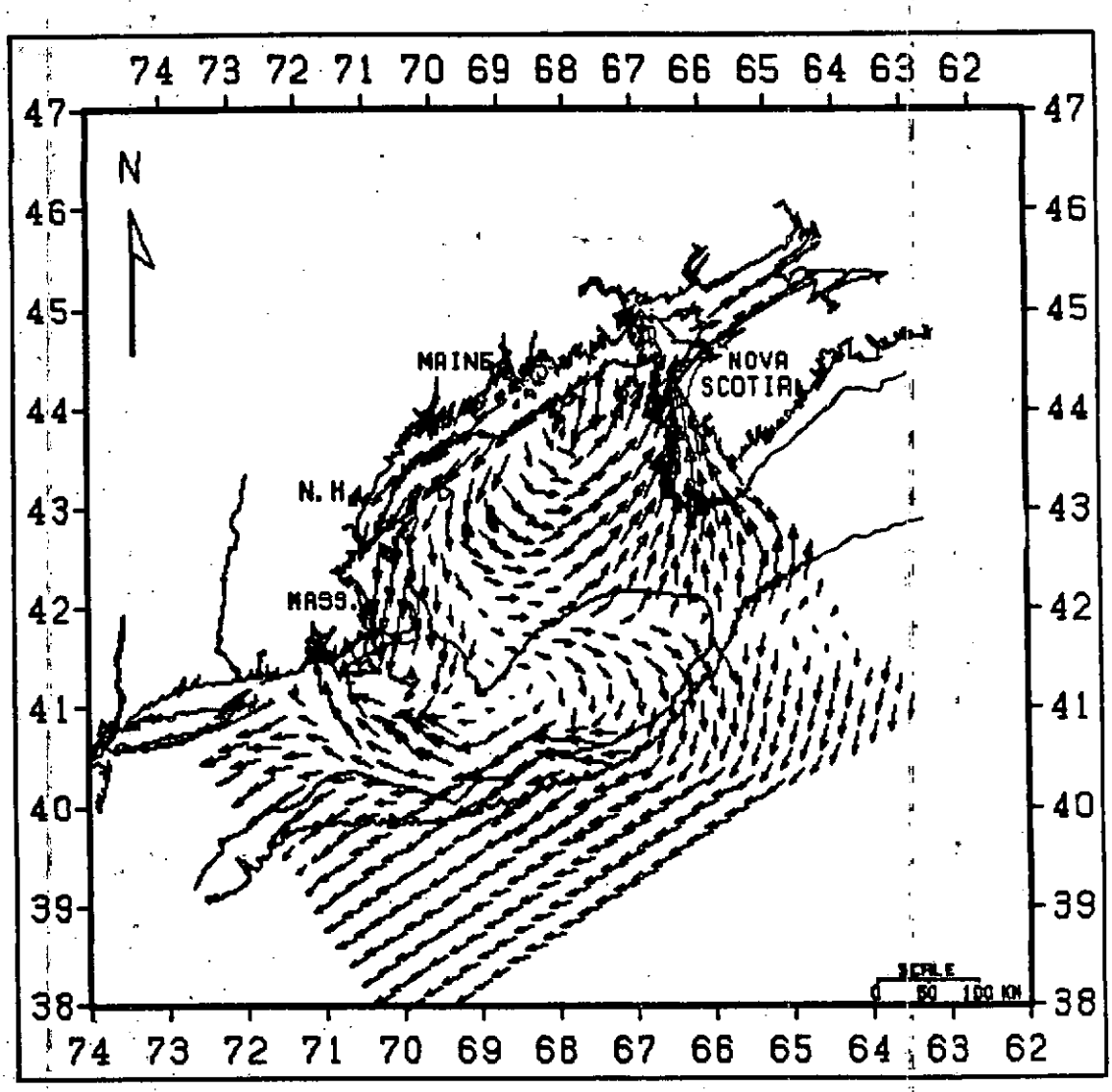

VMAX = 6.49 CM/SEC.

Figure 21. Julian day 244 drifter inferred advective surface currents.

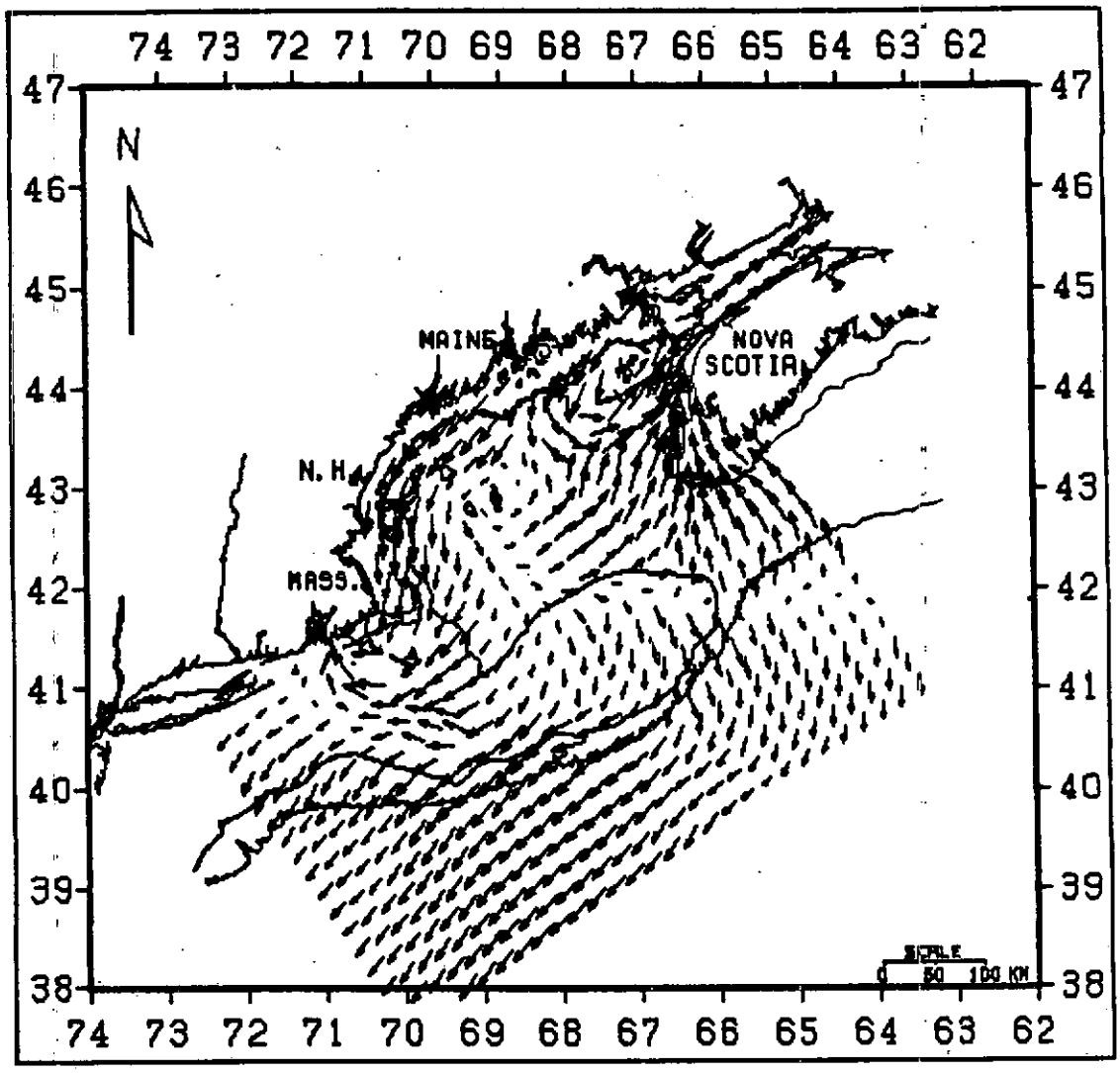

VMAX = 5.82 CM/SEC.

Figure 22. Julian day 335 drifter inferred advective surface currents.

nearly as high as that of 4268.060, even though the sites are on opposite sides of the Bank. At 4167, spring, autumn and winter spill events are governed by southerly transport. Only a summer event may be associated with a northward surface trajectory, subject to typically northeasterly summer winds. The seasonality of winds in this region is consistently reflected in the 11 year (1966-1976) wind record (Appendix A).

6. COD ICHTHYOPLANKTON TRANSPORT AND FATES ANALYSIS

Using as input the surface and subsurface hydrocarbon distributions estimated by the oil spill behavior and fates model, the ichthyoplankton transport and fates model was run for each case inside the time range of the cod impact window. Because cod spawning begins on Julian day 335 in the model, ends on day 120, and planktonic time is taken as 120 days, oil spills of 30 days' duration beginning on Julian day 244 (September 1) are outside the cod impact window. It is noteworthy that the impact windows for certain other species (e.g. herring) are open to pollutant impacts at this time of year.

The estimated losses of cod ichthyoplankton resulting from the spills simulated here are summarized in Table 2 and Fig. 23. The table clearly shows that the spring months carry the highest impact potentials for this species. This is a direct result of the intense cod spawning that typically occurs on Georges Bank in March and April, combined with the northward movement of the polar front and the associated wind shift towards the northeast, and the more gyre-like form of the transport fields during the spring and summer months (Figs. 20 and 21, as compared to

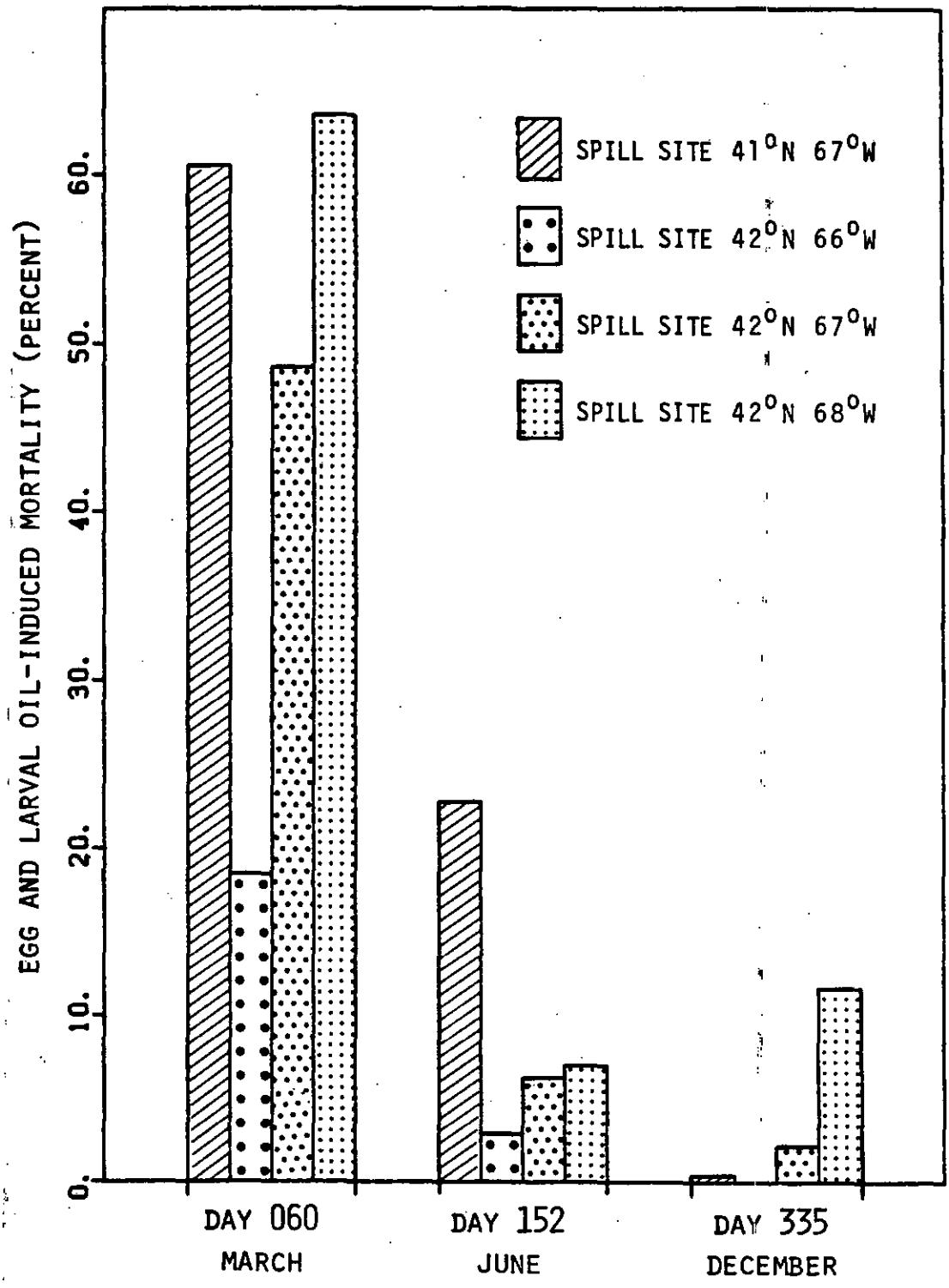

Figure 23. Ichthyoplankton losses associated with each of the 12 cases inside the time range of the Georges Bank cod impact window.

Table 2. Percent Losses of One Year's Spawning Products for Georges Bank - Nantucket Shoals Cod Stock

Spill Date	Spill Site			
	42 N, 66 W	42 N, 67 W	42 N, 68 W	41 N, 67 W
March 1 (Day 60)	18.6	48.7	63.6	60.6
June 1 (Day 152)	*	6.3	7.0	22.9
September 1 (Day 244)	*	*	*	*
December 1 (Day 335)	*	*	11.7	*

*Impacts below 5% are near the error margin of the methodology, and are therefore neglected.

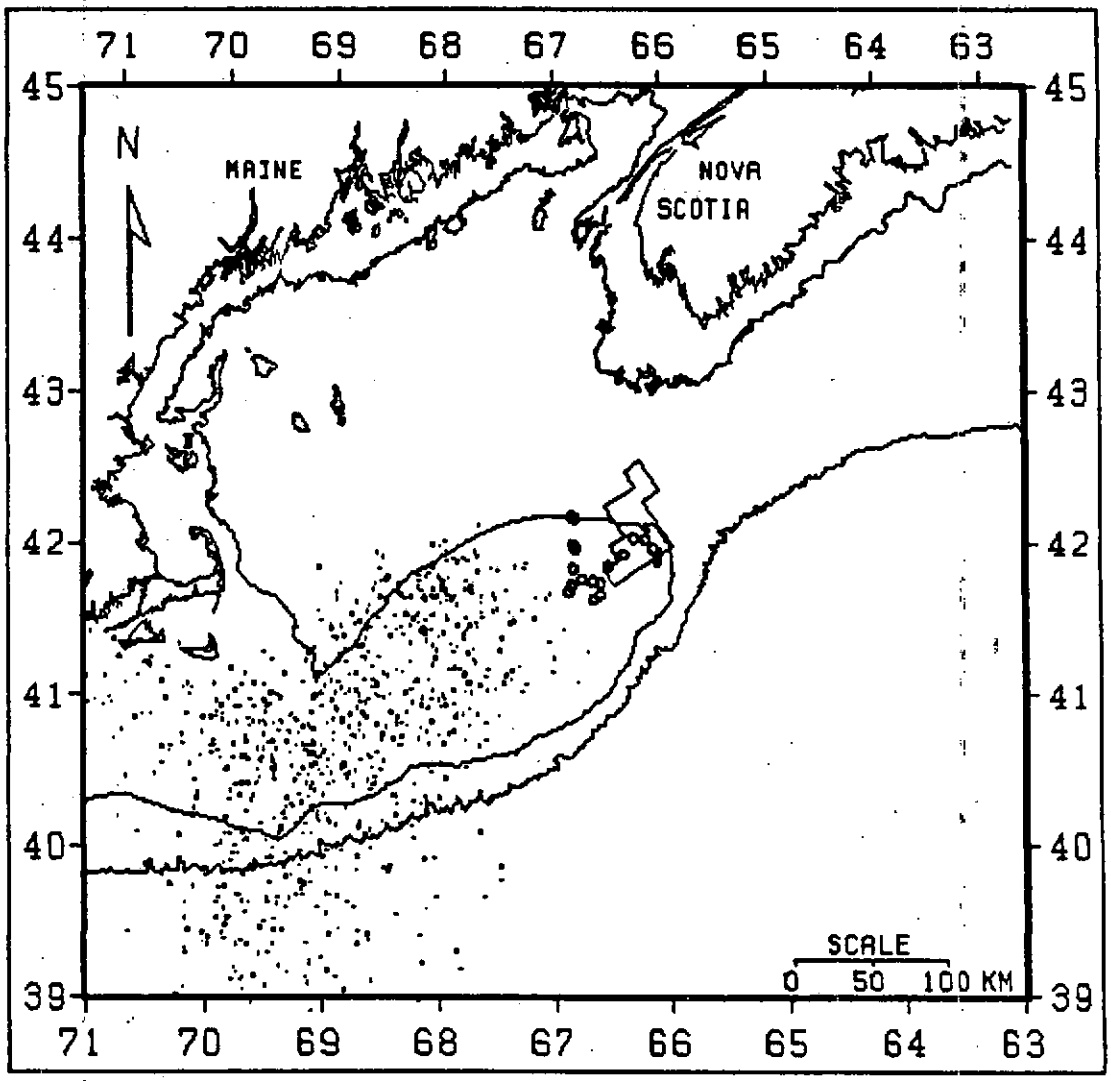

Surface Spillets (circles) and Subsurface 50 ppb Contour (rectangular region)

Spill Site: 42° N, 66° W Spill Start Day: March 1 (10 days after spill start)

Figure 24a.

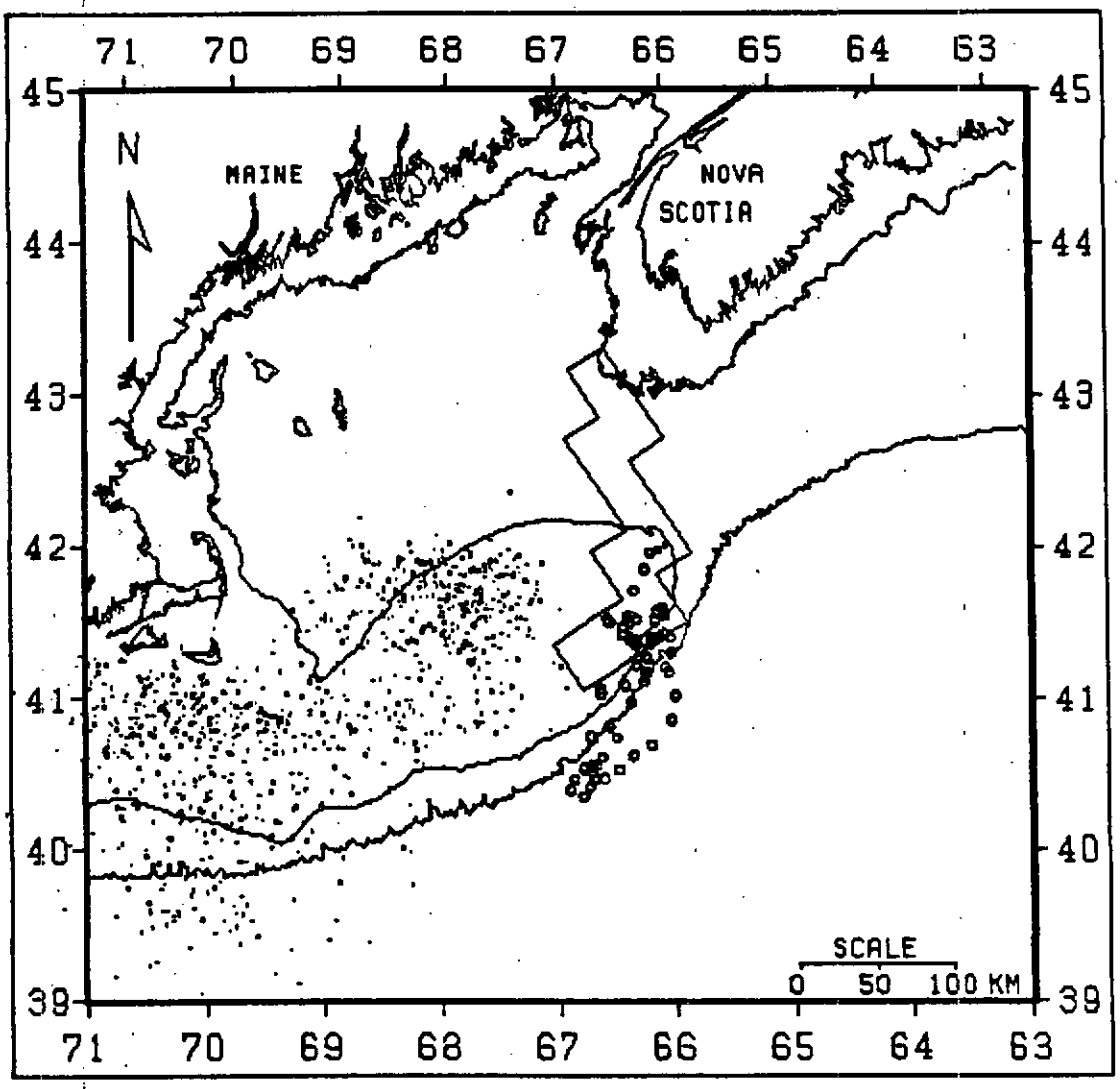

Surface Spillets (circles) and Subsurface 50 ppb
Contour (rectangular region)

Spill Site: 42° N, 66° W Spill Start Day: March 1
(30 days after spill start)

Figure 24b.

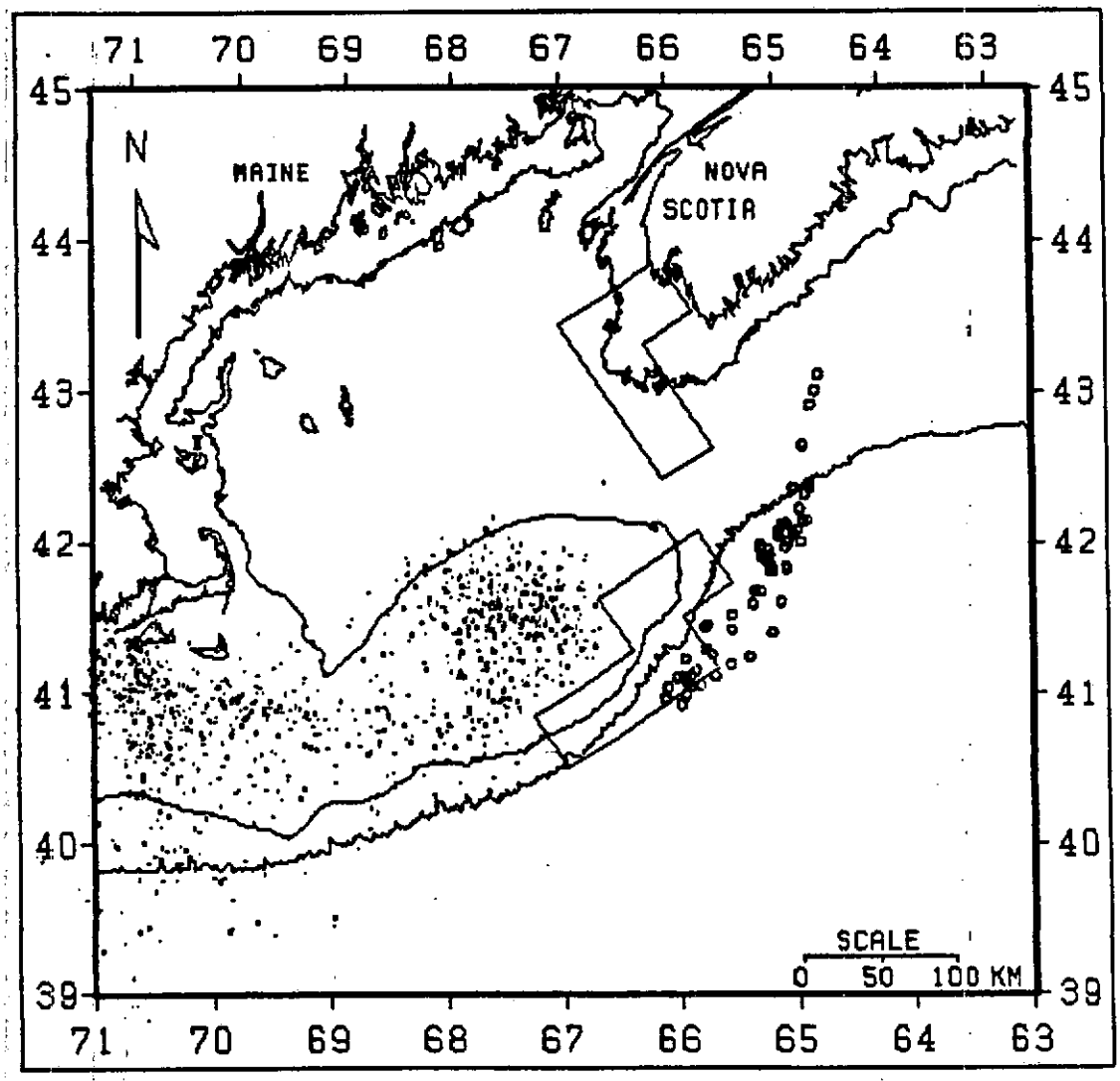

Surface Spillets (circles) and Subsurface 50 ppb
Contour (rectangular region)

Spill Site: 42° N, 66° W Spill Start Day: March 1
(50 days after spill start)

Figure 24c.

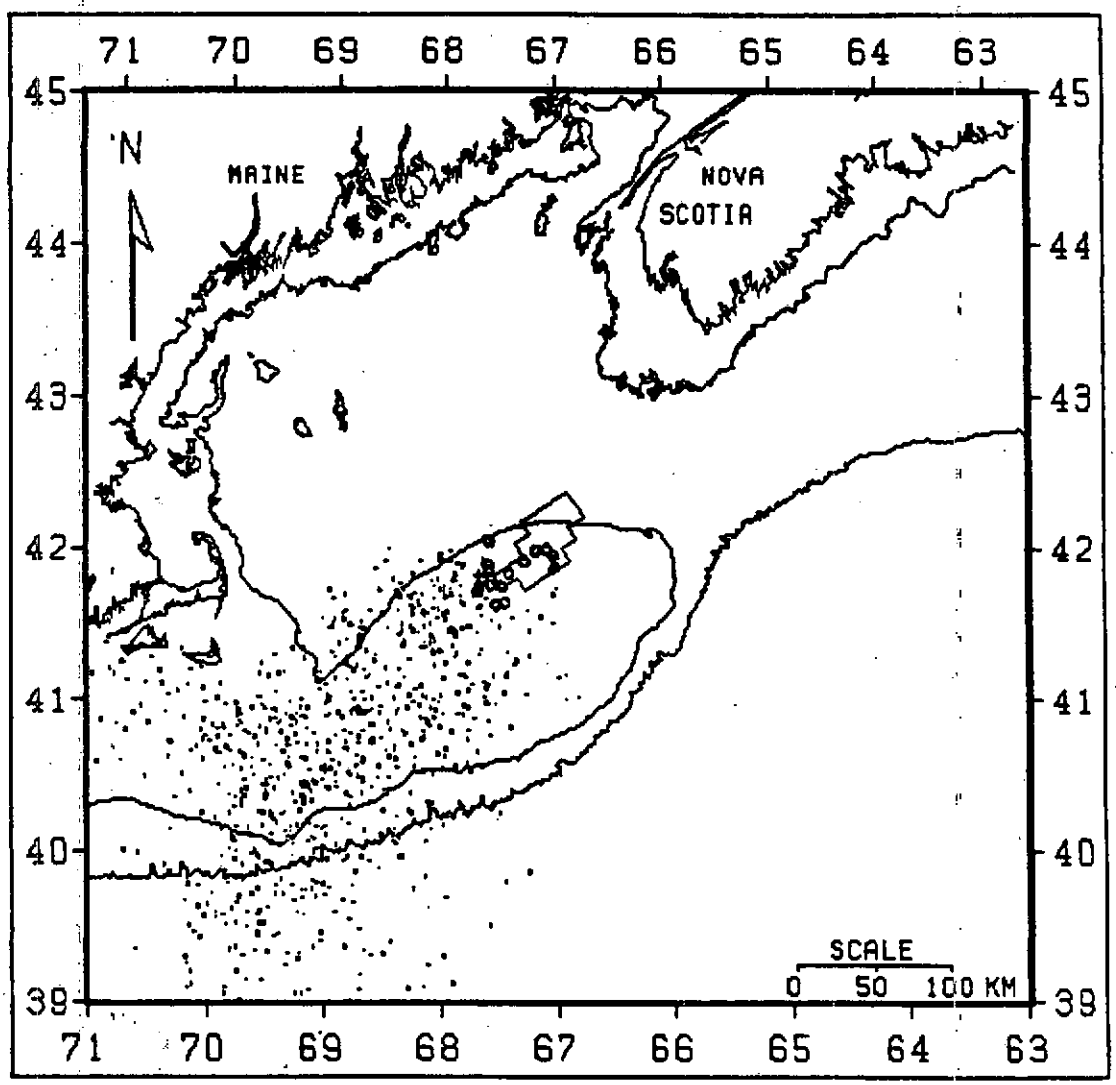

Surface Spillets (circles) and Subsurface 50 ppb
Contour (rectangular region)

Spill Site: 42° N, 67° W Spill Start Day: March 1
(10 days after spill start)

Figure 25a.

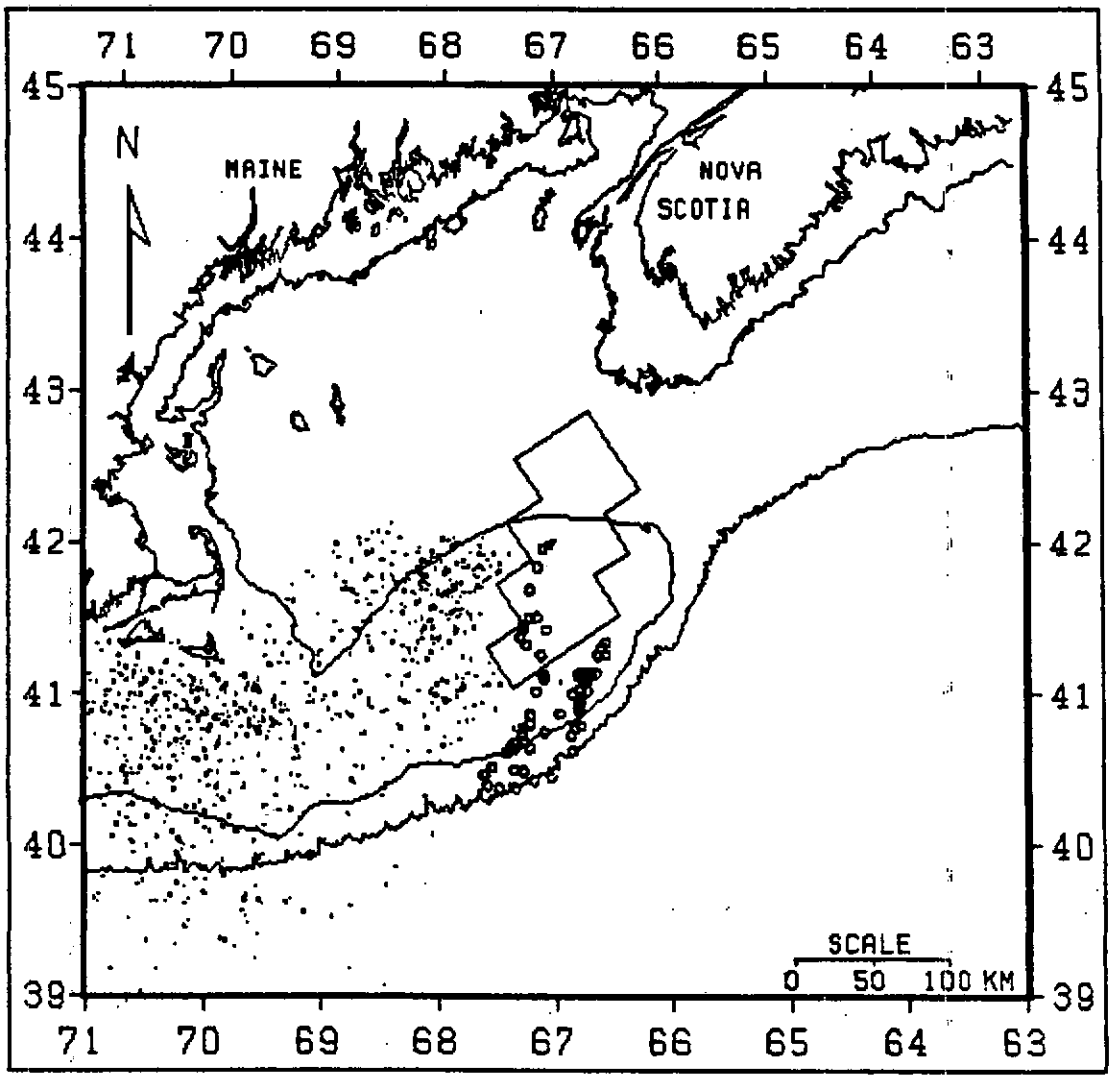

Surface Spillets (circles) and Subsurface 50 ppb
Contour (rectangular region)

Spill Site: 42° N, 67° W Spill Start Day: March 1
(30 days after spill start)

Figure 25b.

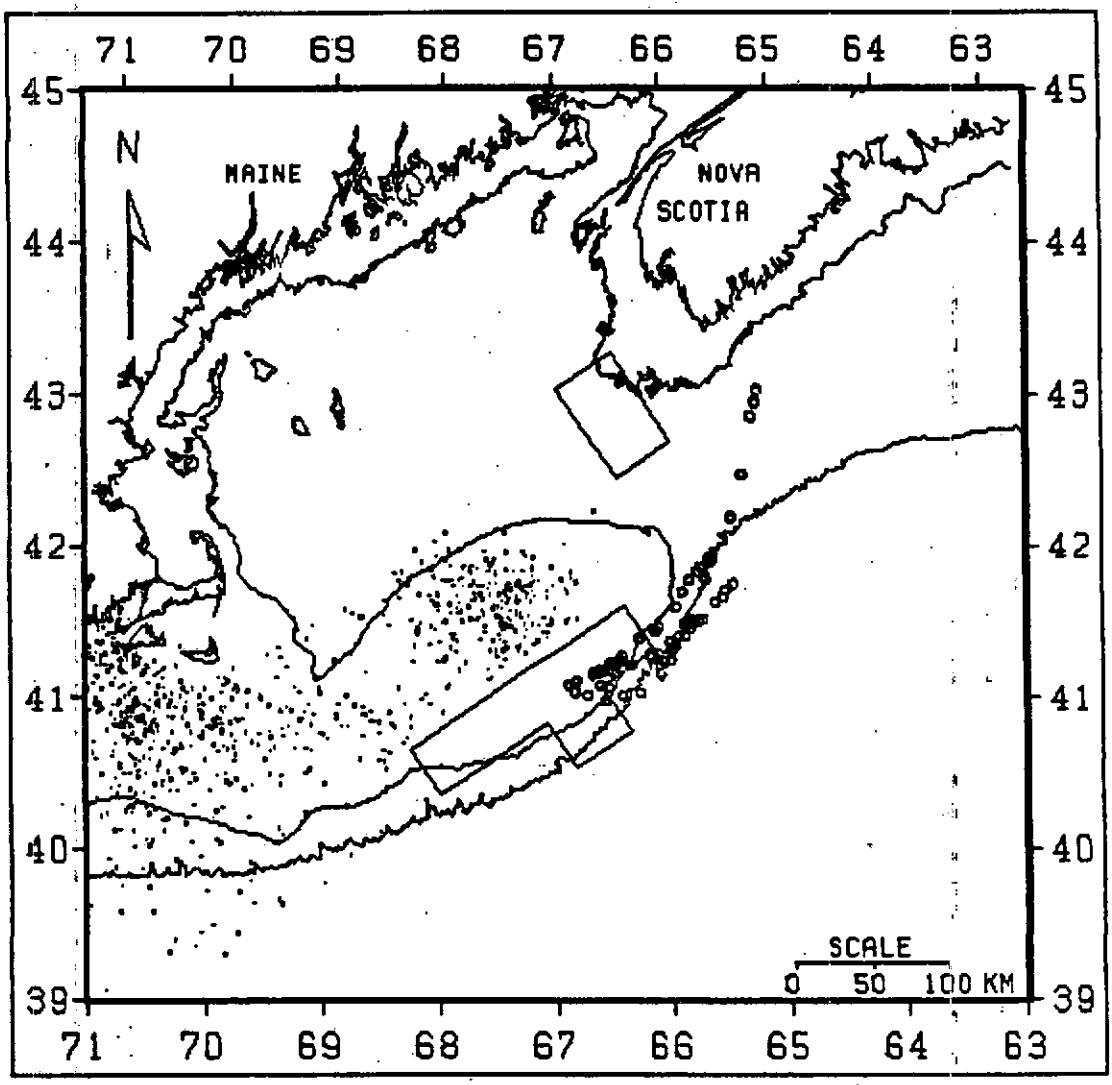

Surface Spillets (circles) and Subsurface 50 ppb Contour (rectangular region)

Spill Site: 42° N, 67° W Spill Start Day: March 1

(50 days after spill start)

Figure 25c.

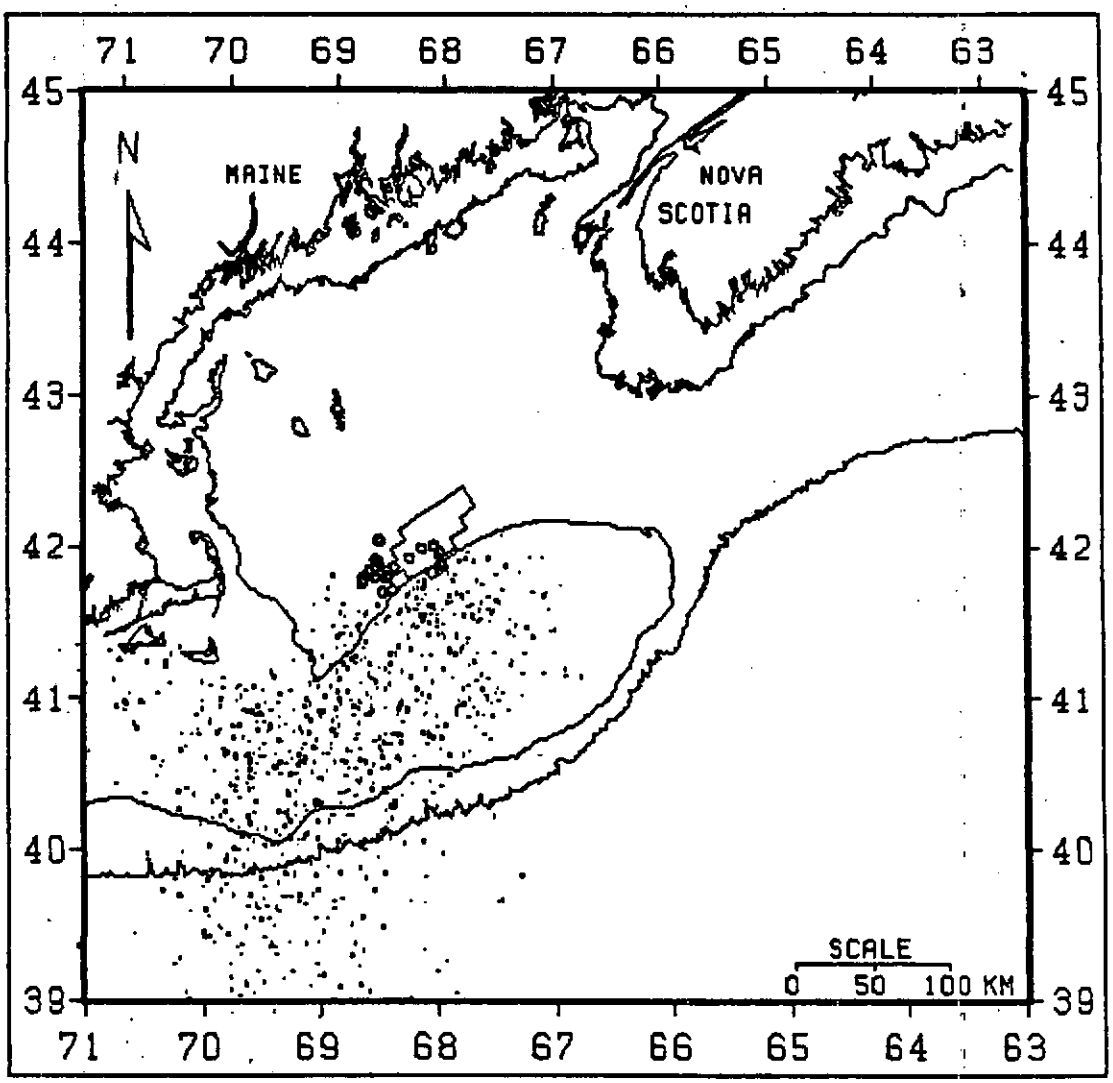

Surface Spillets (circles) and Subsurface 50 ppb
Contour (rectangular region)

Spill Site: 42° N, 68° W Spill Start Day: March 1
(10 days after spill start)

Figure 26a.

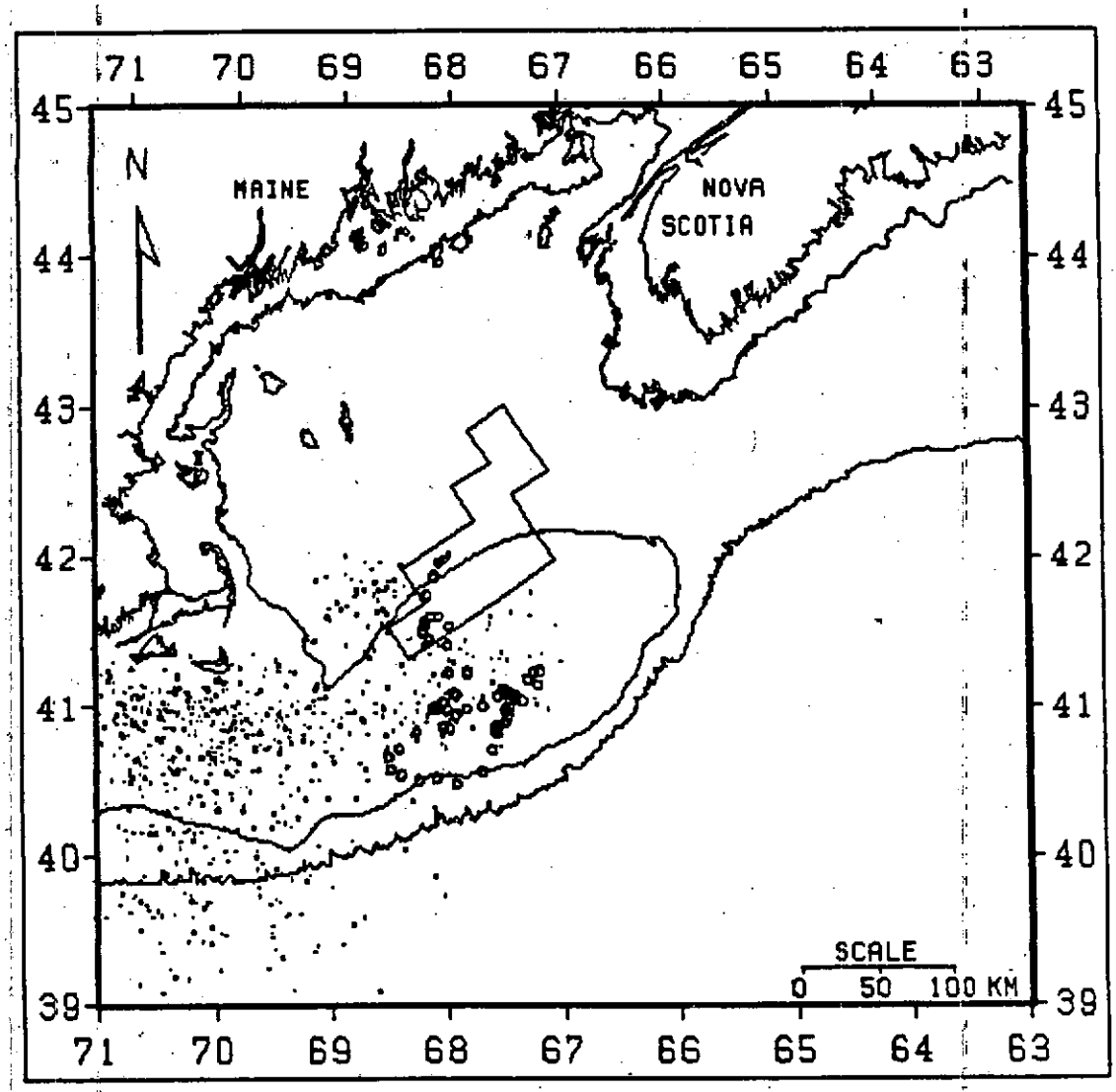

Surface Spillets (circles) and Subsurface 50 ppb
Contour (rectangular region)

Spill Site: 42° N, 68° W Spill Start Day: March 1
(30 days after spill start)

Figure 26b.

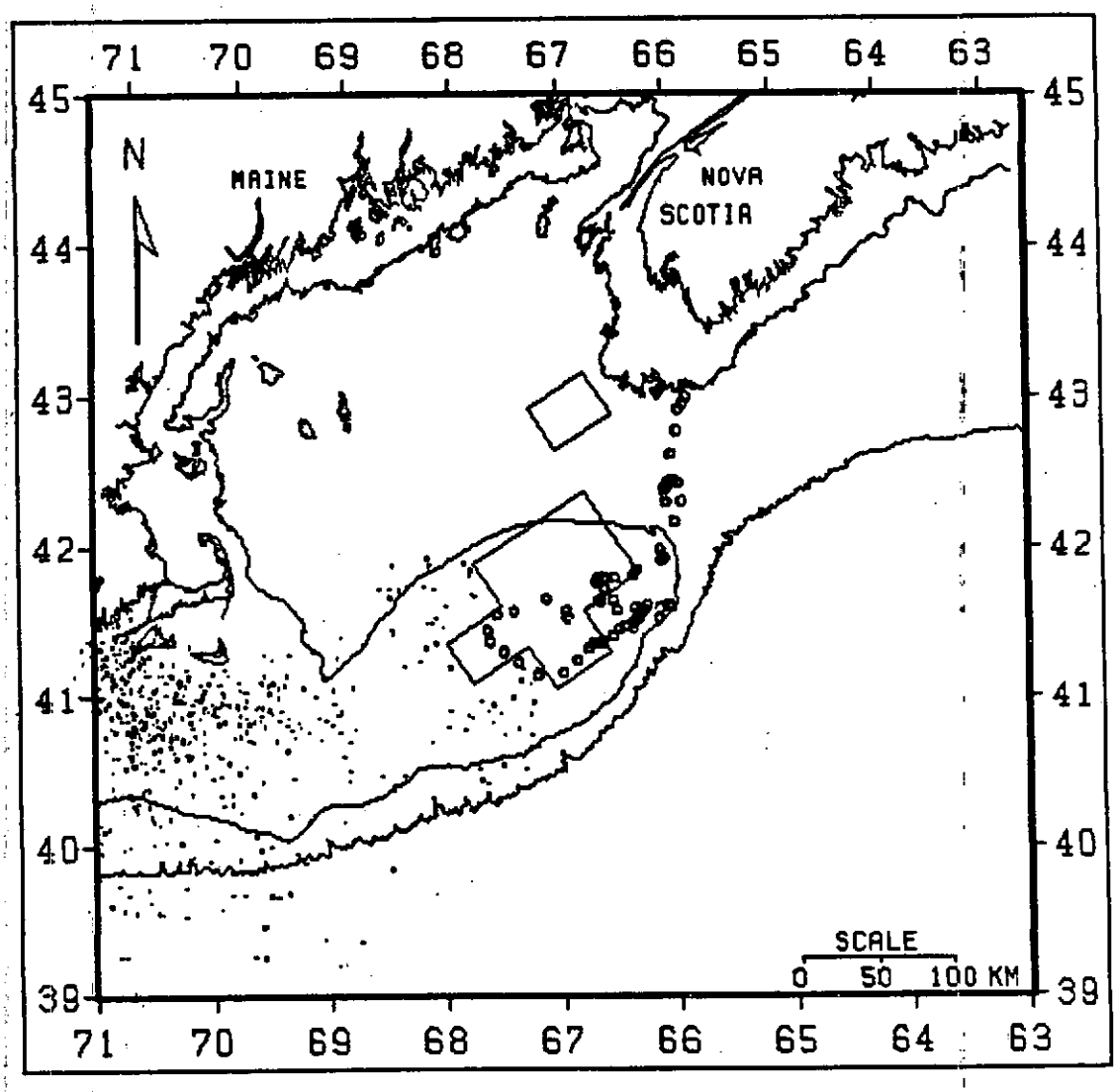

Surface Spillets (circles) and Subsurface 50 ppb
Contour (rectangular region)

Spill Site: 42° N, 68° W Spill Start Day: March 1
(50 days after spill start)

Figure 26c.

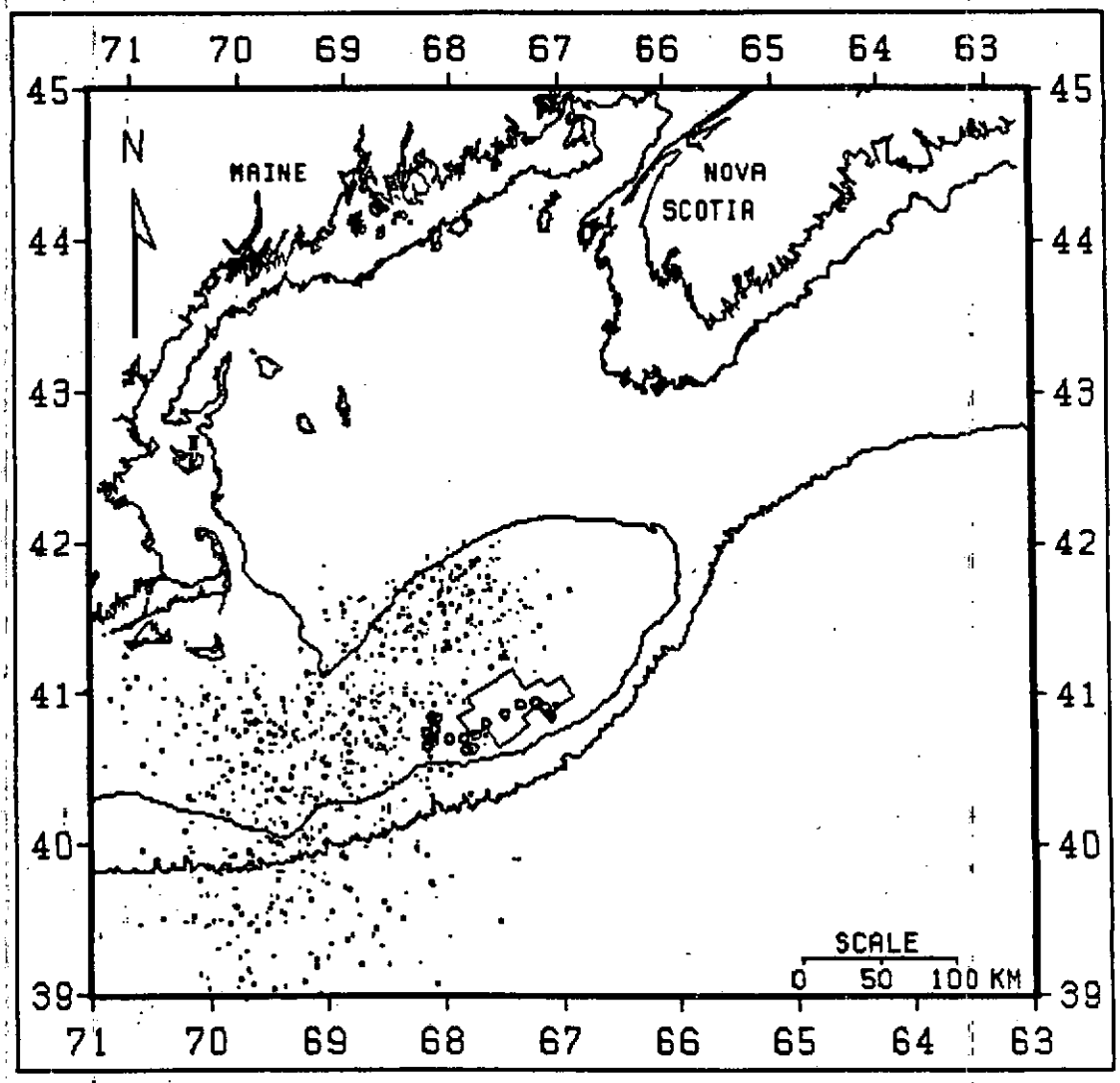

Surface Spillets (circles) and Subsurface 50 ppb
Contour (rectangular region)

Spill Site: 41° N, 67° W Spill Start Day: March 1
(10 days after spill start)

Figure 27a.

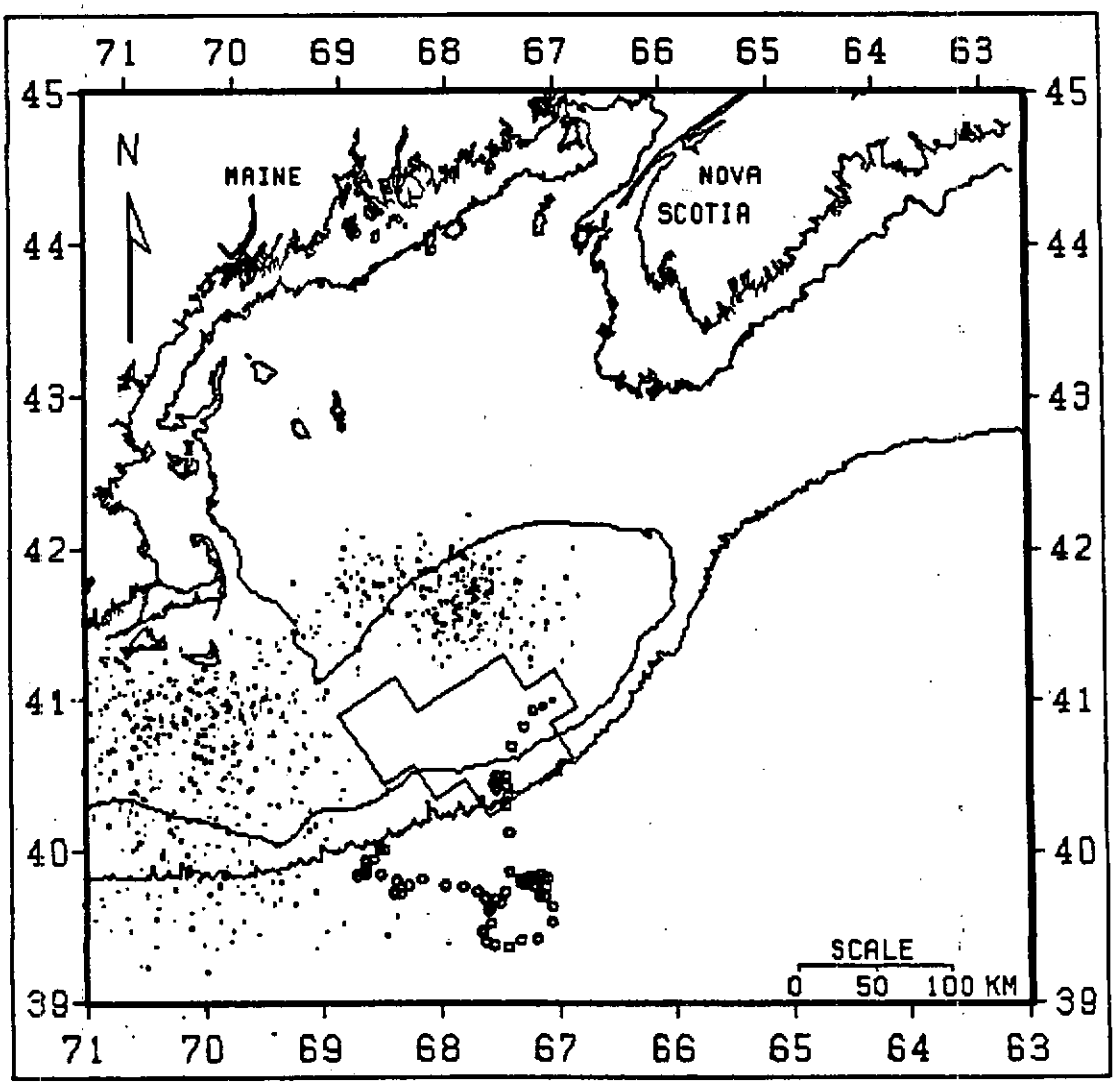

Surface Spillets (circles) and Subsurface 50 ppb
Contour (rectangular region)

Spill Site: 41° N, 67° W Spill Start Day: March 1
(30 days after spill start)

Figure 27b.

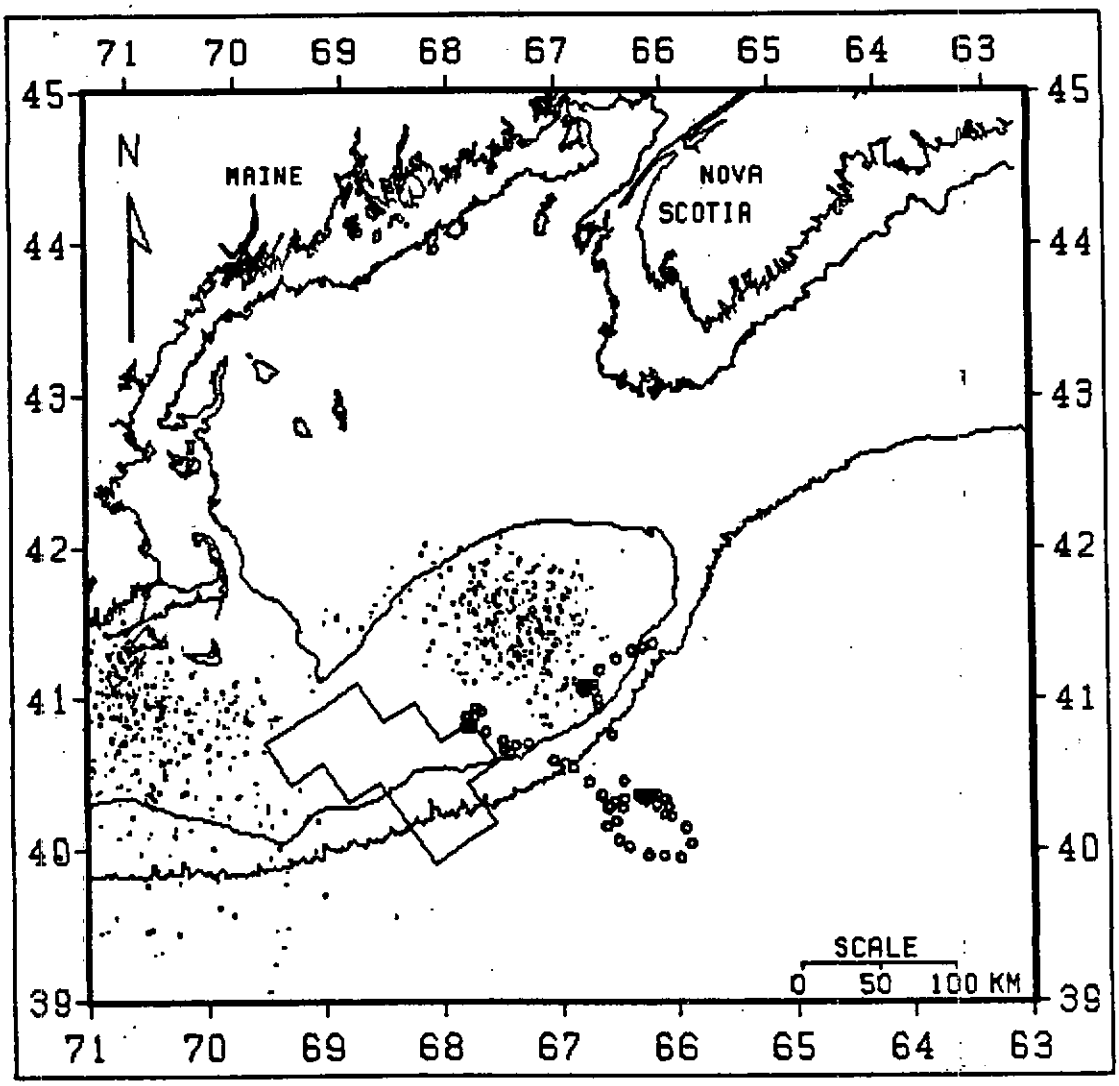

Surface Spillets (circles) and Subsurface 50 ppb
Contour (rectangular region)

Spill Site: 41° N, 67° W Spill Start Day: March 1
(50 days after spill start)

Figure 27c.

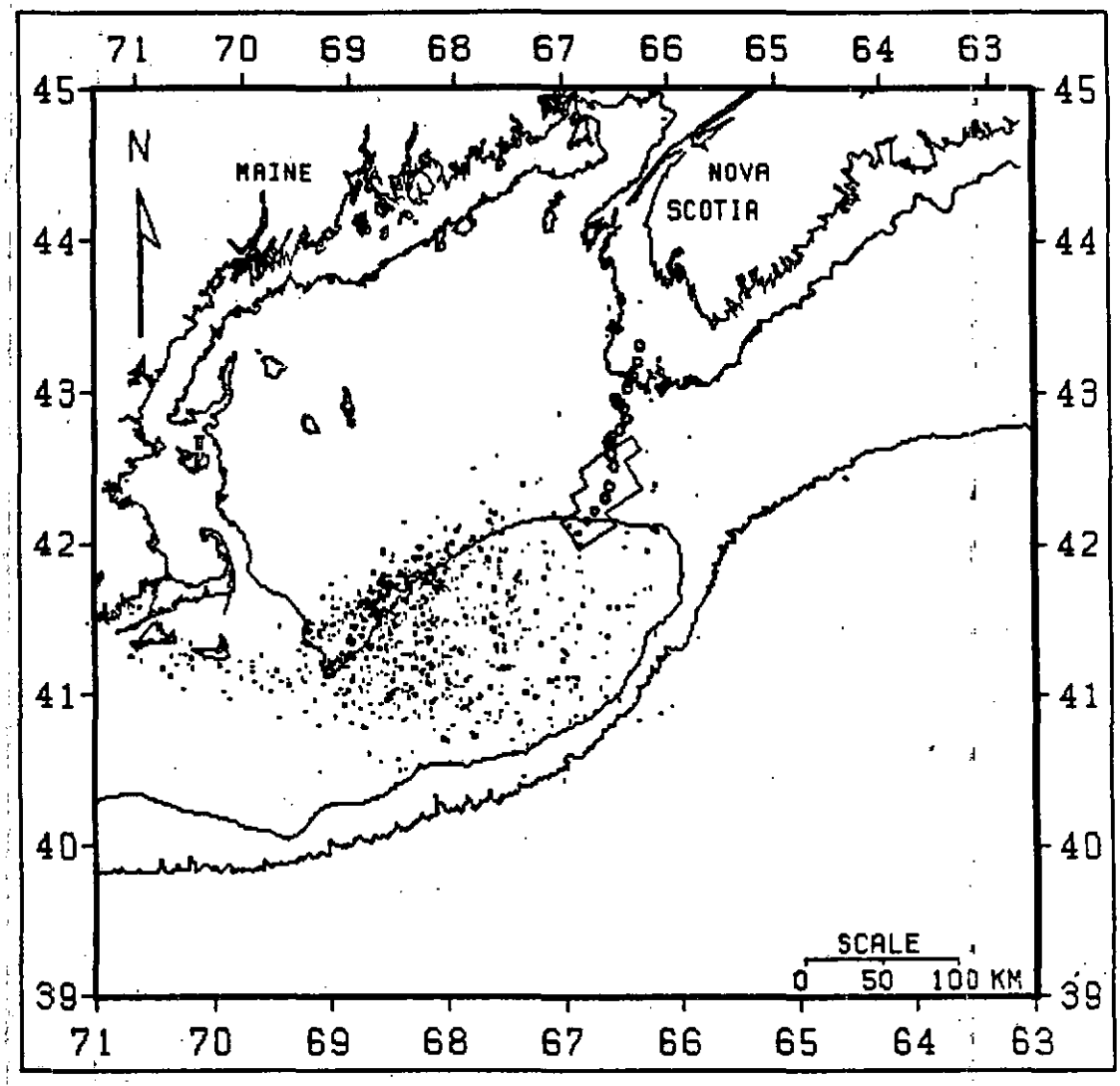

Surface Spillets (circles) and Subsurface 50 ppb Contour (rectangular region)

Spill Site: 42° N, 67° W Spill Start Day: June 1 (10 days after spill start)

Figure 28a.

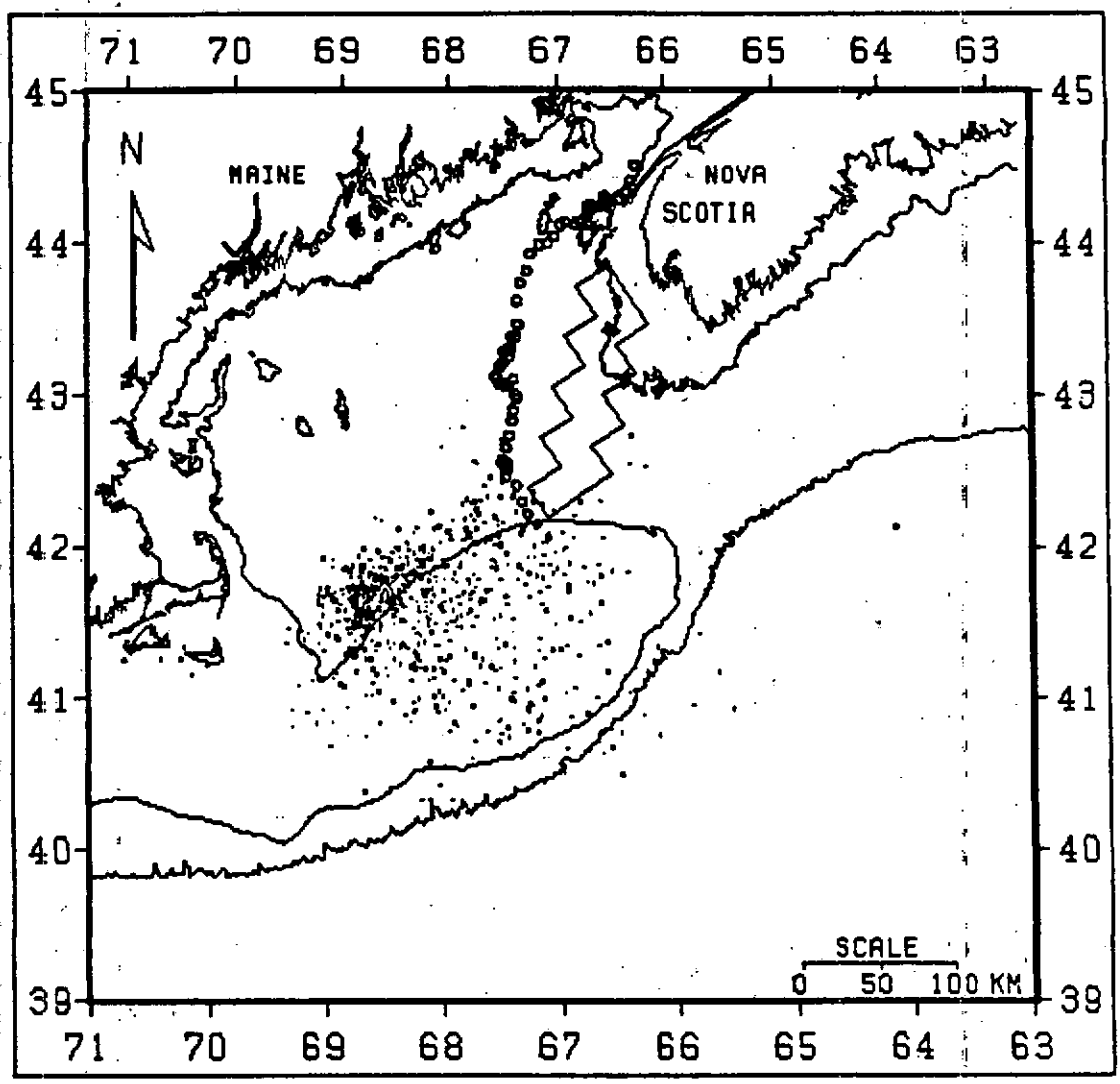

Surface Spillets (circles) and Subsurface 50 ppb
Contour (rectangular region)

Spill Site: 42° N, 67° W Spill Start Day: June 1
(30 days after spill start)

Figure 28b.

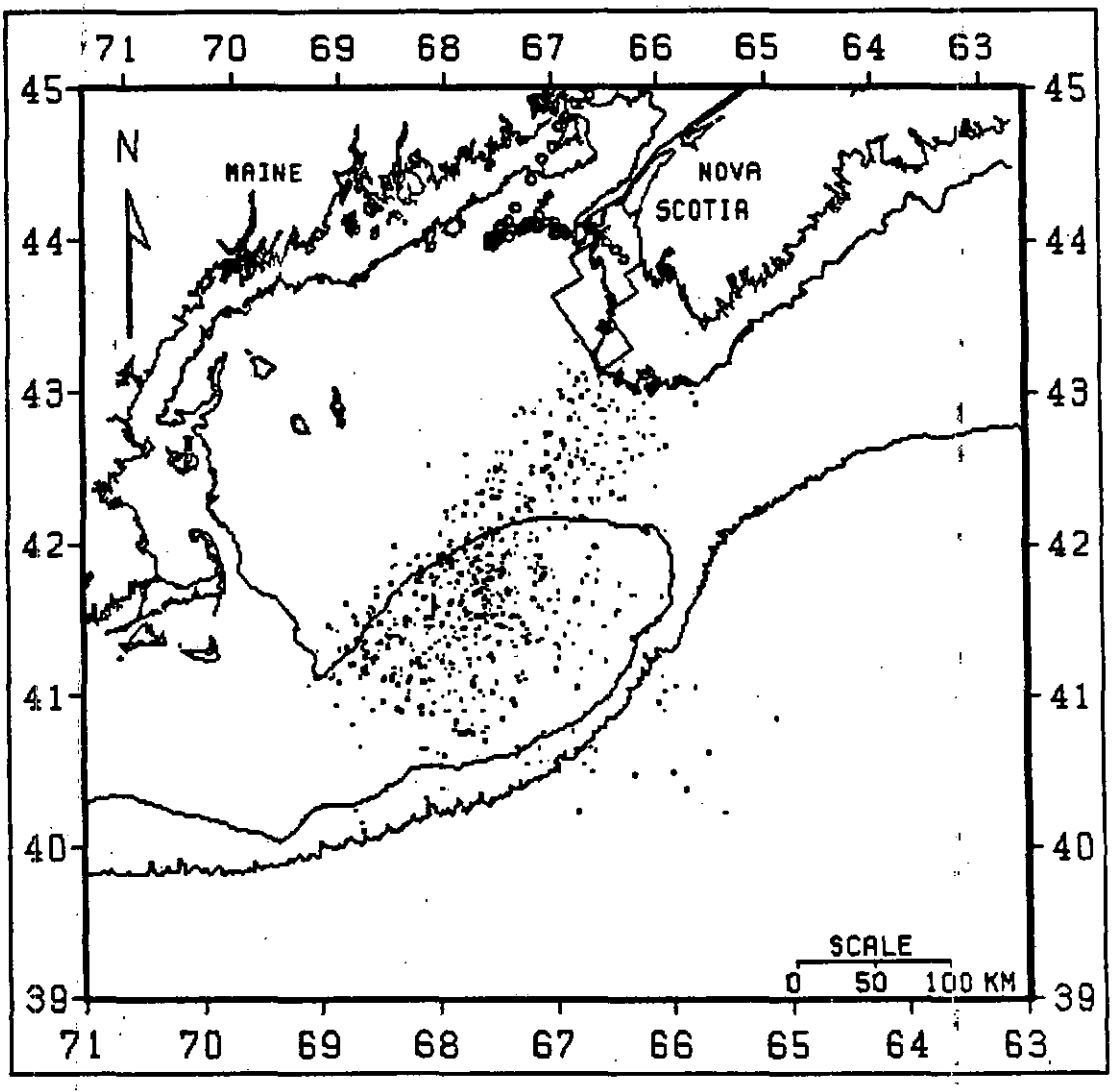

Surface Spillets (circles) and Subsurface 50 ppb
Contour (rectangular region)

Spill Site: 42° N, 67° W Spill Start Day: June 1
(50 days after spill start)

Figure 28c.

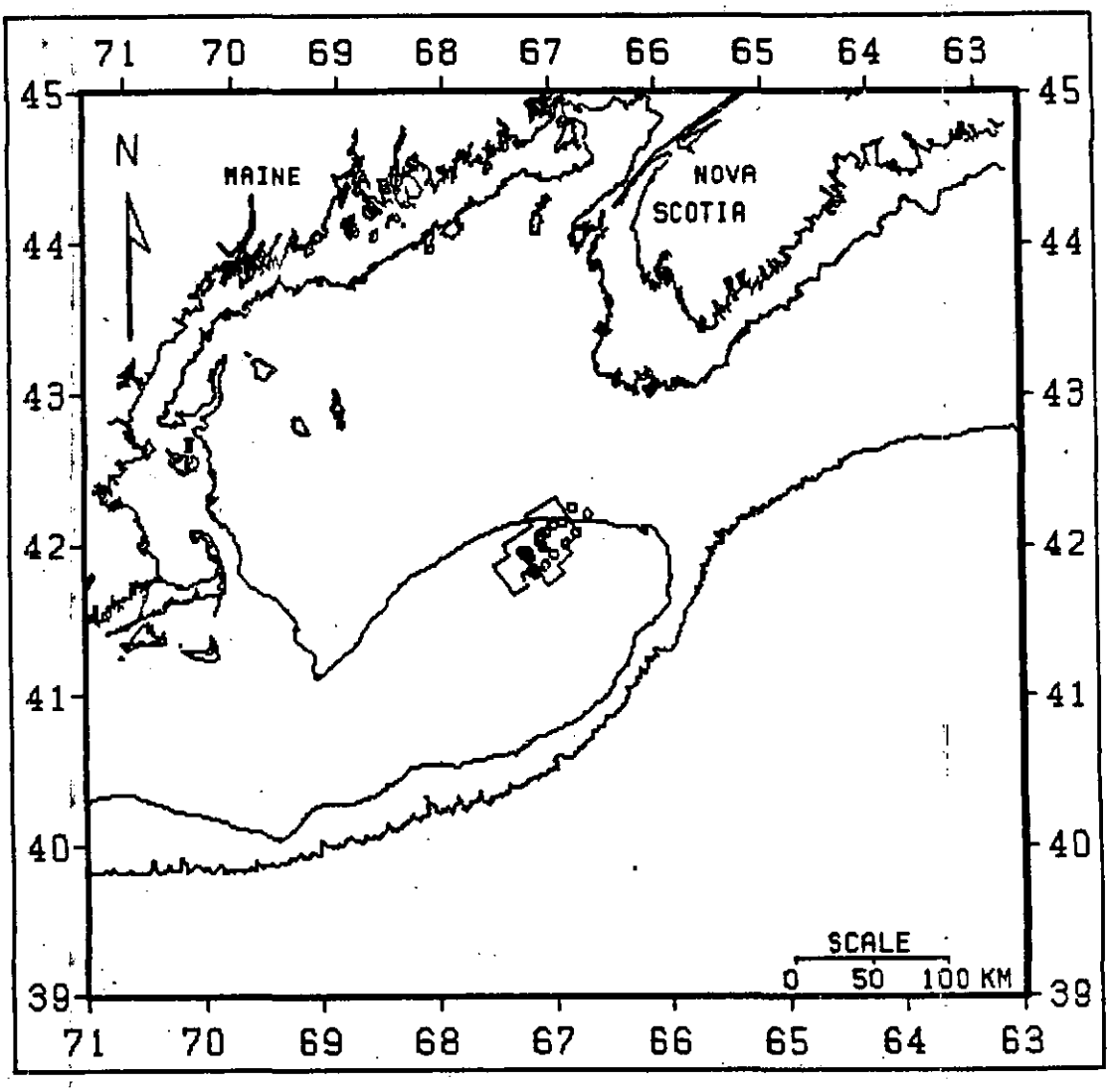

Surface Spillets (circles) and Subsurface 50 ppb
Contour (rectangular region)

Spill Site: 42° N, 67° W Spill Start Day: September 1
(10 days after spill start)

Figure 29a.

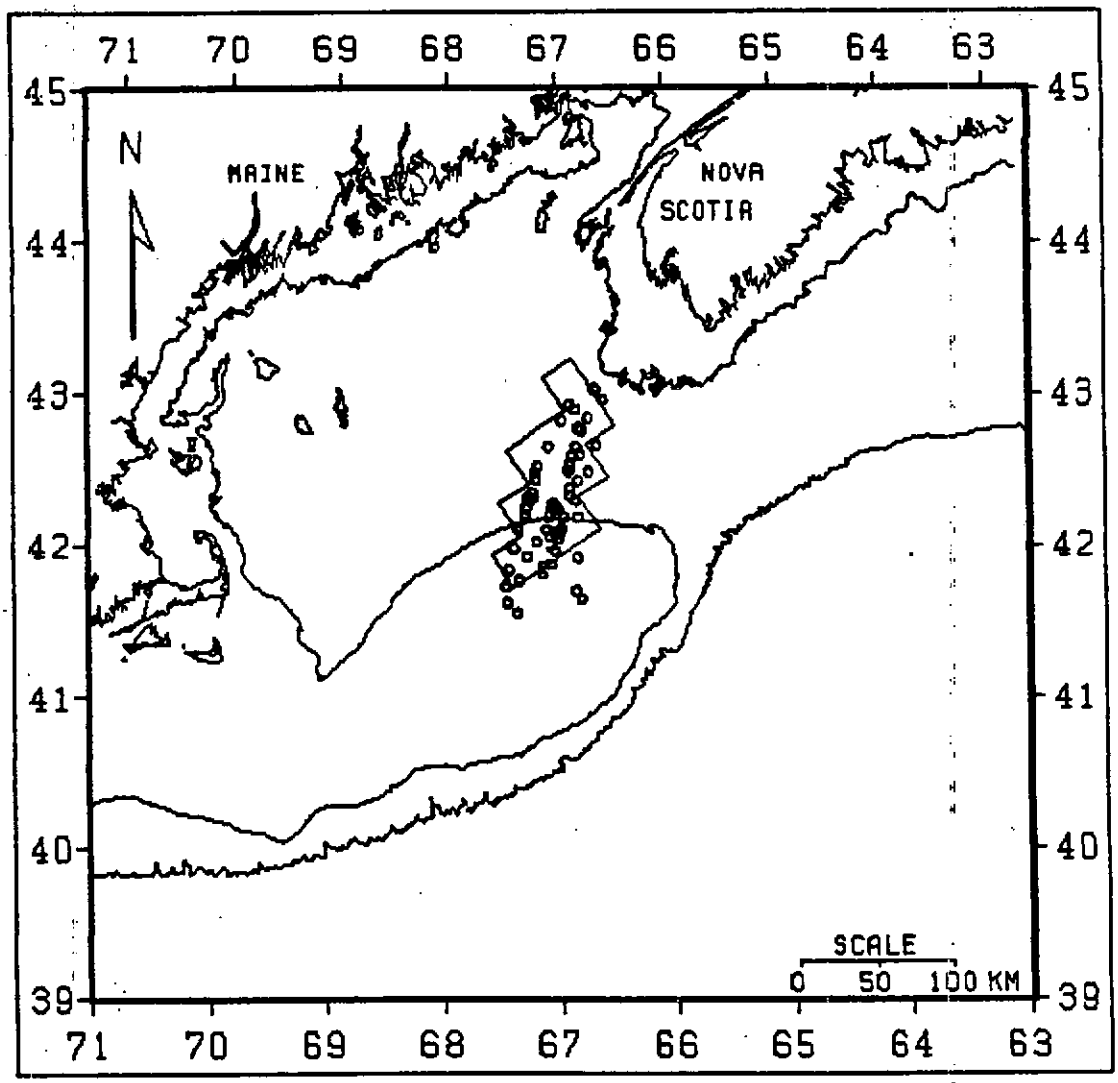

Surface Spillets (circles) and Subsurface 50 ppb
Contour (rectangular region)

Spill Site: 42° N, 67° W Spill Start Day: September 1
(30 days after spill start)

Figure 29b.

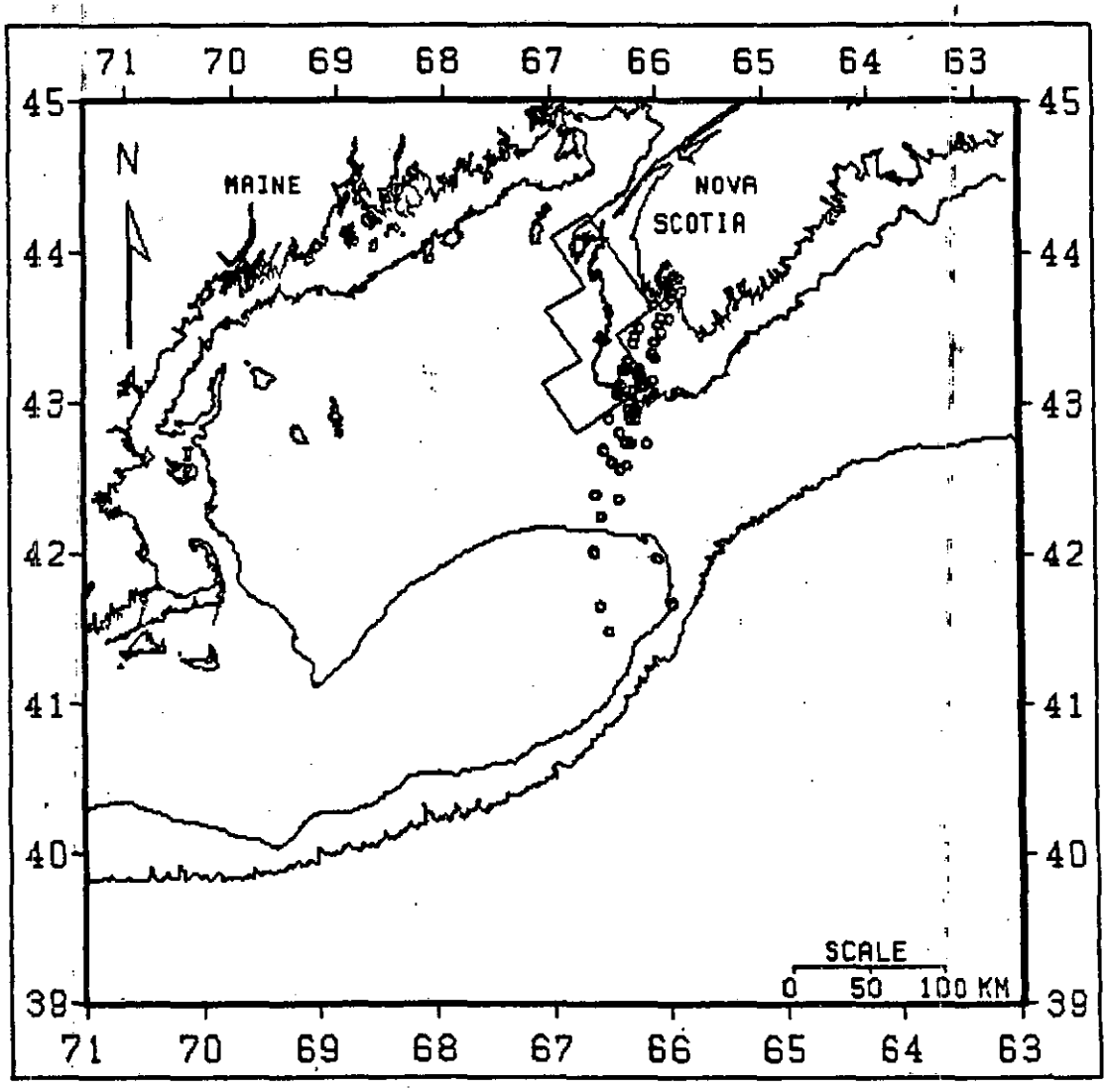

Surface Spillets (circles) and Subsurface 50 ppb
Contour (rectangular region)

Spill Site: 42° N, 67° W Spill Start Day: September 1
(50 days after spill start)

Figure 29c.

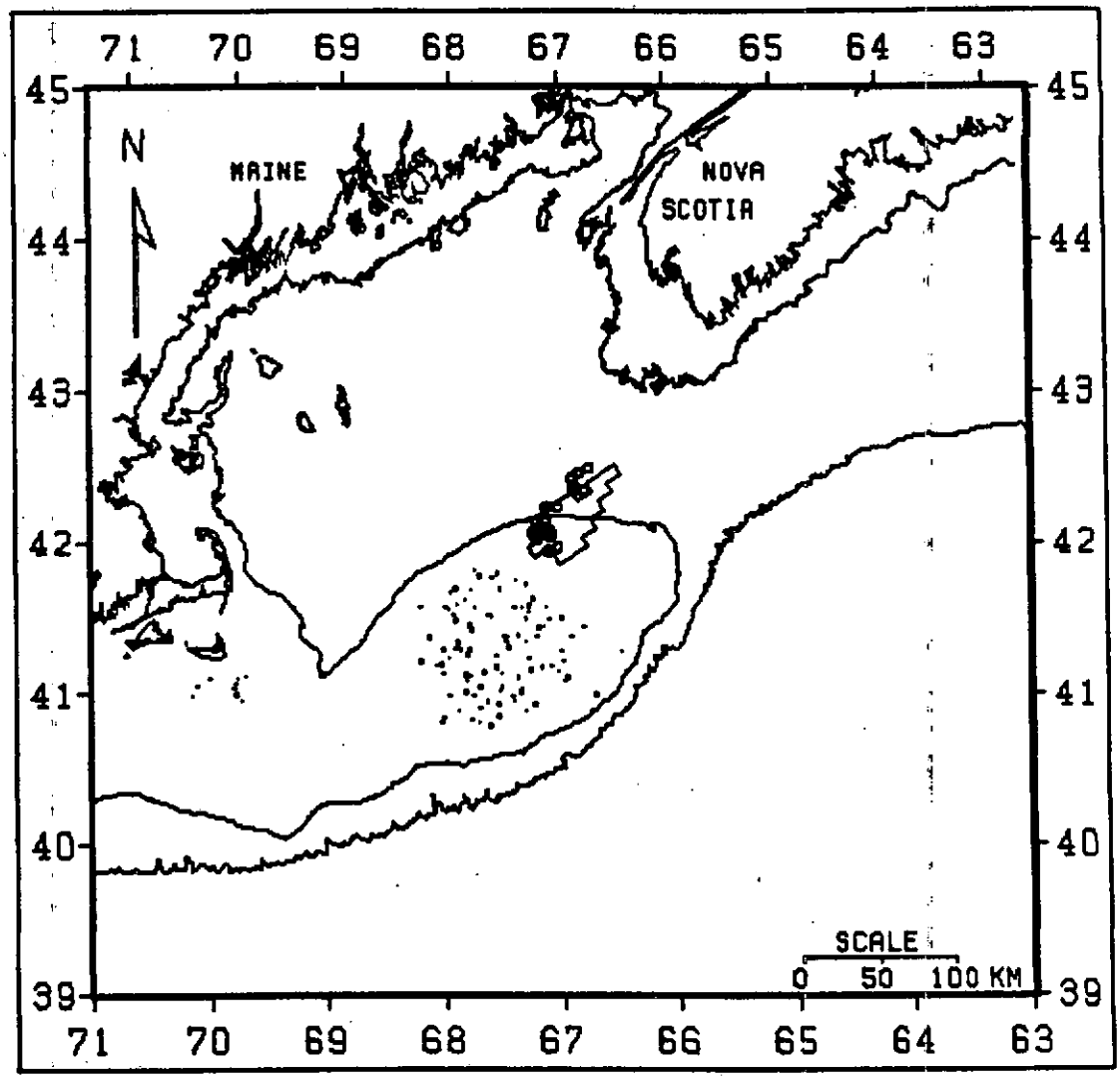

Surface Spillets (circles) and Subsurface 50 ppb
Contour (rectangular region)

Spill Site: 42° N, 67° W Spill Start Day: December 1
(10 days after spill start)

Figure 30a.

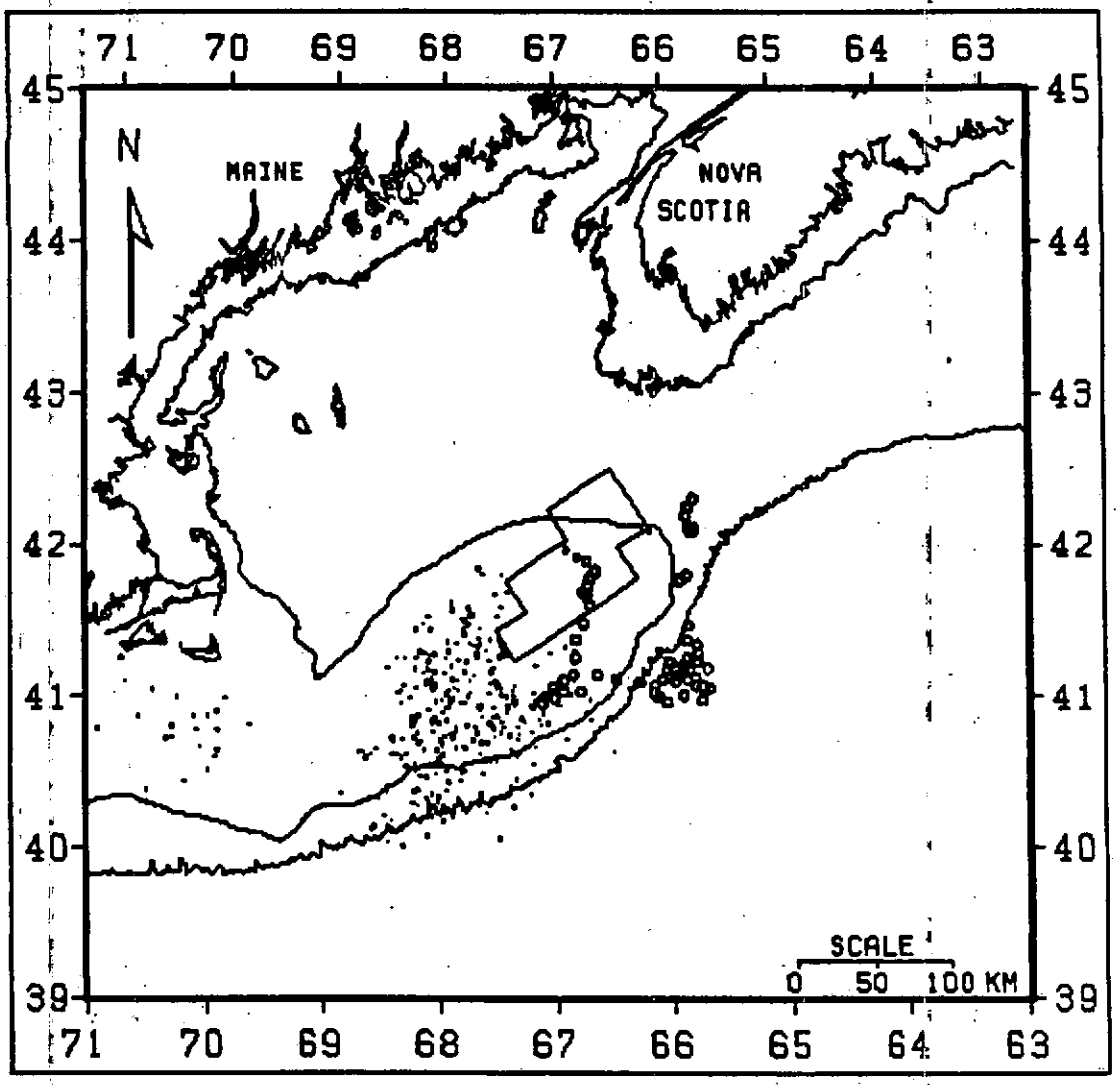

Surface Spillets (circles) and Subsurface 50 ppb
Contour (rectangular region)

Spill Site: 42° N, 67° W Spill Start Day: December 1
(30 days after spill start)

Figure 30b.

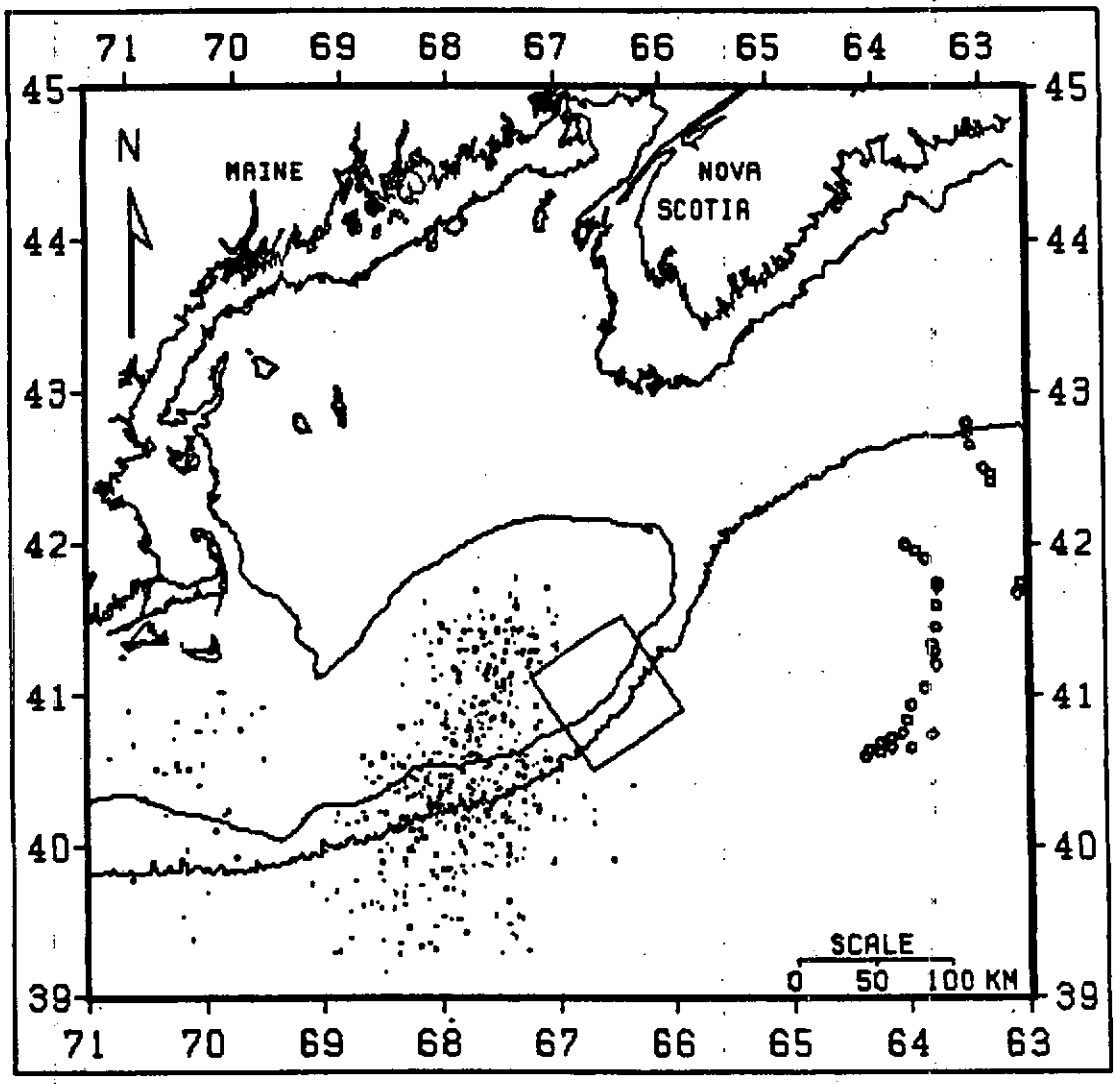

Surface Spillets (circles) and Subsurface 50 ppb
Contour (rectangular region)

Spill Site: 42° N, 67° W Spill Start Day: December 1
(50 days after spill start)

Figure 30c.

Fig. 19). The September spills result in zero impact estimates (see above), while for December only 4268.335 results in an ichthyoplankton loss exceeding 5%.

Details of the spatial and temporal dynamics of the hydrocarbon and ichthyoplankton distributions are shown in Figs. 24 through 30. Figures 24 through 27 show "snapshots" of oil spill and ichthyoplankton transport events for spills beginning on March 1 at each of the 4 selected sites. These are the spills associated with the highest losses of ichthyoplankton. Figures 28 through 30 show events starting on June 1, September 1, and December 1 at 42 N, 67 W, the middle of the three northern spill sites. For each of these cases, snapshots are shown 10, 30, and 50 days after spill commencement. Consideration of these plots, complete at one time for all sites and one site for representative times, combined with the 16 trajectory summaries (Figs. 3-18) and the current plots (Figs. 19-22), should give a relatively complete understanding of the simulations reported here. The other 27 plots (3 sites, 3 seasons, 3 plots per spill event) have not been included. It is felt that these would simply increase the bulk of the report, obscuring rather than illuminating its implications.

7. GEORGES BANK COD FISHERY IMPACTS

As described in Spaulding et al. (1982c), Reed et al. (1982), and Lorda et al. (1982), impacts of oil spills on the Georges Bank cod population are estimated here in a stochastic manner which takes account of natural recruitment variability.

For each case summarized in Fig. 31, the equilibrium population vector was projected over 2000 years to generate a baseline time series of yearly nonimpacted population vectors and annual catch estimates, subject only to randomly fluctuating recruitment rates. Spill events were simulated by adding the oil-induced larval mortalities predicted by the oil spill fates and ichthyoplankton transport models to the stochastic larval density-independent mortalities for each spill scenario being modeled. For each scenario, a total of 200 spill events (of equal magnitude) was simulated independently with the yearly starting points chosen at random along the baseline time series.

In each simulation the impacted population vector was projected using the same random input, matched year by year, as in the baseline time series. The annual catches during the 50 years following each spill event were recomputed and the relative catch losses were obtained as the difference between the nonimpacted and the impacted catches over the same period. The catch loss, relative to the nonimpacted catch during each year, YL(t), and the cumulative catch loss n years after the oil spill, CL(n), relative to the average nonimpacted catch during the same n years, were computed.

The medians of the two loss measures, YL(t) and CL(n), were estimated to summarize the results of the 200 random spill events simulated for each scenario. Thus each of the 50 medians (one for each year after the spill event) was estimated from a sample of 200 random and independent observations (one for each spill event). The simulation "summaries" for all of the scenarios are shown in Fig. 31 with the maximum values of YL(t) and CL(n), and

SUMMARY OF CATCH LOSSES

Spill SITE	Spill DATE	TYPE OF LOSS A	B	C
41°N 67°W	MAR. 1	9.22%	37.13%	15.65%
	JUN. 1	3.48%	14.02%	6.35%
	SEP. 1	*	*	*
	DEC. 1	*	*	*
42°N 66°W	MAR. 1	2.82%	11.38%	5.20%
	JUN. 1	*	*	*
	SEP. 1	*	*	*
	DEC. 1	*	*	*
42°N 67°W	MAR. 1	7.41%	29.85%	12.88%
	JUN. 1	0.96%	3.87%	1.81%
	SEP. 1	*	*	*
	DEC. 1	*	*	*
42°N 68°W	MAR. 1	9.68%	38.98%	16.32%
	JUN. 1	1.07%	4.32%	2.02%
	SEP. 1	*	*	*
	DEC. 1	1.78%	7.19%	3.34%

A: MAX.YEAR LOSS (occurs in the 4th yr. after the spill)
B: MAX.CUMUL LOSS (occurs in the 7th yr. after the spill)
C: LONG TERM CUMULATIVE LOSS
*: Cases with ichthyoplankton losses below 5% (Table 2) have been dropped.

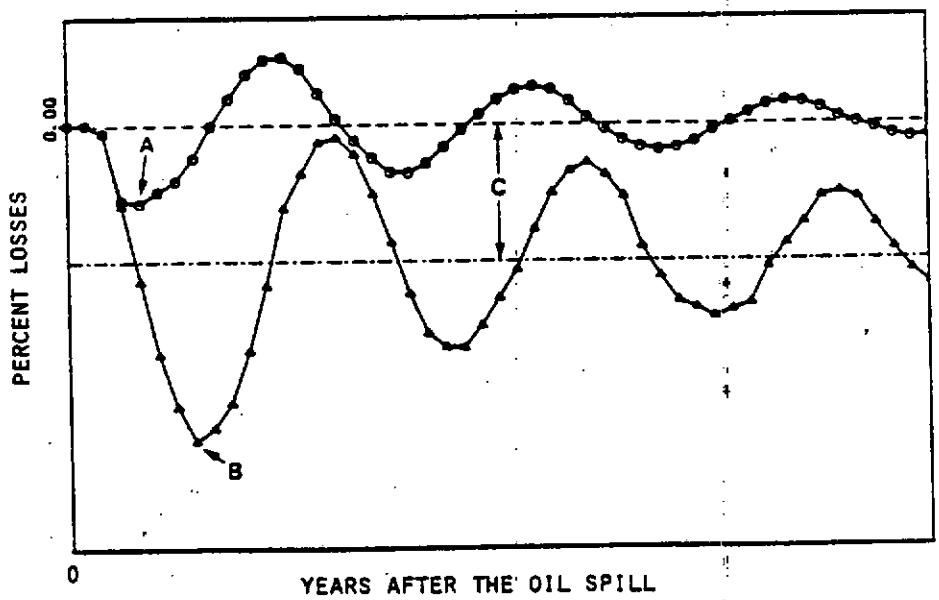

Figure 31. Summary of Median Catch Loss Measures

the long-term cumulative loss listed in tabular form.

Previous numerical analyses (Lorda et al. 1982; Spaulding et al. 1982c) have shown that the probability distributions of these loss measures are lognormally distributed. The two parameters of these lognormal distributions were estimated from the computed catch losses due to the 200 random spill events simulated for each scenario. Tables 3 to 10 summarize these parameters and the incremental probabilities for each scenario.

The tables of probabilities permit the estimation of the risk of a loss being larger than a specified maximum admissible loss, by simply adding the probabilities in the table between the specified loss and the last one listed. Similarly, probabilities may be added to obtain the probability corresponding to any desired loss range. This is equivalent to integrating the area under the curve of the Probability Density Function (PDF) over a given interval.

For example, with reference to Table 5 and the corresponding Fig. 32 (case 4266.060), we see that the most probable value of the maximum cumulative loss is about 13.3% of one year's catch. Table 5 shows the probability of a loss between 10% and 15% as being about 0.224. This corresponds to the area under the curve of Fig. 32 between these two values. The probability that the maximum cumulative catch loss will be less than 25% can be calculated from Table 5 as

$$0.083 + 0.260 + 0.224 + 0.151 + 0.096 = 0.814$$

It can be seen that these tables and figures are extremely valuable for assessing the probabilities associated with the potential ranges of a given impact estimate. Figures 32 through

Table 3

LOG-NORMAL Parameters and Catch Loss Probabilities for Oil Spill at 41°N. 67°W. on March 1st

Max. YEAR-Loss:	Med. =	0.0972	
	G.M. =	0.0926	
	Mode =	0.0694	
	Std. =	0.5803	<-- Log. scale
Max. CUM. Loss:	Med. =	0.4291	
	G.M. =	0.4080	
	Mode =	0.2673	
	Std. =	0.6878	<-- Log. scale

MAXIMUM YEAR-LOSS Probabilities

						P
MAX.YR.LOSS	>	0 %	and	<=	5 %	0.126
" " "	>	5 %	and	<=	10 %	0.394
" " "	>	10 %	and	<=	15 %	0.253
" " "	>	15 %	and	<=	20 %	0.120
" " "	>	20 %	and	<=	25 %	0.055
" " "	>	25 %	and	<=	30 %	0.026
" " "	>	30 %	and	<=	35 %	0.012
" " "	>	35 %	and	<=	40 %	0.006
" " "	>	40 %				0.007

MAXIMUM CUMULATIVE LOSS Probabilities

						P
MAX.CUM.LOSS	>	0 %	and	<=	10 %	0.017
" " "	>	10 %	and	<=	20 %	0.116
" " "	>	20 %	and	<=	30 %	0.168
" " "	>	30 %	and	<=	40 %	0.158
" " "	>	40 %	and	<=	50 %	0.129
" " "	>	50 %	and	<=	60 %	0.099
" " "	>	60 %	and	<=	70 %	0.075
" " "	>	70 %	and	<=	80 %	0.056
" " "	>	80 %	and	<=	90 %	0.042
" " "	>	90 %	and	<=	100 %	0.031
" " "	>	100 %	and	<=	110 %	0.024
" " "	>	110 %	and	<=	120 %	0.018
" " "	>	120 %	and	<=	130 %	0.014
" " "	>	130 %	and	<=	140 %	0.011
" " "	>	140 %				0.043

Losses expressed as % of a nonimpacted average year-catch

Table 4

LOG-NORMAL Parameters and Catch Loss Probabilities for Oil Spill at 41°N. 67°W. on June 1st

Max. YEAR-Loss:	Med. =	0.0367	
	G.M. =	0.0350	
	Mode =	0.0262	
	Std. =	0.5808	<-- Log. scale
Max. CUM. Loss:	Med. =	0.1635	
	G.M. =	0.1552	
	Mode =	0.1009	
	Std. =	0.6946	<-- Log. scale

MAXIMUM YEAR-LOSS Probabilities

						P
MAX. YR. LOSS	>	0 %	and	<=	1 %	0.013
" " "	>	1 %	and	<=	2 %	0.136
" " "	>	2 %	and	<=	3 %	0.217
" " "	>	3 %	and	<=	4 %	0.195
" " "	>	4 %	and	<=	5 %	0.144
" " "	>	5 %	and	<=	6 %	0.098
" " "	>	6 %	and	<=	7 %	0.065
" " "	>	7 %	and	<=	8 %	0.043
" " "	>	8 %	and	<=	9 %	0.029
" " "	>	9 %	and	<=	10 %	0.019
" " "	>	10 %	and	<=	11 %	0.013
" " "	>	11 %	and	<=	12 %	0.009
" " "	>	12 %				0.021

MAXIMUM CUMULATIVE LOSS Probabilities

						P
MAX. CUM. LOSS	>	0 %	and	<=	5 %	0.044
" " "	>	5 %	and	<=	10 %	0.195
" " "	>	10 %	and	<=	15 %	0.211
" " "	>	15 %	and	<=	20 %	0.163
" " "	>	20 %	and	<=	25 %	0.115
" " "	>	25 %	and	<=	30 %	0.079
" " "	>	30 %	and	<=	35 %	0.055
" " "	>	35 %	and	<=	40 %	0.038
" " "	>	40 %	and	<=	45 %	0.026
" " "	>	45 %	and	<=	50 %	0.019
" " "	>	50 %	and	<=	55 %	0.013
" " "	>	55 %	and	<=	60 %	0.010
" " "	>	60 %				0.031

Losses expressed as % of a nonimpacted average year-catch

Table 5

LOG-NORMAL Parameters and Catch Loss Probabilities for Oil Spill at 42°N. 66°W. on March 1st

Max. YEAR-Loss:	Med. =	0.0298	
	G.M. =	0.0286	
	Mode =	0.0211	
	Std. =	0.5868	<-- Log. scale
Max. CUM. Loss:	Med. =	0.1332	
	G.M. =	0.1274	
	Mode =	0.0807	
	Std. =	0.7073	<-- Log. scale

MAXIMUM YEAR-LOSS Probabilities

						P
MAX.YR.LOSS	>	0 %	and	<=	1 %	0.032
" " "	>	1 %	and	<=	2 %	0.218
" " "	>	2 %	and	<=	3 %	0.256
" " "	>	3 %	and	<=	4 %	0.187
" " "	>	4 %	and	<=	5 %	0.119
" " "	>	5 %	and	<=	6 %	0.072
" " "	>	6 %	and	<=	7 %	0.044
" " "	>	7 %	and	<=	8 %	0.026
" " "	>	8 %	and	<=	9 %	0.016
" " "	>	9 %	and	<=	10 %	0.010
" " "	>	10 %				0.019

MAXIMUM CUMULATIVE LOSS Probabilities

						P
MAX.CUM.LOSS	>	0 %	and	<=	5 %	0.083
" " "	>	5 %	and	<=	10 %	0.260
" " "	>	10 %	and	<=	15 %	0.224
" " "	>	15 %	and	<=	20 %	0.151
" " "	>	20 %	and	<=	25 %	0.096
" " "	>	25 %	and	<=	30 %	0.061
" " "	>	30 %	and	<=	35 %	0.039
" " "	>	35 %	and	<=	40 %	0.026
" " "	>	40 %	and	<=	45 %	0.017
" " "	>	45 %	and	<=	50 %	0.012
" " "	>	50 %	and	<=	55 %	0.008
" " "	>	55 %				0.022

Losses expressed as % of a nonimpacted average year-catch

Table 6

LOG-NORMAL Parameters and Catch Loss Probabilities for Oil Spill at 42°N. 67°W. on March 1st

Max. YEAR-Loss:	Med. =	0.0781	
	G.M. =	0.0744	
	Mode =	0.0558	
	Std. =	0.5804	<-- Log. scale
Max. CUM. Loss:	Med. =	0.3452	
	G.M. =	0.3288	
	Mode =	0.2143	
	Std. =	0.6903	<-- Log. scale

MAXIMUM YEAR-LOSS Probabilities

							P
MAX.	YR.	LOSS	>	0 %	and	<= 5 %	0.221
"	"	"	>	5 %	and	<= 10 %	0.444
"	"	"	>	10 %	and	<= 15 %	0.205
"	"	"	>	15 %	and	<= 20 %	0.078
"	"	"	>	20 %	and	<= 25 %	0.030
"	"	"	>	25 %	and	<= 30 %	0.012
"	"	"	>	30 %	and	<= 35 %	0.005
"	"	"	>	35 %			0.005

MAXIMUM CUMULATIVE LOSS Probabilities

							P
MAX.	CUM.	LOSS	>	0 %	and	<= 10 %	0.036
"	"	"	>	10 %	and	<= 20 %	0.178
"	"	"	>	20 %	and	<= 30 %	0.205
"	"	"	>	30 %	and	<= 40 %	0.165
"	"	"	>	40 %	and	<= 50 %	0.120
"	"	"	>	50 %	and	<= 60 %	0.084
"	"	"	>	60 %	and	<= 70 %	0.059
"	"	"	>	70 %	and	<= 80 %	0.041
"	"	"	>	80 %	and	<= 90 %	0.029
"	"	"	>	90 %	and	<= 100 %	0.021
"	"	"	>	100 %	and	<= 110 %	0.015
"	"	"	>	110 %	and	<= 120 %	0.011
"	"	"	>	120 %	and	<= 130 %	0.008
"	"	"	>	130 %			0.027

Losses expressed as % of a nonimpacted average year-catch

Table 7

LOG-NORMAL Parameters and Catch Loss Probabilities for Oil Spill at 42°N. 67°W. on June 1st

Max. YEAR-Loss:	Med. =	0.0101	
	G.M. =	0.0097	
	Mode =	0.0072	
	Std. =	0.5869	<-- Log. scale
Max. CUM. Loss:	Med. =	0.0453	
	G.M. =	0.0434	
	Mode =	0.0274	
	Std. =	0.7089	<-- Log. scale

MAXIMUM YEAR-LOSS Probabilities

							P
MAX.	YR.	LOSS	>	0 %	and	<= 1 %	0.493
"	"	"	>	1 %	and	<= 2 %	0.385
"	"	"	>	2 %	and	<= 3 %	0.091
"	"	"	>	3 %	and	<= 4 %	0.022
"	"	"	>	4 %	and	<= 5 %	0.006
"	"	"	>	5 %			0.003

MAXIMUM CUMULATIVE LOSS Probabilities

							P
MAX.	CUM.	LOSS	>	0 %	and	<= 1 %	0.017
"	"	"	>	1 %	and	<= 2 %	0.108
"	"	"	>	2 %	and	<= 3 %	0.156
"	"	"	>	3 %	and	<= 4 %	0.150
"	"	"	>	4 %	and	<= 5 %	0.125
"	"	"	>	5 %	and	<= 6 %	0.099
"	"	"	>	6 %	and	<= 7 %	0.076
"	"	"	>	7 %	and	<= 8 %	0.058
"	"	"	>	8 %	and	<= 9 %	0.045
"	"	"	>	9 %	and	<= 10 %	0.034
"	"	"	>	10 %	and	<= 11 %	0.027
"	"	"	>	11 %	and	<= 12 %	0.021
"	"	"	>	12 %	and	<= 13 %	0.016
"	"	"	>	13 %	and	<= 14 %	0.013
"	"	"	>	14 %	and	<= 15 %	0.010
"	"	"	>	15 %			0.046

Losses expressed as % of a nonimpacted average year-catch

Table 8

LOG-NORMAL Parameters and Catch Loss Probabilities for Oil Spill at 42°N. 68°W. on March 1st

Max. YEAR-Loss:	Med. =	0.1021	
	G.M. =	0.0972	
	Mode =	0.0729	
	Std. =	0.5802	<-- Log. scale
Max. CUM. Loss:	Med. =	0.4505	
	G.M. =	0.4281	
	Mode =	0.2809	
	Std. =	0.6871	<-- Log. scale

MAXIMUM YEAR-LOSS Probabilities

						P
MAX.YR.LOSS	>	0 %	and	<=	5 %	0.109
" " "	>	5 %	and	<=	10 %	0.377
" " "	>	10 %	and	<=	15 %	0.261
" " "	>	15 %	and	<=	20 %	0.130
" " "	>	20 %	and	<=	25 %	0.062
" " "	>	25 %	and	<=	30 %	0.030
" " "	>	30 %	and	<=	35 %	0.015
" " "	>	35 %	and	<=	40 %	0.008
" " "	>	40 %				0.009

MAXIMUM CUMULATIVE LOSS Probabilities

						P
MAX.CUM.LOSS	>	0 %	and	<=	10 %	0.014
" " "	>	10 %	and	<=	20 %	0.104
" " "	>	20 %	and	<=	30 %	0.158
" " "	>	30 %	and	<=	40 %	0.154
" " "	>	40 %	and	<=	50 %	0.129
" " "	>	50 %	and	<=	60 %	0.101
" " "	>	60 %	and	<=	70 %	0.078
" " "	>	70 %	and	<=	80 %	0.059
" " "	>	80 %	and	<=	90 %	0.045
" " "	>	90 %	and	<=	100 %	0.034
" " "	>	100 %	and	<=	110 %	0.026
" " "	>	110 %	and	<=	120 %	0.020
" " "	>	120 %	and	<=	130 %	0.015
" " "	>	130 %	and	<=	140 %	0.012
" " "	>	140 %	and	<=	150 %	0.009
" " "	>	150 %				0.040

Losses expressed as % of a nonimpacted average year-catch

Table 9

LOG-NORMAL Parameters and Catch Loss Probabilities for Oil Spill at 42°N. 68°W. on June 1st

Max. YEAR-Loss:	Med. =	0.0113	
	G.M. =	0.0109	
	Mode =	0.0080	
	Std. =	0.5869	<-- Log. scale
Max. CUM. Loss:	Med. =	0.0506	
	G.M. =	0.0484	
	Mode =	0.0306	
	Std. =	0.7088	<-- Log. scale

MAXIMUM YEAR-LOSS Probabilities

							P
MAX.	YR.	LOSS	>	0 %	and	<= 1 %	0.418
"	"	"	>	1 %	and	<= 2 %	0.417
"	"	"	>	2 %	and	<= 3 %	0.117
"	"	"	>	3 %	and	<= 4 %	0.032
"	"	"	>	4 %	and	<= 5 %	0.010
"	"	"	>	5 %			0.006

MAXIMUM CUMULATIVE LOSS Probabilities

							P
MAX.	CUM.	LOSS	>	0 %	and	<= 1 %	0.011
"	"	"	>	1 %	and	<= 2 %	0.084
"	"	"	>	2 %	and	<= 3 %	0.135
"	"	"	>	3 %	and	<= 4 %	0.140
"	"	"	>	4 %	and	<= 5 %	0.123
"	"	"	>	5 %	and	<= 6 %	0.102
"	"	"	>	6 %	and	<= 7 %	0.081
"	"	"	>	7 %	and	<= 8 %	0.064
"	"	"	>	8 %	and	<= 9 %	0.051
"	"	"	>	9 %	and	<= 10 %	0.040
"	"	"	>	10 %	and	<= 11 %	0.032
"	"	"	>	11 %	and	<= 12 %	0.025
"	"	"	>	12 %	and	<= 13 %	0.020
"	"	"	>	13 %	and	<= 14 %	0.016
"	"	"	>	14 %	and	<= 15 %	0.013
"	"	"	>	15 %	and	<= 16 %	0.010
"	"	"	>	16 %			0.052

Losses expressed as % of a nonimpacted average year-catch

Table 10

LOG-NORMAL Parameters and Catch Loss Probabilities for Oil Spill at 42°N. 68°W. on December 1st

Max. YEAR-Loss:	Med. =	0.0188	
	G.M. =	0.0181	
	Mode =	0.0133	
	Std. =	0.5869	<-- Log. scale
Max. CUM. Loss:	Med. =	0.0842	
	G.M. =	0.0806	
	Mode =	0.0510	
	Std. =	0.7082	<-- Log. scale

MAXIMUM YEAR-LOSS Probabilities

						P
MAX.YR.LOSS	>	0 %	and	<=	1 %	0.141
" " "	>	1 %	and	<=	2 %	0.401
" " "	>	2 %	and	<=	3 %	0.245
" " "	>	3 %	and	<=	4 %	0.114
" " "	>	4 %	and	<=	5 %	0.051
" " "	>	5 %	and	<=	6 %	0.024
" " "	>	6 %	and	<=	7 %	0.011
" " "	>	7 %	and	<=	8 %	0.006
" " "	>	8 %				0.007

MAXIMUM CUMULATIVE LOSS Probabilities

						P
MAX.CUM.LOSS	>	0 %	and	<=	5 %	0.231
" " "	>	5 %	and	<=	10 %	0.365
" " "	>	10 %	and	<=	15 %	0.197
" " "	>	15 %	and	<=	20 %	0.096
" " "	>	20 %	and	<=	25 %	0.049
" " "	>	25 %	and	<=	30 %	0.026
" " "	>	30 %	and	<=	35 %	0.014
" " "	>	35 %	and	<=	40 %	0.008
" " "	>	40 %				0.014

Losses expressed as % of a nonimpacted average year-catch

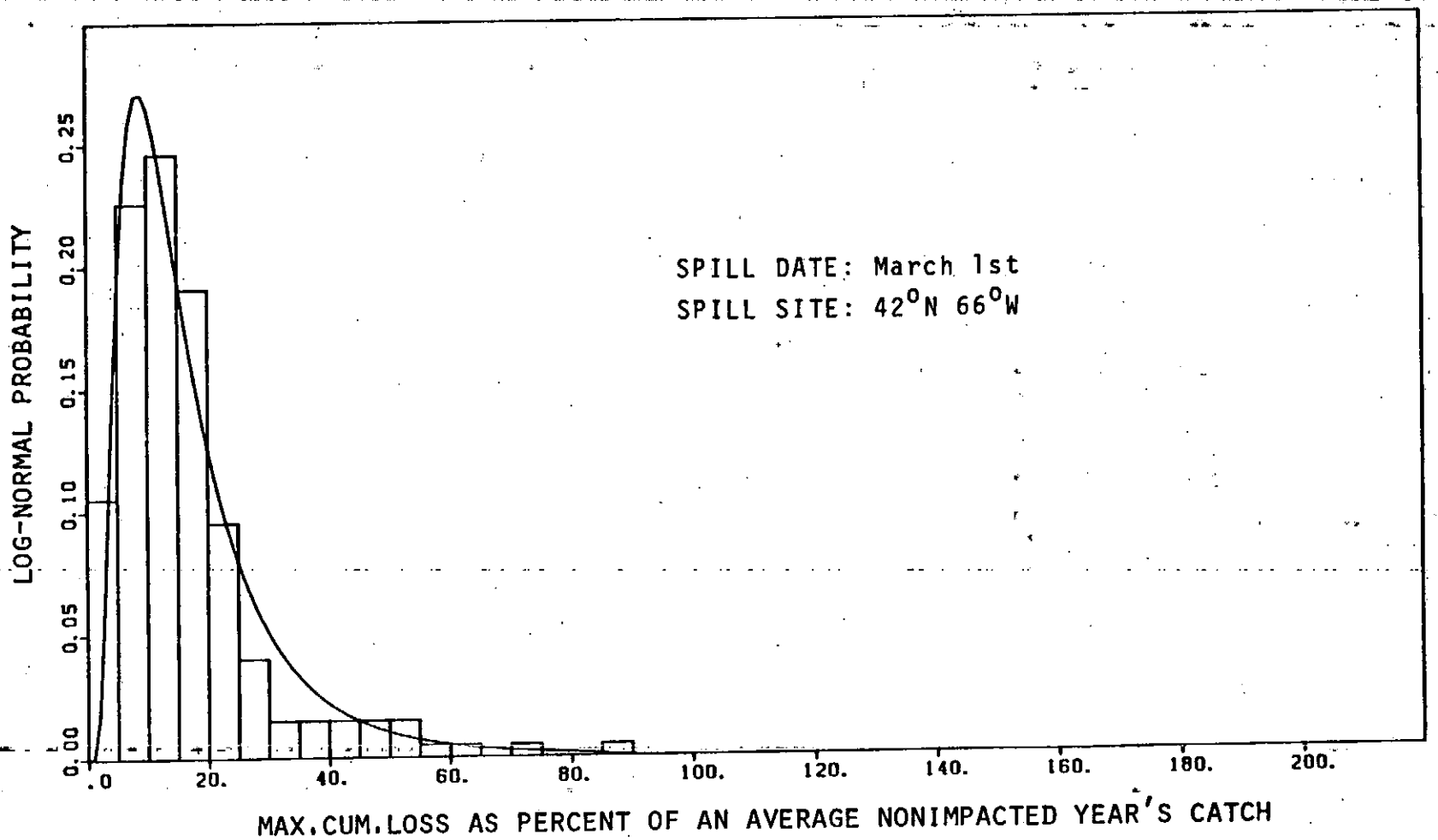

Figure 32. Catch loss probability distribution.

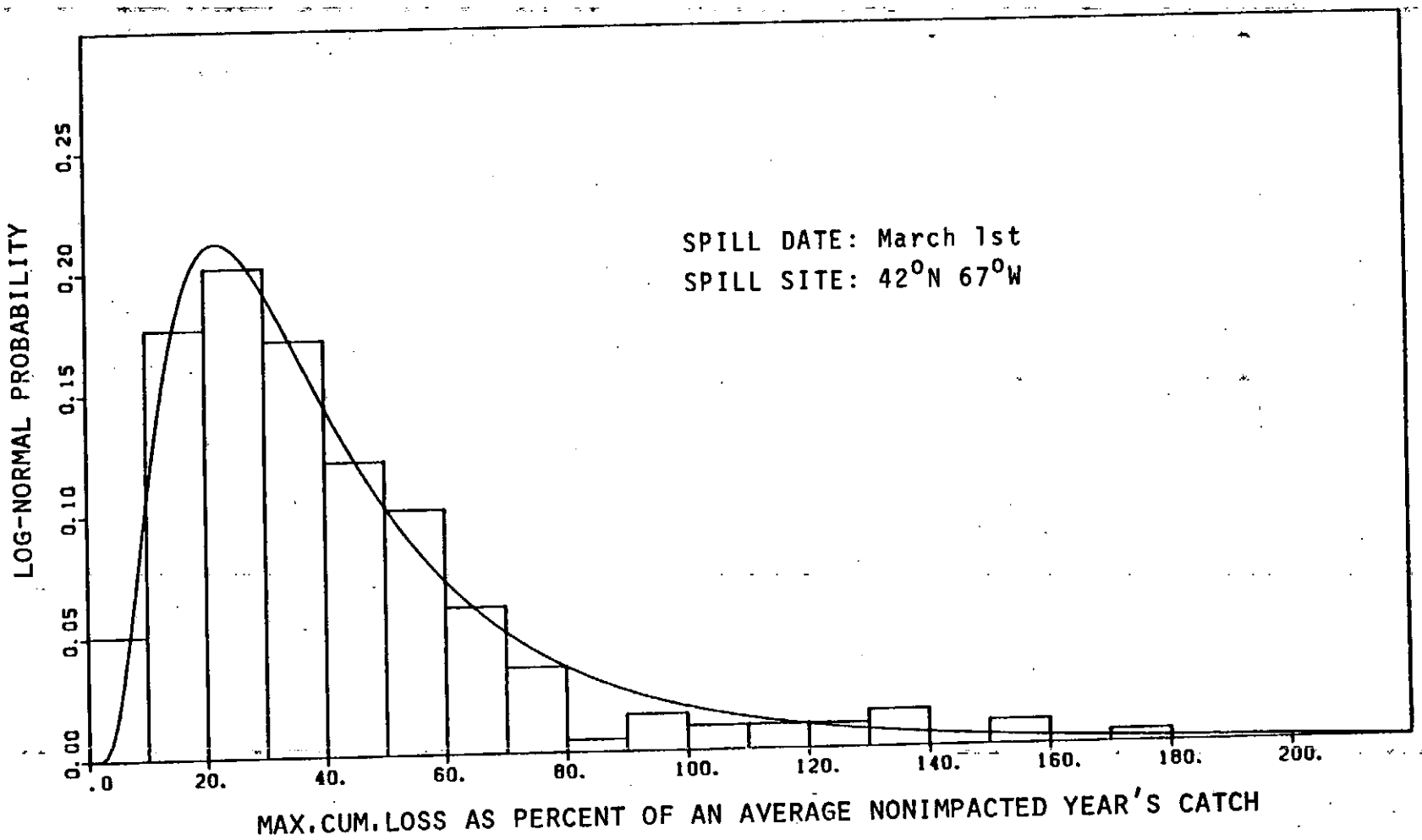

Figure 33. Catch loss probability distribution.

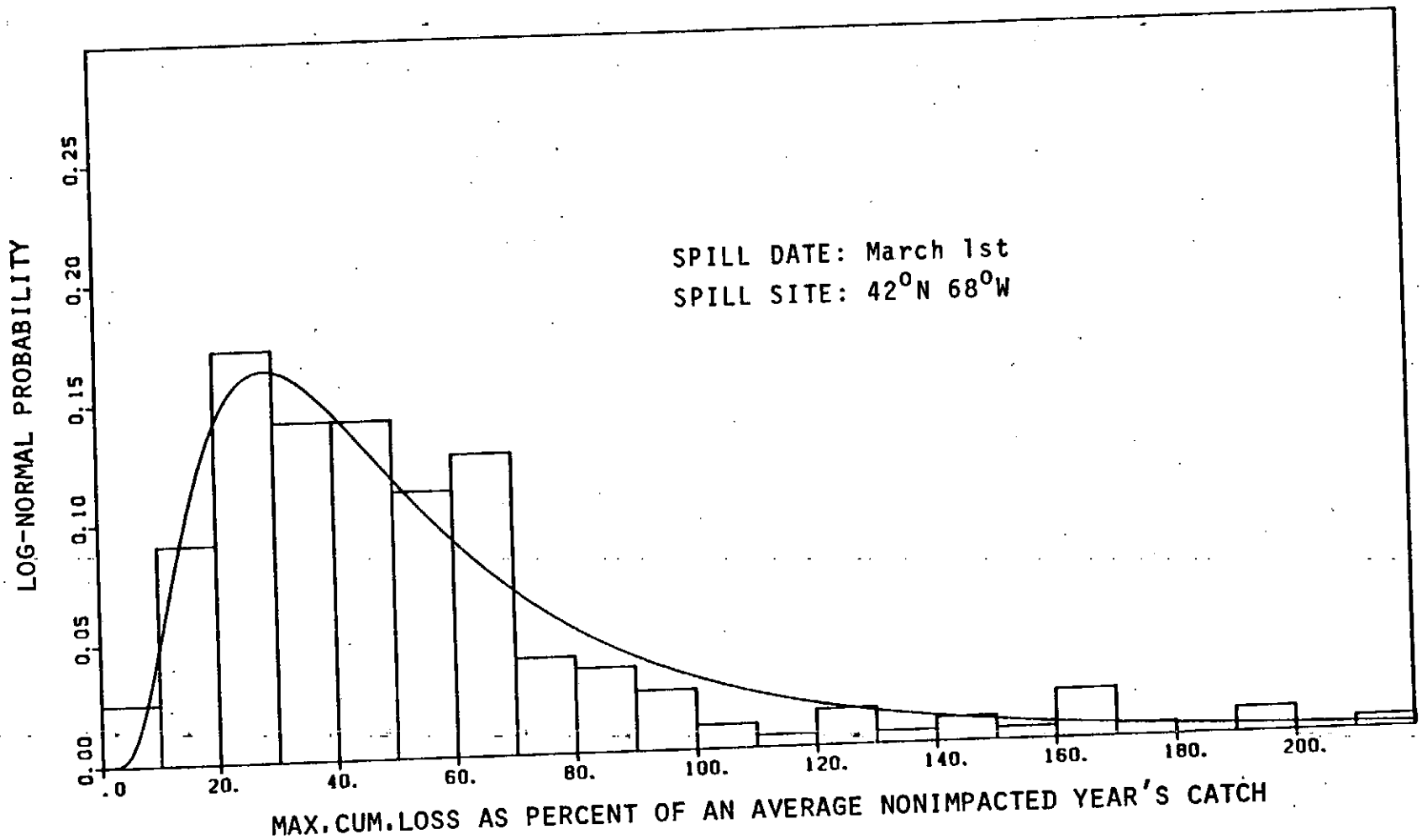

Figure 34. Catch loss probability distribution.

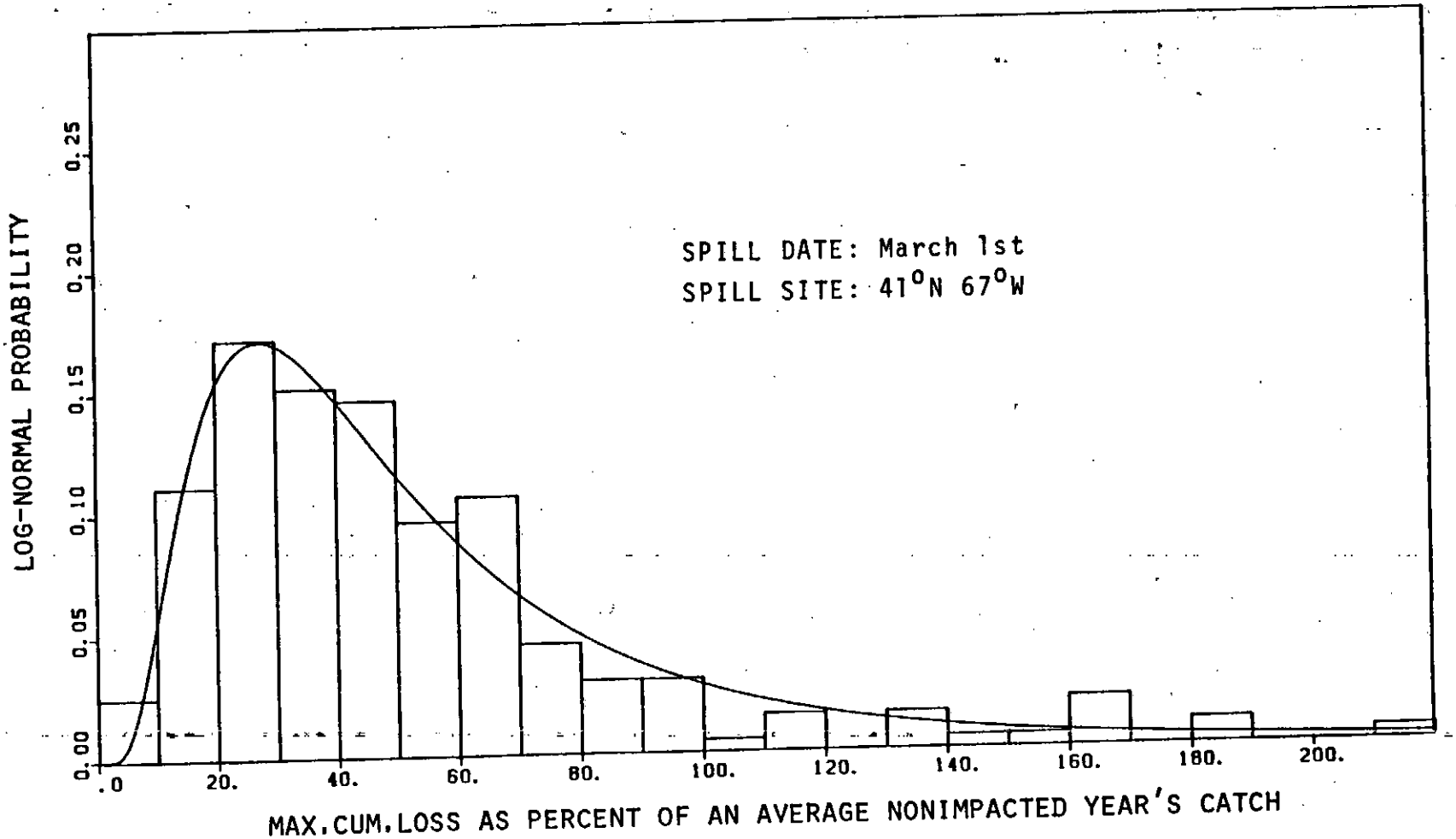

Figure 35. Catch loss probability distribution.

35 also show that, as the magnitude of the median impact estimate increases, so does the standard deviation of the associated probability density function.

Figures 32 to 35 illustrate the agreement between the histograms of the computed MAX.CUM.LOSS for the four scenarios with the largest oil-induced mortalities (March 1 spills) and the PDF of their corresponding estimated lognormal probability distributions plotted in the same scale. These four plots are graphical realizations of the data given in Tables 3, 5, 6, and 8.

8. SUMMARY OF FINDINGS

(1) Assessed by site, a spill at 42 N, 66 W is least likely to cause cod ichthyoplankton mortality on Georges Bank. As the potential oil spill site is moved west and south, the total probability of an impact increases, the sum of the impact estimates for the four seasonal cases being approximated equal for 42 N, 68 W, and 41 N, 67 W. Given an oil spill event probability distribution constant throughout the year, (i.e. equal probability of a spill regardless of season), these two sites carry approximately equal damage potential. If winter spills are more probable, then 42 N, 68 W has the highest damage potential.

(2) The trajectories of both surface and subsurface pollutants released along the northern edge of Georges

Bank (i.e. near latitude 42 N) are governed largely by the interaction of the currents set up by the dominant southwest flows on the Scotian Shelf with the relatively deep Northeast Channel and Gulf of Maine and the shallows of Georges Bank. This complex topography produces a strong north-south flow divergence in the Northeast Channel. The transport of subsurface hydrocarbons in Figs. 24a, b, and c demonstrates the effects of this divergence. The drifter-inferred current patterns underlying the simulations presented here place this divergence a little south of 42 N latitude (Figs. 19-22). Poor drifter returns from this region (5%) give low confidence in the placement of this flow detail. Application of a fine gridded numerical hydrodynamic model is the suggested remedy for this problem.

(3) The clockwise flow around Georges Bank during the spring and summer (Figs. 19-20) combined with the high cod spawning activity in March and April produce the high impact estimates associated with spills beginning on day 60 (Figs. 24-27).

9. FURTHER SUPPORTING STUDIES

There are several ways in which the work described here could be scientifically strengthened. Ranked in order of priority, these are:

(1) Using extant oceanographic observations and a numerical hydrodynamic model, evaluate the seasonal and geographical details of the circulation patterns along the northern flank of Georges Bank, to better assess the probable surface and subsurface trajectories of oil spills.

(2) Apply alternate formulations of the wind field to investigate the effects of spatial and year-to-year variability. (Isaji et al. 1982)

(3) Given improvements (1) and (2) above, and the information gained from the 16 simulations described here, perform additional simulations for better estimates of biological and coastal impacts.

(4) The passage of Gulf Stream rings is known to alter the local flows. The effect of such an event on both oil and ichthyoplankton is of potential importance to questions of recruitment and impact assessment.

(5) Poor drifter returns for the Scotian Shelf make the Bumpus-derived transport fields used here highly questionable in that area. The ASA three dimensional numerical hydrodynamic model of this region (Isaji, Spaulding, and Swanson, 1982) could be used to assess the potential impacts of Sable Island spills on Georges Bank and Brown's Bank species.

Although we believe that the simulations reported here give an excellent first order estimate of both trajectories and impacts, we recommend at least efforts (1), (2), and (3) to bring this evidence in line with current state-of-the-art capabilities.

REFERENCES

Anderson, E., and M.L. Spaulding, 1981. Application of an Oil Spill Fates Model to Environmental Management on Georges Bank, The Environmental Professional - Special Issue on Toxic and Hazardous Substances, 3(1): 119-132.

Bigelow, , H.B., 1927. Physical Oceanography of the Gulf of Maine, Bull. U.S. Bureau of Fisheries 40(2): 511-1027.

Bumpus, D.F., and C.G. Day, 1957. Drift Bottle Records for Gulf of Maine and Georges Bank, 1931-56, U.S. Fish and Wildlife Service, Special Science Report, Fisheries No. 242, p. 61.

Bumpus, D.F. and L.M. Lauzier, 1965. Serial Atlas of the Continental Shelf off Easter North American Between Newfoundland and Florida. American Geographical Society Serial Atlas, Folio 7.

Devanney III, J.W., et al. 1974. Analysis of Oil Spill Statistics, In: Primary Physical Impacts of Offshore Petroleum Developments, Report No. MITSG 74-20, Massachusetts Institute of Technology, Cambridge, MA, 126 p.

EG&G, 1978. Data Report Moored Instruments, January - May 1978, Appendix B of Seventh Quarterly Progress Report, New England Outer Continental Shelf Physical Oceanography Program, U.S. Department of the Interior.

EG&G, 1978. Data Report Moored Instruments, September 1977 - February 1978, Appendix B of Sixth Quarterly Progress Report, New England Continental Shelf Physical Oceanography Program, U.S. Department of the Interior.

EG&G, 1981. Interpretation of the Physical Oceanography of Georges Bank. Preliminary Report, Contract #AA851-CT1-39, prepared for U.S. Dept. of the Interior, Bureau of Land Management.

Godshall, F.A., et al. 1980. A Climatologic and Oceanographic Analysis of the Georges Bank Region of the Outer Continental Shelf, Final Report to the Bureau of Land Management, U.S. Department of the Interior, 290 p.

Isaji, T., M.L. Spaulding, J.C. Swanson, 1982. A Three-Dimensional Hydrodynamic Model of Wind and Tidally Induced Flows on Georges Bank, Applied Science Associates, Inc., Wakefield, Rhode Island, 47 p.

Lorda, E. and S.B. Saila, 1980. A Stochastic Nonlinear Leslie Matrix Model for Simulating the Effect of Increased, Age-Specific, Density-Independent Mortality of Fish Populations. Paper presented at the Symposium on Age-Structured Models in Fishery Science, 110th Annual Meeting of the Amer. Fisheries Soc., Sept. 22-24, 1980. Louisville, Kentucky.

Lorda, E., S.B. Saila, and H.A. Walker, 1982. The Stochastic Simulation of the Dynamics of Fish Populations Using Nonlinear Leslie Matrix Models: Methodology, Probablistic Analysis and Application to the Georges Bank Cod Fishery, (in preparation).

Reed, M. and M.L. Spaulding, and P.C. Cornillon, 1979. An Oil Spill-Fishery Interaction Model: Comparison of Treated and Untreated Spill Impacts. Proc. of 1979 Oil Spill Conference, EPA-API, L.A., p. 63-73.

Reed, M., 1980. An Oil Spill Fishery Interaction Model -- Development and Applications. Ph.D. Thesis, Department of Ocean Engineering, University of Rhode Island, Kingston, Rhode Island.

Reed, M., M.L. Spaulding, and P. Cornillon. 1981. A Fishery-Oil Spill Interaction Model: Simulated Consequences of a Blowout, Proc. of NATO Symposium on Applied Operations Research in Fishing, 1981 Plenum Press, New York, p. 99-114.

Reed, M., M.L. Spaulding, and E. Lorda, 1982. Oil Spill Fishery Impact Assessment Modeling: The Fisheries Recruitment Problem, Proceedings of a Technological Conference: Georges Bank Hydrocarbon Exploration and Development, Nantucket, Massachusetts, April 27-30, 1982.

Spaulding, M.L. and M. Reed, 1982. Oil Spill Fishery Impact Assessment Modeling: Application to Georges Bank, Proceedings of NOAA/EDIS/CEAS Workshop on Ecosystems Modeling, Frederick, MD., April 5-8, 1982, (In press).

Spaulding, M.L., and S.B. Saila, 1981. Oil Spill - Fishery Impact Assessment Modeling: Application to Selected Georges Bank Fish Species, Estuarine, Coastal, and Shelf Science, in press.

Spaulding, M.L. and S.B. Saila, M. Reed, J.C. Swanson, T. Isaji, E. Anderson, E. Lorda, V. Pigoga, K. Marti, J. Hoenig, H. Walker, C. Jones, F. White, R. Glazman, and K. Jayko. 1981. Assessing the Impact of Oil Spills on a Commercial Fishery. First Interim Report, prepared for the Bureau of Land Management NYOCS Office under Contract No. AA851-CTO-75.

Spaulding, M.L., K.B. Jayko, and E.L. Anderson, 1982a. Hindcast of the Argo Merchant Spill Using the URI Oil Spill Fates Model, Journal of Ocean Engineering (in review).

Spaulding, M.L. et al. 1982b. Assessing the Impact of Oil Spills on a Commerical Fishery, Second Interim Report, prepared for the Bureau of Land Management NYOCS Office under Contract No. AA851-CTO-75. January, 1982.

Spaulding, M.L., et al. 1982c. Assessing the Impact of Oil Spills on a Commercial Fishery, Third Interim Report, prepared for the Bureau of Land Management NYOCS Office under Contract No. AA851-CTO-75. May, 1982.

ENVIRONMENTAL DATA INPUT: WIND

(Appendix A)

The wind data used as input to the model runs presented in this report is a one year long actual record, (Julian day 72-244 to 73-243) collected at Nantucket Airport, and archived on a standard National Climatic Center TDF-14 weather tape. The sampling interval is three hours, giving eight observations per day. Table 1 shows monthly statistics for the two components of velocity for this wind record: U positive East, V positive North. WSbar is the monthly mean wind speed. The oceanographic convention is used, a northerly wind flows northward. Units are meters per second; NMS shows the number of missing values by month.

TABLE 1
Monthly Simulation Wind Statistics

YR MO	NMS	Ubar m/sec	Usig m/sec	Vbar m/sec	Vsig m/sec	WSbar m/sec
73 01	0	3.05	4.02	-1.22	4.67	6.41
73 02	0	0.51	4.62	-2.63	5.02	6.69
73 03	0	-1.19	4.66	-1.05	4.93	6.13
73 04	0	2.06	5.02	0.48	3.50	6.09
73 05	0	0.87	3.68	1.23	3.50	4.91
73 06	0	1.48	3.38	1.66	3.07	4.60
73 07	0	1.38	3.21	1.67	3.41	4.68
73 08	0	0.41	3.38	0.64	2.92	4.12
72 09	0	0.02	4.07	-0.12	3.14	4.47
72 10	0	-0.02	3.56	-0.54	4.14	4.98
72 11	0	-0.87	3.36	-1.50	4.37	5.23
72 12	0	0.80	4.72	-0.75	3.77	5.54

In any simulation requiring environmental input data the question of the representativeness of this data must be addressed. Comparisons of the 72-73 wind dataset used to drive the model simulations with ten other contiguous years of the same wind dataset follow. The total wind record examined spans the calender years 1966 through 1976. Table 2 gives

the ensemble averaged monthly statistics for the eleven year dataset.

TABLE 2
Statistics of Ensemble Averaged Monthly
Means Over Years 1966 through 1976

MO	Ubar m/sec	Usig m/sec	Vbar m/sec	Vsig m/sec	WSbar m/sec	WSsig m/sec
01	2.17	0.30	-1.54	0.90	5.98	0.30
02	1.73	1.21	-1.36	1.91	6.30	0.65
03	1.33	1.18	-0.84	0.59	6.26	0.04
04	1.44	0.66	-0.45	1.15	6.12	0.38
05	0.84	0.53	0.77	0.57	5.57	0.35
06	0.80	0.66	1.49	0.25	4.95	0.08
07	1.24	0.52	1.66	0.40	4.61	0.17
08	0.99	0.34	0.99	0.28	4.54	0.10
09	0.40	0.45	-0.00	0.33	4.83	0.15
10	0.76	0.98	-0.40	0.86	5.31	0.20
11	1.14	2.23	-1.19	0.23	5.71	0.34
12	1.47	0.87	-1.35	0.45	6.05	0.42

Figure 1, a plot of the eleven year U component monthly mean range and Figure 2, the corresponding V monthly range plot gives a graphical feel for the between year monthly variability. The eleven year monthly mean ranges are presented as the vertical lines. The horizontal marks are the ensemble averaged monthly means, and the circles are the monthly means for the 72-73 dataset. Figure 2 shows the characteristic summer - winter shift of north-south net wind drift. The ranges of both components tend to be greater during the spring and fall transitions than during the middle of either the summer or winter season. January, March and November of the 72-73 dataset are extremes of their respective monthly mean ranges.

A more useful comparison is to display a progressive vector diagram for the wind data. Figures 3 through 6 show the progressive vector diagrams of the 72-73 wind data (top) and an overlay of all 11 years' data (bottom) for the four simulation times. The start days are Julian 60, 152, 244, and 335;

each plot covers ninety days duration, and in each case the starting location for the plot is on the center of the cross-hair. The expected general characteristics of the seasonal winds for this location are evident. The summer (152) plot shows the result of the prevailing northeasterly wind. All four plots show eastward drift associated with the overall prevailing wind pattern. The plots for the summer (152) and winter (335) runs show the most directional consistency among the eleven years presented, and the 72-73 data track lies in a mediate position. The 72-73 tracks for the spring (6) and fall (244) simulations show less westward drift than does the summation of the eleven year runs.

Figure 1, month 3 (March) shows a 72-73 value at the western extreme of the eleven year range. Since the March simulations for all four spill locations have the highest impacts, one must look closely at this wind statistic. The 72-73 U component means for April and May show greater eastward net flow and equivalent net flow to the ensemble averaged mean, respectively. Comparison of the top and bottom of Figure 3 shows the progressive vector position at the end of March, and the extreme westerly drift compared to the eleven year ensemble average for March. The April and May 72-73 values push the eventual termination of the 72-73 progressive vector to a position closer to the center of the cluster of the eleven ninety day endpoints.

This comparative net westward drift of the first month of the 3 month simulation would tend to keep the surface oil within the spawning areas in the vicinity of Georges Bank for a longer time than the "average" of the eleven years, and thus could be expected to result in relatively greater larval mortality ("worst case" estimate).

Scanning the length of the range bars in Figures 1 and 2, it is clear that the greatest among-year variability of the monthly means occurs during the spring and fall. The relative consistency of the summer and winter seasons is evident also from the coherence of the progressive diagrams for these months as mentioned above.

As discussed by Godshall et al. (1980), the dataset reflects the consistent passage of the North Polar front through the 40° N - 45° N latitudes during spring and autumn. This frontal passage can be seen in the wind shift from southeasterly (winter) to northeasterly (summer), as well as in the increased variability associated with the transitional seasons.

Figure 1. 11 Year U Component Range of Monthly Mean Winds

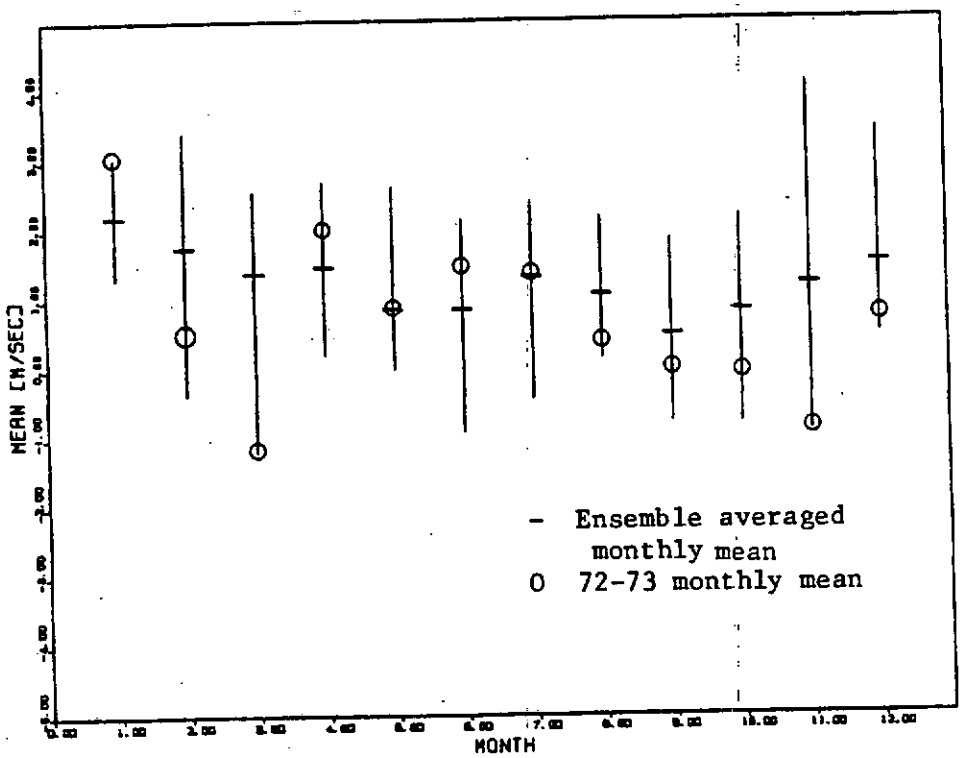

Figure 2. 11 Year V Component Range of Monthly Mean Winds

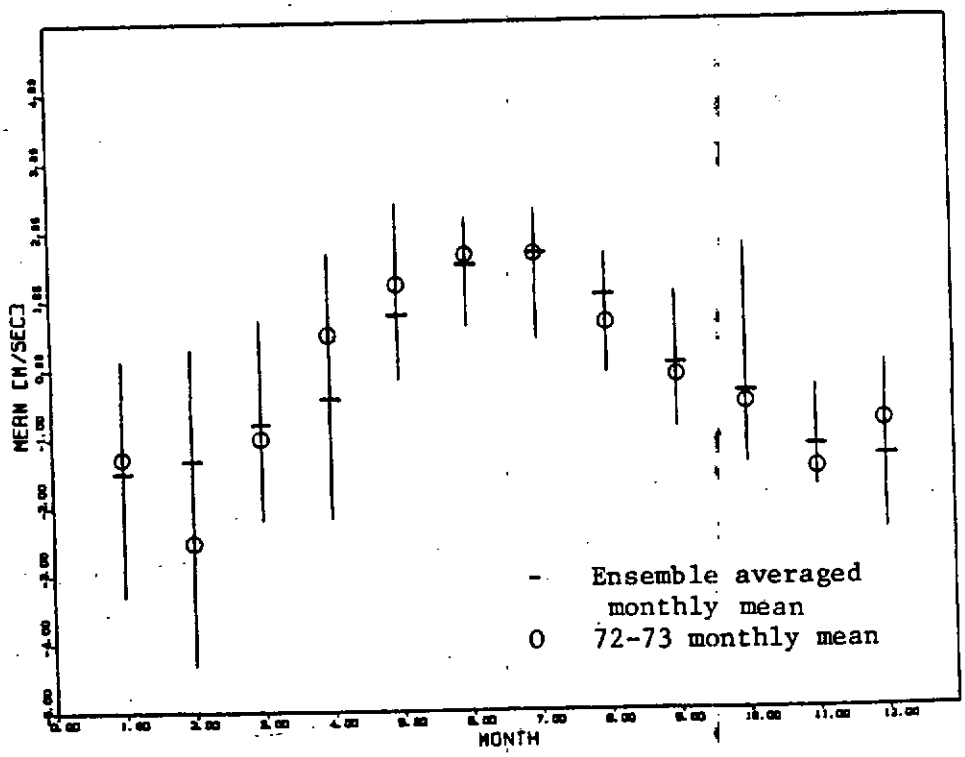

Figure 3. 90 Day Progressive Wind Vector Plot
Start Day: 60

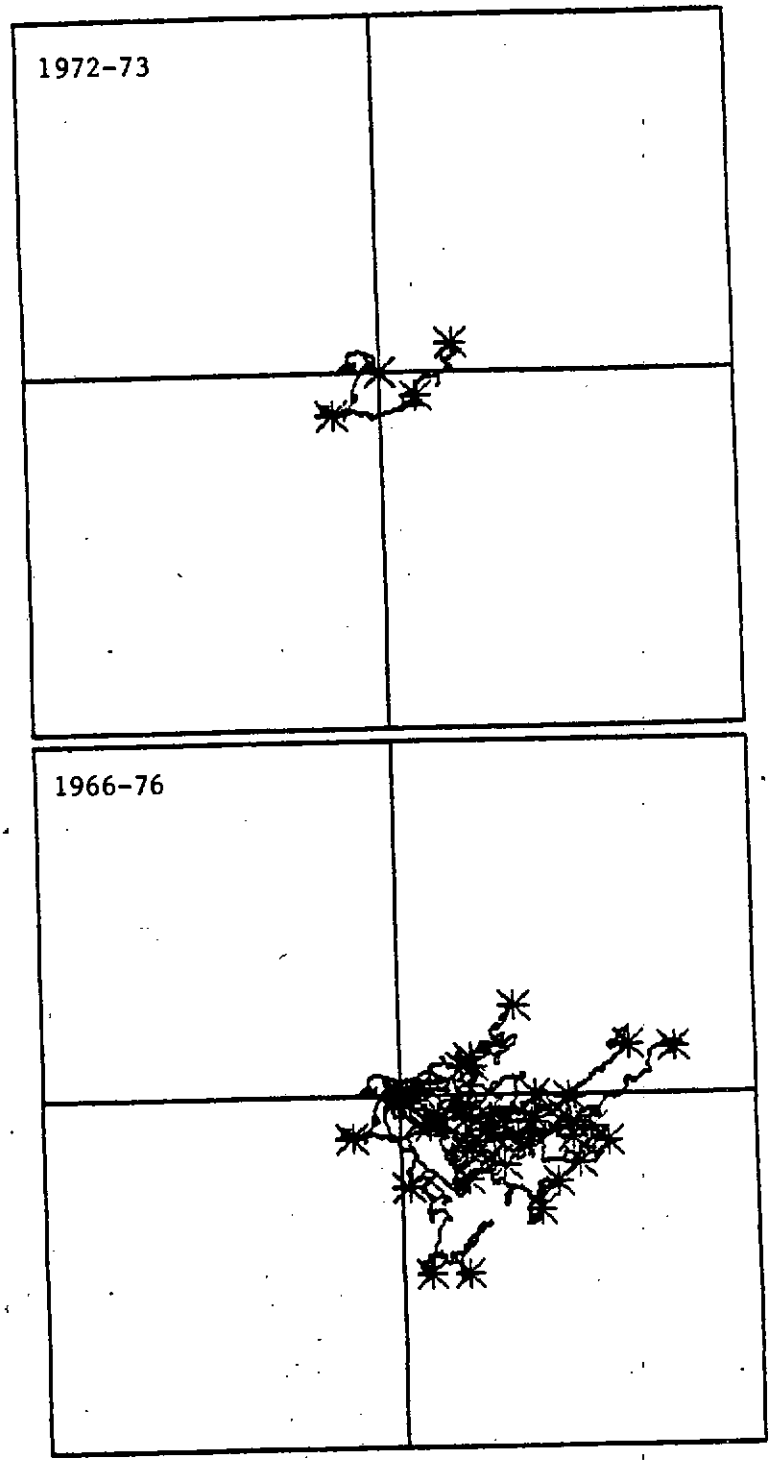

Figure 4. 90 Day Progressive Wind Vector Plot
Start Day: 152

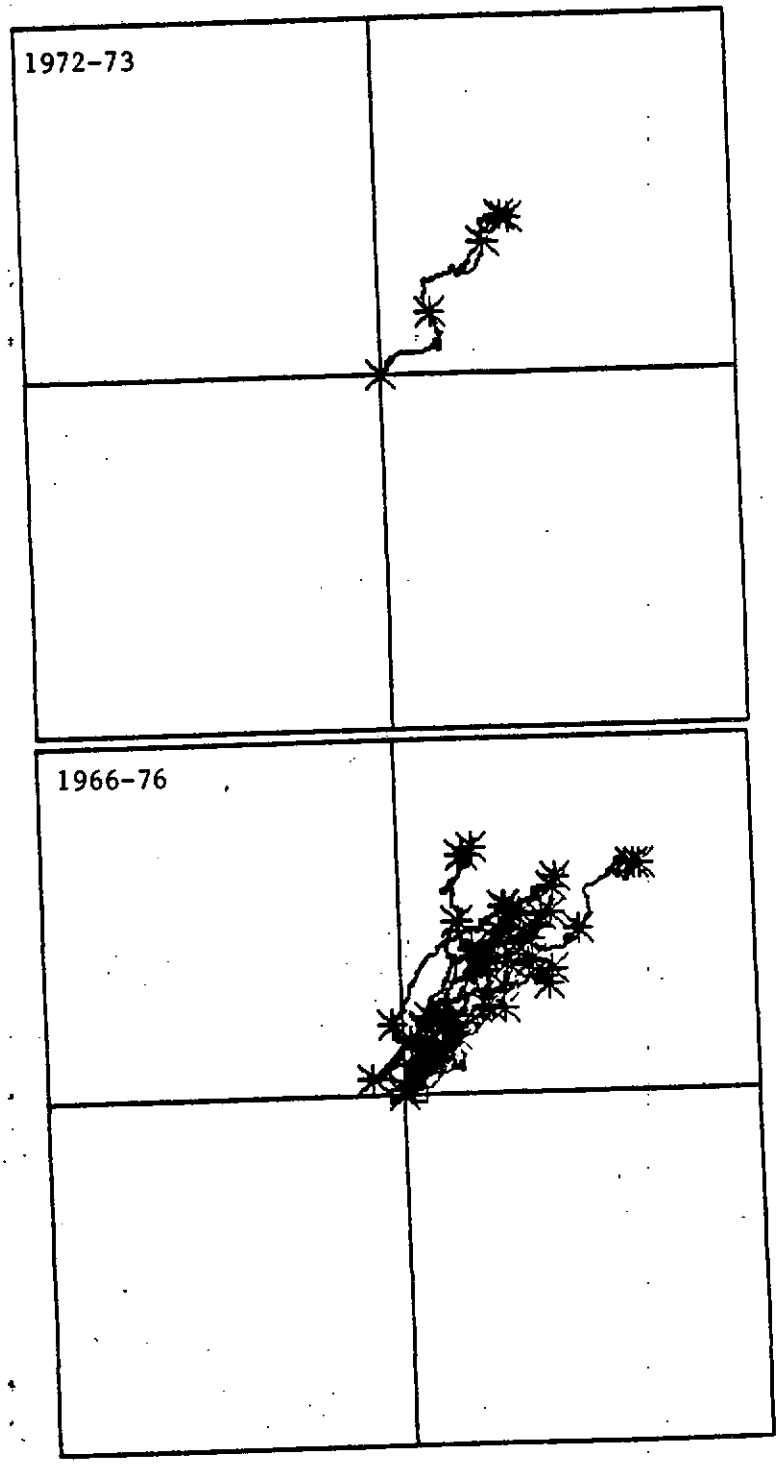

Figure 5. 90 Day Progressive Wind Vector Plot
Start Day: 244

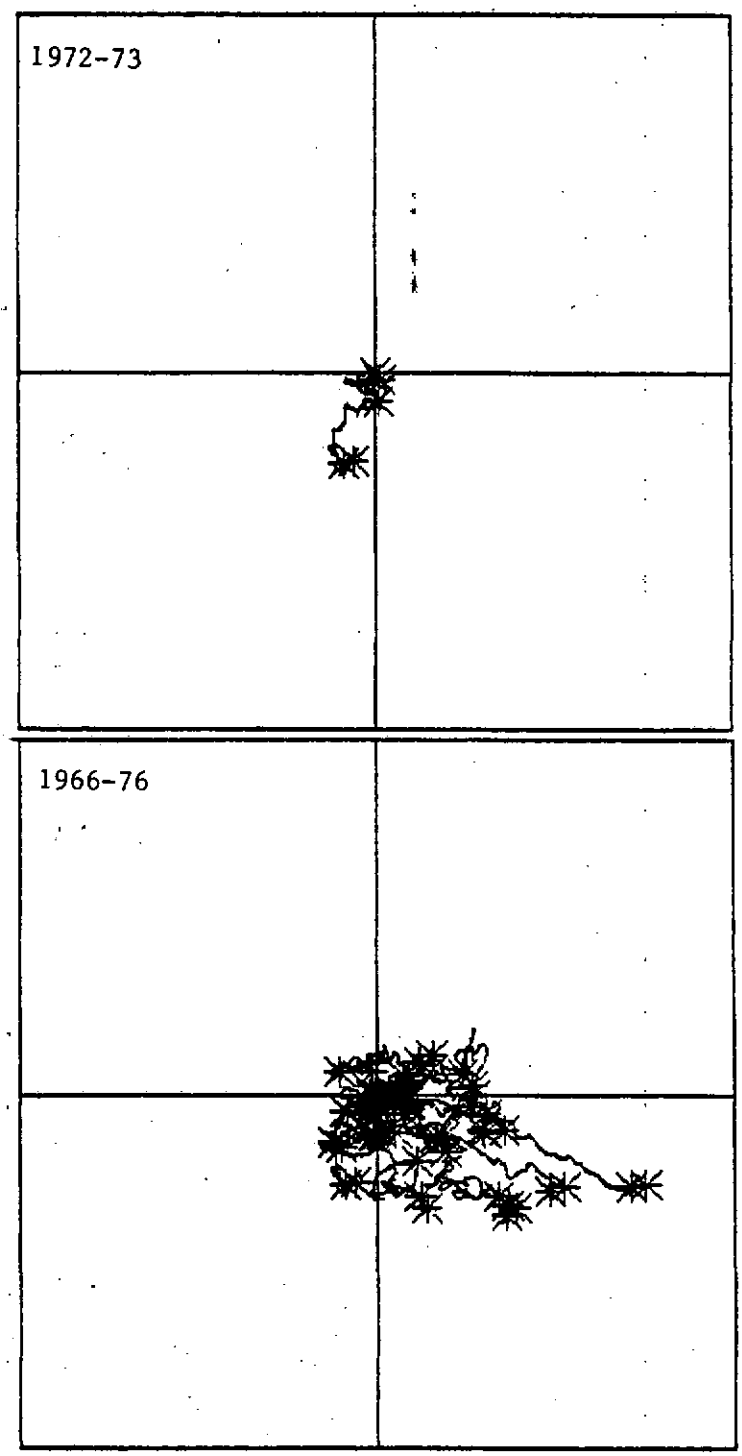
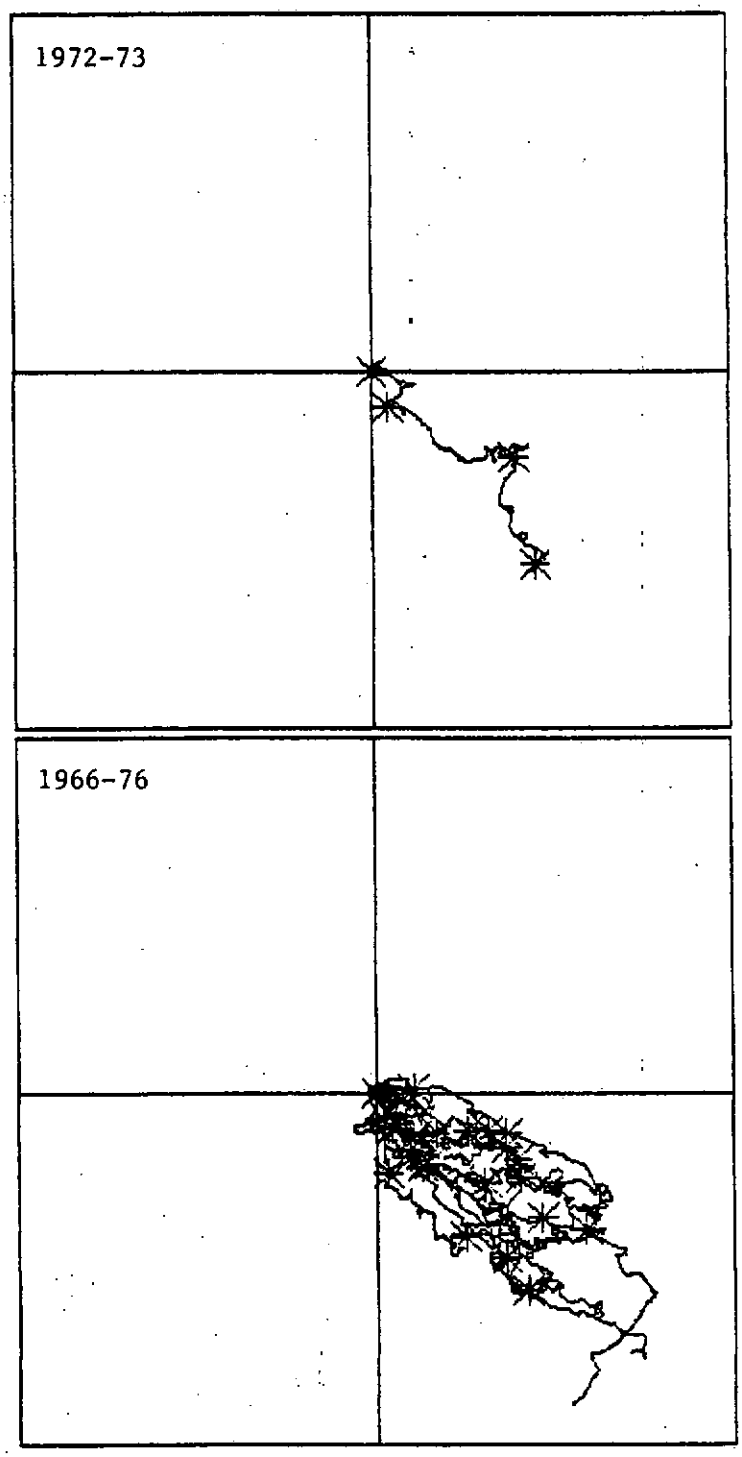
Figure 6. 90 Day Progressive Wind Vector Plot
Start Day: 335